2014

Additives to Control Mechanical Properties and Drug Delivery of Injectable Polymeric Scaffolds

Paul Fisher
University of Kentucky, pdpescador@gmail.com

STUDENT AGREEMENT:

I represent that my thesis or dissertation and abstract are my original work. Proper attribution has been given to all outside sources. I understand that I am solely responsible for obtaining any needed copyright permissions. I have obtained needed written permission statement(s) from the owner(s) of each third-party copyrighted matter to be included in my work, allowing electronic distribution (if such use is not permitted by the fair use doctrine) which will be submitted to UKnowledge as Additional File.

I hereby grant to The University of Kentucky and its agents the irrevocable, non-exclusive, and royalty-free license to archive and make accessible my work in whole or in part in all forms of media, now or hereafter known. I agree that the document mentioned above may be made available immediately for worldwide access unless an embargo applies.

I retain all other ownership rights to the copyright of my work. I also retain the right to use in future works (such as articles or books) all or part of my work. I understand that I am free to register the copyright to my work.

REVIEW, APPROVAL AND ACCEPTANCE

The document mentioned above has been reviewed and accepted by the student's advisor, on behalf of the advisory committee, and by the Director of Graduate Studies (DGS), on behalf of the program; we verify that this is the final, approved version of the student's thesis including all changes required by the advisory committee. The undersigned agree to abide by the statements above.

Paul Fisher, Student

Dr. David A. Puleo, Major Professor

Dr. Abhijit Patwardhan, Director of Graduate Studies

ADDITIVES TO CONTROL MECHANICAL PROPERTIES AND DRUG DELIVERY OF INJECTABLE POLYMERIC SCAFFOLDS

_____

DISSERTATION

_____

A dissertation submitted in partial fulfillment of the
requirements for the degree of Doctor of Philosophy in the
College of Engineering
at the University of Kentucky

By

Paul Daniel Fisher

Lexington, Kentucky

Director: Dr. David Puleo, Professor of Biomedical Engineering

Lexington, Kentucky

2014

ABSTRACT OF DISSERTATION

ADDITIVES TO CONTROL MECHANICAL PROPERTIES AND DRUG DELIVERY OF INJECTABLE POLYMERIC SCAFFOLDS

In situ forming implants (ISIs) are popular due to their ease of use and local drug delivery potential, but they suffer from high initial drug burst, and release behavior is tied closely to solvent exchange and polymer properties. Additionally, such systems are traditionally viewed purely as drug delivery devices rather than potential scaffold materials due to their poor mechanical properties and minimal porosity. The aim of this research was to develop an injectable ISI with drug release, mechanical, and microstructural properties controlled by micro- and nanoparticle additives.

First, an injectable ISI was developed with appropriate drug release kinetics for orthopedic applications. Poly(β-amino ester) (PBAE) microparticles were loaded with simvastatin or clodronate, and their loading efficiency and drug retention after washing was quantified. Drug-loaded PBAE microparticles and hydroxyapatite (HA) microparticles were added to a poly(lactic-co-glycolic acid) (PLGA)–based ISI. By loading simvastatin into PBAE microparticles, release was extended from 10 days to 30 days, and burst was reduced from 81% to 39%. Clodronate burst was reduced after addition of HA, but was unaffected by PBAE loading. Scaffold mass and porosity fluctuated as the scaffolds swelled and then degraded over 40 days.

Next, the mechanical properties of these composite ISIs were quantified. Both micro- and nanoparticulate HA as well as PBAE microparticle content were varied. Increasing HA content generally improved compressive strength and modulus, with a plateau occurring at 30% nano-HA. Injectability remained clinically acceptable for up to 10% w/w PBAE microparticles. Ex vivo injections into trabecular bone improved both strength and modulus.

Lastly, HA-free ISIs were investigated for drug delivery into the gingiva to treat periodontitis. Doxycycline and simvastatin were co-delivered, with delivery of doxycycline over 1 week accompanied by simvastatin release over 30 days. PBAE-containing ISIs exhibited higher initial and progressive porosity and accessible volume than PBAE-free ISIs over the course of degradation. Additionally, PBAE-containing ISIs provided superior tissue retention within a simulated periodontal pocket. The ISIs investigated here have a wide range of potential applications due to their flexible material and drug release properties, which can be controlled by both the chemistry and concentration of various particulate additives.

KEYWORDS: Injectable tissue engineering scaffolds, biodegradable polymers, controlled drug delivery, biodegradable hydrogels, *in situ* forming drug delivery implant

Paul Daniel Fisher
Student's Signature

11/24/2014
Date

ADDITIVES TO CONTROL MECHANICAL PROPERTIES AND DRUG DELIVERY OF INJECTABLE POLYMERIC SCAFFOLDS

By

Paul Daniel Fisher

Dr. David Puleo
Director of Dissertation

Dr. Abhijit Patwardhan
Director of Graduate Studies

11/24/2014
Date

ACKNOWLEDGMENTS

It would be impossible to mention every person who has played an impactful role in my time here at the University of Kentucky. There are so many people who have been involved, directly or indirectly, in this journey, and rest assured that all of the help, attention, or advice I received did not go unappreciated. In particular, I wish to thank my advisor, Dr. David Puleo, who has the uncanny ability to provide every answer in the form of a new question, which has continued to spark my scientific curiosity. My co-advisor, Dr. Zach Hilt, has provided insight and expertise that helped guide my work as it progressed. I also wish to thank the members of my committee: Dr. Todd Milbrandt has provided clinical input that shaped many of my research aims, and Dr. Hainsworth Shin and Dr. Thomas Dziubla have provided fresh perspectives.

My lab mates, both past and present, are a collection of odd and wonderful people that made the days fly by, except for the times when the radio was commandeered to play country music all day. Thank you for your support – I would list all of you, but the fact that the list would be incredibly long is probably a sign that it's time for me to graduate!

This section would be meaningless without a dedication to my wife Paulina, without whom I would have never considered graduate school. She has been patient when my nerves were frayed, encouraging when progress was slow, supportive when things were difficult, and most importantly, she was always there with me to share in this adventure. She deserves more than a short paragraph, but as a Californian, I believe I can put it most succinctly by simply stating that she is totally rad.

Finally, my family! My mom and dad have been, and continue to be, a tremendous source of encouragement and guidance, and I have difficulty putting into words how grateful I am for their tireless dedication to raising me well. I truly lucked out with my older brother Greg and my younger sister Julia – I simply could not ask for more caring and supportive siblings.

Table of Contents

List of Tables

List of Figures

Chapter 1 Introduction

In situ forming implants (ISIs) made from poly(lactic-co-glycolic acid) (PLGA) have been thoroughly investigated for drug delivery applications, and these systems have been commercialized due to their simplicity and effectiveness as sustained, local drug delivery depots. The release kinetics from these systems are generally controlled by modifying the polymer or solvent used, but very little information is available on the impact that particulate additives may have on the material properties and release kinetics. In particular, PLGA ISIs are not favored for applications requiring tissue ingrowth or mechanical support because their microarchitecture and mechanical properties are inferior to pre-formed scaffolds. Here, composite PLGA/hydroxyapatite/hydrogel ISIs were developed for orthopedic applications, and PLGA/hydrogel ISIs were also further investigated for soft tissue applications.

Chapter 2 provides a brief history of synthetic biodegradable polymers used for drug delivery, and includes properties of some of the most popular materials. Then, the applications for these materials are discussed, and particular focus is placed on micro- and nanoparticle systems, as well as the different types of ISIs. Next is an overview of two conditions that were targeted in this research – osteonecrosis of the femoral head and periodontitis. The specific aims of this dissertation conclude Chapter 2.

Chapters 3 and 4 are both related to the development of a locally injectable PLGA ISI suitable for orthopedic applications. The work in Chapter 3 is devoted to quantifying the effects of hydrogel and hydroxyapatite additives on drug release from a PLGA ISI. A significant portion of this chapter focused on developing drug-loaded, hydroxyapatite-coated, hydrogel microparticles. The objective of this chapter was to demonstrate that particulate additives could modify release kinetics and provide a suitable microarchitecture for trabecular bone augmentation. Chapter 4 focused on the effects of hydroxyapatite and hydrogel particles on the material properties of the

system. Specifically, mechanical properties and injectability were quantified, and injection into artificial bone and *ex vivo* bone samples were used to demonstrate feasibility of the system as a mechanically supportive, injectable scaffold.

In Chapter 5, PLGA ISIs containing a high concentration of hydrogel microparticles were investigated for soft tissue applications, and the periodontal pocket was considered the target tissue. Here, hydrogels were processed into microparticles using a wet grinding technique without using hydroxyapatite additives. The purpose of adding hydrogel was to improve the space-filling, microarchitecture, and co-delivery of an antibiotic and osteogenic drug. The objective of this chapter was to show the potential of these materials for future consideration as tissue scaffolds.

Chapter 2 Background and Significance

2.1. Synthetic biodegradable polymers for drug delivery

Biomaterials are classically defined, distinctly from drugs, as materials used to augment or replace tissues or processes in the body. With the advent of synthetic, biodegradable polymers, however, the line becomes blurred, as these materials are capable of blending the roles of biomaterials and drugs into a single system [1]. The recognition that certain polymers containing hydrolytically or enzymatically labile groups could be degrade naturally after implantation led to a revolution in the field of drug delivery [2-8]. By incorporating drugs into a biodegradable polymer matrix, spatial and temporal control of release kinetics was possible. As seen in Figure 2.1, the publication rate for biodegradable polymeric drug delivery systems has grown exponentially since their first uses in the 1970s. This growth is due in no small part to the vast array of synthetic polymer properties that can be controlled by both chemical syntheses and material processing steps, resulting in an extremely versatile platform. Controlling and understanding mechanisms by which these polymers degrade is important when designing or choosing a material for drug delivery, because the degradation behavior influences drug release rates and host response [9]. Some of the most popular materials and their potential applications are presented in the subsequent sections, with an emphasis placed on their mechanisms and rates of degradation.

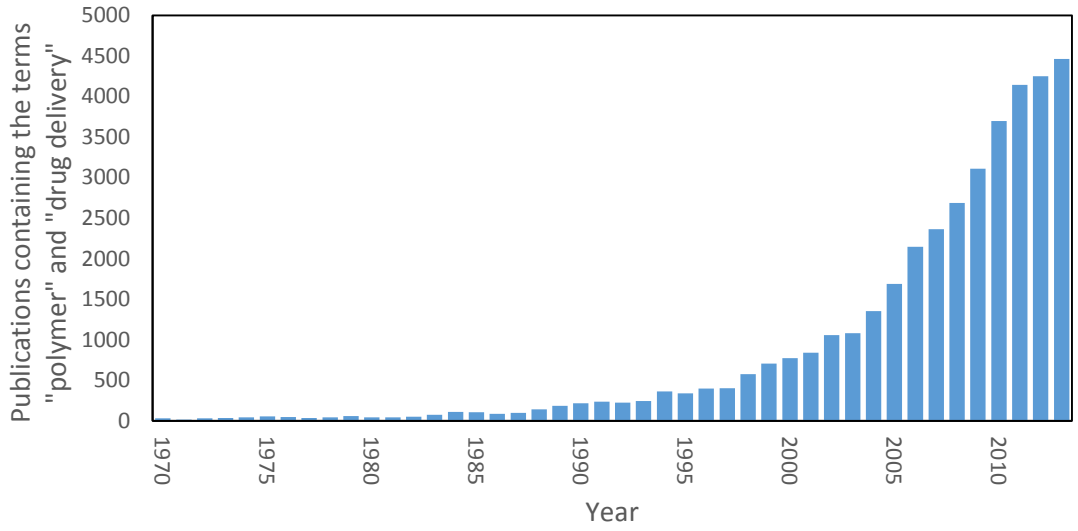

Figure 2.1. Annual publications containing the search terms “polymer” and “drug delivery.” Via PubMed.

2.1.1. Polyanhydrides

Polyanhydrides are named for the anhydride bonds that link repeating units of the polymer backbone (Figure 2.2A), and were originally synthesized in the early 1980s with the objective of matching polymer degradation rate to drug release [10]. The anhydride bonds can be hydrolyzed to produce dicarboxylic acids, and these materials degrade through surface erosion, as the water uptake rate is generally far lower than the rate of surface chain scission [11]. As a result of this degradation mechanism, linear drug release rates that closely match the material degradation rate can be achieved [10, 12]. Since the bulk of the polymer does not appreciably hydrate as it degrades, processing methods that affect the microstructure or the implant geometry can strongly influence degradation kinetics by limiting or increasing the accessible surface area [13, 14]. Copolymers of polyanhydrides are also used to control the properties of these materials. For example, polyanhydrides copolymerized with more hydrophilic blocks can be produced to accelerate degradation and drug release from months to hours [10, 13, 15-17], while

poly(anhydride-co-imides) possess mechanical properties more suitable for orthopedic applications [18]. Polyanhydrides have been further modified via cross-linking to improve mechanical strength [19, 20]. The incorporation of hydroxyapatite (HA) via surface-grafting can promote bone cell attachment, and homogeneously incorporated HA can improve mechanical properties [20, 21]. Polyanhydrides have exhibited good biocompatibility in animal *in vivo* studies, with no observed toxicity, inflammation, or other adverse effects noted after implantation in a variety of tissues [22-25]. The FDA first approved their use in 1996 in the form of Gliadel®, a polyanhydride wafer loaded with chemotherapeutic carmustine, which is placed directly onto brain tissue after removal of cancerous tumors.

2.1.2. Poly(lactic-co-glycolic acid)

The most well-characterized and prevalent biodegradable polymers in drug delivery are composed of lactic or glycolic acid subunits, forming poly(lactic acid) (PLA), poly(glycolic acid) (PGA), or poly(lactic-co-glycolic acid) (PLGA) (Figure 2.2B). Investigation of these polymers began in the 1970s with PLA [3, 26, 27]. Because the monomers in PLA possesses methyl side groups, optically pure, semicrystalline polymers made from either D or L enantiomers can be produced, but PLA is most commonly used in drug delivery in amorphous form as the product of a racemic mixture [28]. PGA is highly crystalline, though it is hydrolyzed rapidly compared to PLA due to its more hydrophilic nature, and as a homopolymer was popularized as the first biodegradable synthetic suture, Dexon® [29]. PLGA is generally amorphous, and degradation times are highly dependent on the lactide:glycolide ratio [29-32]. As with most degradable polymers, the degradation rate also decreases with molecular weight [33]. PLGA containing a 50:50 lactide:glycolide ratio degrades most rapidly, and degradation time can be modified by varying molecular weight, hydrophilicity of the chain end species, or the lactide:glycolide ratio [33, 34]. PLGA, PLA, and PGA are primarily bulk-degrading because the polymer chains are hydrophilic

enough to allow water penetration before surface erosion occurs, so a progressive molecular weight decrease occurs throughout the material [32]. Chain scission eventually produces lactic and glycolic acid, both of which are endogenously produced during metabolic processes, and soluble acidic oligomers may autocatalyze degradation [35, 36]. PLA and PLGA are used in many commercial drug delivery systems, including antibiotic delivery (Atridox®, Arestin®), hormone therapy (Nutropin®), and cancer treatment (Lupron Depot®, Trelstar Depot®, Eligard®).

2.1.3. Poly(caprolactone)

Poly(caprolactone) (PCL) is a biodegradable, semi-crystalline polymer characterized by its hydrophobicity, long degradation time, and low melting point (Figure 2.2C). PCL was one of the earliest polymers investigated as a degradable biomaterial, and was originally tested as a biodegradable alternative to silicon rubber implants for long-term delivery of contraceptives in the 1970s [5, 37]. However, its usefulness as a homopolymer was limited due to its 2-4 year degradation time [38]. Because it is easily blended or copolymerized, PCL is often used to produce copolymers or polymer blends with versatile rheological, viscoelastic, and drug release properties that depend on the ratios of each component [39-43]. The glass transition temperature of PCL is around -60˚C, meaning PCL is far more flexible and less brittle than PLGA and PLA at ambient and physiological temperatures, which can improve physical properties of blends and copolymers [44-46]. Additionally, its low melting temperature (approximately 60˚C) makes PCL one of the more workable materials, so it is a popular choice for 3-D printing, extrusion, and melt blending [47-50]. Amphiphilic copolymers of PCL and poly(ethylene glycol) (PEG) or other hydrophilic components have been investigated as solid particles, hydrogels, or micelles, with the highly hydrophobic PCL regions appropriate for sustained delivery of hydrophobic drugs [51-53]. The physical properties of PCL allow it to be easily blended with particle additives and formed into scaffolds with complex geometries, and PCL composites containing HA or other bioceramics have

been extensively investigated for orthopedic applications, although their lower mechanical properties limit their load-bearing potential [49, 54-57]. A block copolymer of PCL and PGA, now marketed as Monocryl®, was developed to reduce the stiffness of resorbable PGA sutures.

2.1.4. Poly(ortho esters)

In the 1980s, poly(ortho esters) (POEs), along with polyanhydrides, were among the first polymers specifically synthesized for drug delivery [58]. The ortho ester bonds (Figure 2.2D) result in more hydrophobic polymer chains than carbonyl-containing polymers such as PLGA, slowing water penetration and limiting hydrolysis to the polymer-water interface. This results in a pH-sensitive, surface-eroding material that produces low-molecular weight, soluble byproducts, although longer-degrading POEs will eventually become permeated with water. Degradation rates can be further controlled by the incorporation of glycolic acid or other acidic species into the polymer backbone to autocatalyze degradation [59-61]. Conversely, surface erosion can be prolonged by incorporating basic excipients with poor water solubility to stabilize the polymer and prevent water imbibition [62]. During synthesis, the concentration of flexible diols and acid diols used in the polymer backbone determines the glass transition temperature, so very brittle or semi-solid POEs can be easily produced [63]. The latest generation of POEs have been specifically investigated as intraocular delivery systems because they are a viscous, easily injectable liquid at room temperature yet still provide erosion-based drug release [64, 65]. Because POEs are surface-eroding, they offer an advantage over PLA and PCL because small-molecule, hydrophilic drugs can be released concomitantly with degradation as long as a stabilizing excipient is used [66].

2.1.5. Poly(β-amino esters)

Poly(β-amino esters) (PBAEs) are a class of biodegradable polymers that are synthesized through a condensation reaction between a diacrylate and a primary amine (Figure 2.2E) or

secondary-secondary diamine [67, 68]. This initial reaction occurs through a step-growth polymerization process, and a molar excess of diacrylate will produce acrylate-terminated macromers [69]. These macromers can be cross-linked using free radical initiated chain-growth polymerization to form hydrogels that can biodegrade at their ester bonds [69-71]. Many factors determine the degradation rate and swelling behavior of these hydrogels in aqueous environments, including diacrylate and amine chemistry, macromer synthesis time and temperature, and cross-link density [69-71]. PBAEs have been extensively investigated for their potential in DNA therapy. For example, PBAEs incorporated into PLGA microparticles were shown to improve loading efficiency and delivery of plasmid DNA, preserve integrity of the delivered plasmid DNA, and improve transfection efficiency [72-74]. Microparticulate copolymers of PBAE and PEG have been investigated for pH-sensitive delivery of drugs to cancer cells [75-77], and PBAE hydrogels have been investigated as both passive porogens and drug delivery vehicles [78-82].

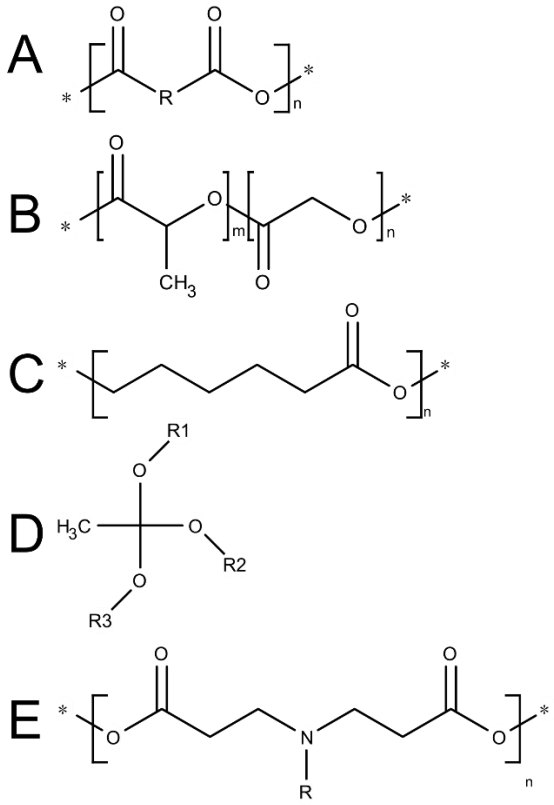

Figure 2.2. Chemical structures of common synthetic biodegradable polymers. A) Polyanhydride. B) Poly(lactic-co-glycolic acid). C) Poly(caprolactone). D) A simple ortho ester. Poly(ortho esters) tend to contain repeated cyclic units and therefore have a variety of possible structures. E) Poly(β-amino ester) synthesized using a primary amine.

2.2. Injectable drug delivery systems

As biodegradable polymers gained traction as versatile drug delivery platforms, research began to focus on improving the structure of these materials to simplify implantation and take advantage of their long lifespan *in vivo*. Pre-formed, monolithic implants require surgical implantation at the treatment site, and this approach is undesirable or even impossible for targeted treatments such as drug delivery to intratumoral or intraosseous tissue. Two distinct approaches to this problem are discussed below. First, drug-loaded polymeric micro- or

nanoparticles allow targeted delivery of biodegradable polymers via simple injection. Second, injections containing drug-loaded liquid precursors designed to solidify *in situ* permit formation of a monolithic implant at the injection site.

2.2.1. Micro- and nanoparticle delivery

Micro- and nanoparticles can be synthesized using a variety of techniques. Most commonly, the polymer is dissolved in an appropriate solvent, and is subjected to a series of emulsion steps that both entrap drug and stabilize spherical polymer droplets as they solidify during solvent evaporation. For hydrophilic drugs, a water/oil/water double emulsion technique is used. First, an aqueous drug solution is dispersed in the polymer/solvent phase (W1/O emulsion 1). Next, the W1/O phase is emulsified in a second aqueous phase, creating a W1/O/W2 emulsion, and solid particles can be created through solvent removal. Frequently, surfactants are used to stabilize these emulsions, preventing collapse or coalescence of particles prior to solidification. For hydrophobic drugs, a single emulsion technique is sufficient, with the drugs added directly to the polymer phase, skipping the W1/O emulsion. Particle size can be controlled by adjusting the solvent:water ratios, the surfactant content, temperature, and stirring parameters throughout the process [83-87].

Microparticles can be created from films or slabs of material by simple grinding followed by sieving to the desired particle size, although this works best for weak, brittle materials.[88] Stronger materials are difficult to mechanically break apart, while soft or sticky materials such as PBAE hydrogels will re-aggregate during the grinding process, necessitating a powder additive to act as a dispersant. For particles that swell in water or other solvents without degrading quickly, drugs can be more easily loaded after particle formation by swelling the particles in a drug solution followed by solvent removal [81, 89-91]. This list of methods is by no means exhaustive – many other techniques have been developed to create drug-loaded micro- and nanoparticles beyond

these popular few listed, including spray drying [92-95], hot melt microencapsulation [96], phase inversion microencapsulation [97], non-aqueous solvent removal [98], and interfacial polymerization [99, 100].

One major advantage of using a microparticle carrier is that particles can easily be injected as a powder or aqueous suspension to the target site. For example, Arestin® is the product name of a PLGA microparticle system, approved in 2001, containing the antibiotic minocycline. Arestin is injected as a powder directly into periodontal pockets to treat infection, and can achieve up to 21 days of continuous drug release. Similarly, Lupon Depot ® is another PLGA microsphere-based system that was FDA-approved in 1989 for the treatment of prostate cancer, and is capable of delivering leuprolide acetate for 30 days. However, the properties of micro- and nanoparticles do not always behave consistently with monolithic implant degradation and release kinetics. First, particles have a much higher surface area to volume ratio, and thus the rate of water permeation is increased. For surface eroding polymers such as poly(anyhydrides) and poly(ortho esters), this means a faster, but generally still linear, release rate occurs since there is a larger polymer:water interface for a given mass of material. For bulk degrading polymers such as PLGA, this means a burst effect is often seen as the material hydrates much more rapidly, and diffusive release is accelerated due to the smaller diffusion distance required to escape the material [101].

2.2.2. In situ forming implants

Compared to micro- or nanoparticle systems, *in situ* forming implants (ISIs) are simpler, with fewer and less costly fabrication steps, and 100% encapsulation efficiency [102, 103]. The principle underlying all ISIs is that a precursor solution or mixture can be injected at the treatment site, and this mixture can be induced or will passively adopt a solid form, resulting in a monolithic delivery system at the site of injection. Typical shortcomings of such systems include the

propensity for burst release during the solidication period, toxicity of any additives required for solidification (solvents, heat, or initiators), and heterogeneity of the ISI microstructure [102, 103].

2.2.3. Thermoplastics

Thermoplastics used as ISIs are polymers with a relatively low melting point, which enables them to be injected as a melt and solidify upon cooling to body temperature. Thermoplastics are an appealing choice for ISI because no solvents or chemical initiator is required to solidify. Initial attempts to develop a thermoplastic ISI focused on block copolymers of PEG and PLA and blends of L-PLA and PCL, however these materials exhibited melting or glass transition points around 60˚C, which can cause pain, tissue necrosis, and scar tissue formation [104]. Additionally, such systems exhibited slow release, with less than 50% drug released by 30 or 60 days, depending on the material. Blending PCL with methoxyPEG was able to reduce the melting temperature [105]. Poly(ortho esters) have also been investigated as thermoplastic ISIs, because low-molecular weight POEs can be created with low viscosity at ambient temperatures [106]. POE ISIs have been copolymerized with PLA or PGA to accelerate degradation and allow autocatalysis of hydrolysis [107]. Thermoplastics have been most thoroughly investigated for drug delivery into tumors because the local hyperthermia can be utilized as treatment, rather than a disadvantage.

2.2.4. Sol-gel transitioning materials

Sol-gels refer to materials that undergo a solution to gel phase transition due to a rise in temperature that shifts the hydrogen bonding equilibrium from water-polymer to polymer-polymer [108]. The temperature at which this transition occurs is referred to as the lower critical solution temperature (LCST), and this kinetics with which this phenomenon occurs can affect the initial drug burst [109]. Poly(*N*-isopropyl acrylamide) (PNIPAAM) is one of the most studied sol-gels due to its rapid phase transition and its natural LCST of 32˚C, which can be adjusted to 37˚C through additives [110-112]. Unfortunately, cell toxicity and platelet activation hinder PNIPAAM

as a potential implantable material, and it must be copolymerized to become biodegradable [113, 114]. Copolymerizing PNIPAAM with known biodegradable species can allow hydrolytic degradation into oligomers small enough to be cleared [115, 116]. Poly(ethylene oxide) (PEO) and poly(propylene oxide) (PPO) have been investigated in the form PEO-PPO-PEO triblock copolymers, called Poloxamers, which undergo the sol-gel transition at a temperature dependent upon the polymer concentration [117]. Most popular in this family of copolymers is Poloxamer 407 (Pluronic® F127), which has been well-tolerated after implantation in animals [118, 119]. However, Pluronic® F127 tends to disintegrate rapidly, limiting release to hours or days, and the gel transition temperature and rate is susceptible to additives, including drugs [120, 121]. PCL-PEG copolymers and PEG-PLGA-PEG triblock copolymers have been investigated because the gelling temperature is easily controlled by varying PEG content, and have garnered interest due to their low observed toxicity [122-124].

2.2.5. Cross-linking systems

In situ cross-linking systems differ from the previous *in situ* forming materials because an additional stimulus is required to promote solidification. The stimulus can be heat, light, an ionic species, or a reactive chemical [102]. Thermosets, which require heat as well as a chemical initiator, are cured irreversibly as the cross-linking reaction proceeds. These systems have many safety considerations before they can be considered, including heat generated, free radical production, and toxicity of the monomers present in the prepolymer [103]. As such, relatively little academic research is available on thermosets as biodegradable ISIs for drug delivery applications, though several patents have explored the concept [125-127]. Photocrosslinked polymers are advantageous because they can be rapidly polymerized via fiber optic cables inserted during the injection, or by a penetrating light source, without excess heat needed. Similar, non-degradable photocrosslinked materials have historically been used in dentistry for

many years [128]. An ISI created by cross-linking a PEG-containing, acrylate-terminated polymer with the photonitiator 2,2-dimethoxy-2-phenylacetophenone (DMPA), resulted in hydrogels with significant tensile strength that released the (now discontinued) antibiotic sulfamethoxazole over 3 days [129]. PLA modified to allow cross-linking has been researched as an orthopedic material, and PEG-based cross-linked hydrogels have been developed for protein release [130, 131]. Photocrosslinked polymers can be difficult to fully polymerize, because irregular geometry and the presence of tissue limits light penetration, and just as in thermally cross-linked polymers, the generation of free radicals can have toxic side effects. Furthermore, short-wavelength UV irradiation rapidly damages tissues and is a known carcinogen, though even long-wave UV sources are potentially carcinogenic [132]. Chemically cross-linked polymers begin polymerizing immediately after addition a cross-linking reagent to the prepolymer, and as such are unique among these *in situ* forming systems because they have a setting time that begins prior to injection. Thiol-containing, PEG-based polymers were cross-linked into hydrogels within 3 minutes using a divinylsulfone-based cross-linking reagent, and these hydrogels were capable of releasing a model protein, bovine serum albumin, for 20 days [133]. For chemically cross-linked ISIs, monomer and initiator toxicity are of concern because the process generally proceeds more slowly than thermal- or photocrosslinking, which can allow these species to leach out of the injectate. Physically cross-linked materials are unique in that instead of creating covalent cross-links via an initiator, the prepolymer forms strong physical associations that cause solidification. Although not a synthetic material, one of the best examples of these materials is alginate, which can utilize divalent cations (typically calcium) to form a physically cross-linked gel from a precursor solution. Generally, physiological conditions do not have sufficient calcium concentrations to promote gelation, so calcium can be co-delivered in temperature-sensitive vesicles that release calcium at body temperature, resulting in gelation shortly after injection [134, 135]. However,

because the vesicles had poor shelf-stability, the formulation would gradually gel prematurely as calcium was slowly released even at low temperatures. An interesting application for injectable alginate systems is ocular drug delivery, because fluids in the eye possess sufficient calcium chloride concentrations to permit gelation. Such a system was able to release pilocarpine, a glaucoma treatment, over 24 hours [136]. Degradation of alginate can be unpredictable because these hydrogels are sensitive to ionic and pH fluctuations.

2.2.6. Solvent exchange

Phase inversion occurs when a hydrophobic polymer dissolved in a water-miscible solvent is introduced to an aqueous environment. This process is appealing for drug delivery systems because the formulation is quite simple, and a wide variety of polymers can be utilized. A drug is freely mixed into the dissolved polymer, and upon injection, the polymer immediately begins to precipitate, entrapping drug in the solid phase as solvent exchange occurs. However, drug release is characterized by an initial burst, especially for hydrophilic drugs, because drug can easily escape during solvent exchange prior to complete solidification. PLA and PLGA are the two most popular materials for phase inverting ISIs, and they are used in two FDA-approved delivery systems – Atridox® and Eligard®. Many factors can influence the microstructure and drug release kinetics of these ISIs: choice of polymer, polymer concentration and molecular weight, water miscibility of solvent, and the size and hydrophilicity of the drug [137-141]. Generally, highly water-miscible solvents such as N-methyl-2-pyrrolidone (NMP) are used because they allow rapid solidification, yet this also contributes to higher burst release and a hetereogeneous microstructure, as surface solidification occurs more rapidly [142]. Such systems exhibit elongated pores oriented radially towards the surface, as well as an outer, low-porosity “skin” layer [137, 143]. Solvents with low miscibility, such as benzyl benzoate or triacetin, cause lower burst and longer release periods as well as more spherical, uniformly-distributed pores [137, 143]. There is evidence that these

hydrophobic solvents may lead to the formation of an intermediate gel phase that gradually solidifies [144, 145]. However, these slow-forming systems can take days or weeks to solidify, and the semisolid implants with liquid cores can rupture if they are subjected to stresses. Increasing polymer concentration slows drug release by forming a thicker “skin” layer, which hampers drug diffusion as well as solvent exchange [142, 146]. Increasing polymer concentration will also increase the viscosity of the system and slow solidification. Hydrophilic, small-molecule drugs are the most challenging to control in these systems, because a large initial burst occurs during solvent exchange, while proteins or hydrophobic small molecule drugs are entrapped in the solid phase more efficiently and exhibit lower burst. ISIs formed by phase inversion comprise the focus of the subsequent chapters.

2.3. Clinical applications for *in situ* forming systems

ISIs can be utilized in two different ways: either the ISI can be injected with the objective of sustained, systemic delivery of drugs, or it can be injected into a target tissue to provide a local treatment with limited systemic availability. A specific focus will be made on solvent-exchange systems, as these are the foundation of this work, and several commercially available and preclinical forms are currently available. Because PLGA is present in many FDA-approved formulations, its clinical safety has been well-established, and the solvents used are considered nontoxic, with side effects limited to mild irritation [147]. By comparison, other *in situ* forming materials are still in their infancy, with many unknowns including material stability, *in vitro* vs *in vivo* behavior, and potential side effects. In particular, factors such as heat, free radicals, and potentially toxic polymer precursors or initiators are all components of other systems that require extensive research before they can be considered for clinical applications.

2.3.1. Systemic treatments

Systemic drug delivery can achieved from ISIs by injection into a tissue where the released drug can freely enter circulation. The subcutaneous route is most popular because it is easily accessed with a simple injection, and there is sufficient circulation and fluid flow to distribute the drug and clear the polymer as it degrades. ISIs for systemic drug delivery are advantageous because they can provide sustained delivery of a drug from a single injection (typically monthly), while a simple drug solution may require daily injections to maintain a therapeutic concentration [102]. Two technologies, both based on solvent exchange, are commercially available or in clinical trials. Eligard® is an FDA-approved treatment for advanced prostate cancer, which is composed of a PLGA solution in NMP that is mixed with leuprolide acetate prior to subcutaneous injection [148]. Previous treatments required daily subcutaneous injection of a leuprolide solution, while Eligard® is available in 1-month, 3-month, and 6-month formulations, with longer-lasting formulations containing PLGA at higher concentrations and with larger lactide:glycolide ratios. For patients with advanced prostate cancer, these infrequent treatments are an effective palliative treatment requiring minimal hospitalization time. Another systemic treatment utilizing solvent removal from PLGA ISIs is Relday™, which recently completed phase I clinical trials. Relday™ delivers risperidone from a subcutaneous or intramuscular implant in a once-monthly injection for the treatment of schizophrenia and bipolar disorder.

2.3.2. Targeted therapies

Closer attention will be paid to targeted injections to treat specific tissues with local dosages, as ISIs offer potential advantages over existing technologies. Because they solidify upon injection, ISIs can be retained within the target tissue, while drug solutions or microparticle suspensions can potentially be cleared from the injection site due to natural fluid flow. Limiting systemic dosages is a major goal for modern targeted drug delivery systems, because it enables

lower overall drug loading (reducing cost), and reduces or eliminates side effects. As an example, expensive and potent growth factors such as bone morphogenetic protein 2 (BMP-2) can have severe side effects such as heterotopic ossification and tumor formation when they reach tissues outside the treatment area [149, 150]. A solid delivery depot could greatly reduce both treatment costs and the chance of these serious adverse effects by efficiently delivering drug only to the target tissue. This concept, in the form of a solvent-exchange ISI, has been explored in numerous research articles as well as one commercial product designed for the treatment of periodontitis.

2.3.3. Periodontitis

Periodontitis is a term for inflammatory diseases oral tissue, specifically gingival tissue, alveolar bone, and ligamentous tissue all involved in tooth support [151]. In the United States alone, 48% of adults suffer from chronic periodontitis, and it is estimated that 90% of the world's population is affected [151, 152]. Beyond its effects on oral health, periodontitis has also been implicated in development of systemic conditions such as cardiovascular disease, stroke, and diabetes [153, 154]. An initial buildup of bacteria that is not addressed properly by oral hygiene will eventually form larger colonies in gingival pockets residing below the gingival sulcus. These pockets, if left untreated, become periodontal pockets, in which the fibrous attachment of gingival tissue to the tooth is destroyed and destruction of alveolar bone occurs [151]. Bacteria adhering to the tooth surface can form a biofilm, called dental plaque, which begins as a sticky layer that hardens within 48 hours [155]. Once the plaque has hardened, it requires professional cleaning to reliably remove, and can act as a barrier that limits drug penetration to the underlying bacteria. The combination of a periodontal pocket and plaque barrier protect the bacteria and allow the infection to flourish, and the surrounding tissues exhibit inflammation and resorption due to the spreading bacterial front. Ultimately, as the fibrous tissue and alveolar bone is

destroyed, tooth loosening and loss will occur, and severe infections can spread beyond the oral cavity if they reach the bloodstream [151].

Treatment of periodontitis begins with a proper oral hygiene, which can halt the disease at its early stages [156]. Advanced periodontitis requires a deep, professional cleaning, termed scaling and root planing. Scaling is the removal of tartar (hardened plaque) from the tooth surface, and root planing is the process of smoothing the tooth root and removing infected tissue [157]. Together, these techniques are effective at combatting periodontitis, though infections can still persist and the missing tissue often fails to regenerate. Antibiotics are therefore frequently used as an adjuvant therapy in the treatment of advanced periodontitis where persistent infection can occur [158, 159]. Tetracyclines such as doxycycline are the most popular antibiotic for this disease, because they effectively inhibit the growth of *A. actinomycetemcomitans*, one of the most common bacteria involved in aggressive periodontitis, and are also lethal to other bacterial species [160, 161]. Doxycycline also has anti-matrix metalloproteinase (MMP) activity, therefore slowing or preventing the resorption of connective tissue [161-163]. This secondary anti-MMP effect occurs even at subantimicrobial doses, and has been shown to improve outcomes when combined with scaling and root planing [164]. Further, there is evidence that doxycycline has anti-inflammatory and anti-bone resorptive properties [165-167]. Looking towards the future, an ideal treatment for periodontitis can be envisioned, in which local delivery of an antibiotic is coupled with restorative drugs (for example, an osteogenic agent to help regenerate lost alveolar bone). In cases where alveolar bone loss is extensive, tissue grafts as well as synthetic scaffolds have been employed to guide bone regeneration [168, 169]. Therefore, a single injection that provides drug delivery as well as scaffold potential can serve multiple purposes as a periodontitis treatment. Currently, a solvent removal-based ISI, Atridox®, is commercially available as a

sustained local doxycycline treatment that is injected directly into the periodontal pocket after scaling and root planing.

2.3.4. Osteonecrosis of the femoral head

Osteonecrosis of the femoral head is the death of bone tissue in the proximal femoral epiphysis, generally due to an interruption in blood supply. An estimate from the 1990s indicated that osteonecrosis of the femoral head affects over 10,000 new patients each year in the United States, and is also responsible for more than 10% of all hip arthroplasties annually [170]. A more recent study in Korea found that the incidence of confirmed diagnoses nearly doubled between 2002 and 2006, with prevalence rising from 20 per 100,000 to 38 per 100,000 [171]. There are many identified risk factors, including chronic steroid use, alcohol use, trauma, and smoking, and up to 10-25% of cases are idiopathic [172]. Most of the blood supply to the femoral head comes from the large branch of the medial femoral circumflex artery and smaller branches of the lateral femoral circumflex artery. The superior and inferior gluteal arteries and the ligamentum teres also contribute to the epiphyseal vasculature [173]. Though the exact mechanism causing progression of osteonecrosis is unclear, it is believed that infarction in some of these blood sources can lead to cell necrosis as well as pathological apoptosis of osteoblasts and osteocytes [174]. As a result, the balance between osteoclast and osteoblast activity is disrupted, resulting in proportionally more resorption. Because the femoral head is weight-bearing, microfractures due to osteonecrosis can easily propagate and lead to structural collapse. Osteonecrosis in the femoral head begins asymptomatically, then appears as a small, crescent-shaped region of radiolucency adjacent to the weight-bearing region at the articular surface. This region progresses to a flattened or otherwise deformed femoral head as the bone collapses, and this process is associated with pain and stiffness in the joint [170, 175-177]. If osteonecrosis is diagnosed in the

early stages, before collapse has occurred, there are surgical options that have had varying degrees of success.

The most common treatment for osteonecrosis of the femoral head is core decompression, which has a success rate inversely proportional to the amount of necrosis, with "success" determined as halting or reversing the progression of the disease [178]. However, patients with successful intervention are still subject to recurrence, as well as elevated rates of osteoarthritis and eventual arthroplasty later in life [179, 180]. A major issue with the treatment options for osteonecrosis is that a diagnosis is frequently not made until the condition has already progressed to a stage where collapse is inevitable. Core decompression is thought work by alleviating high pressure and promoting a bone healing response to the removed tissue, but it does not rescue mechanically compromised bone. Recent research has focused on pharmaceutical intervention using targeted delivery systems to treat osteonecrosis. Patients receiving systemic bisphosphonate treatments to inhibit resorption had better outcomes if their disease was still in the early stages, although follow-up studies have had mixed results regarding incidence of arthroplasties within two years following treatments [181-184]. Contemporary research has utilized a targeted injection of bisphosphonate solution to prevent systemic exposure, as well as the addition of BMP-2 to the injection to promote osteogenesis, with promising results.[185, 186] However, there were issues with heterotropic ossification, indicating that the injection was not fully retained within the femoral head [186]. Recently, an injectable system for co-delivery of clodronate and simvastatin was also developed for the treatment of pediatric idiopathic osteonecrosis [90]. Clodronate is a bisphosphonate whose mechanism of action causes apoptosis of osteoclasts, while simvastatin has recently been extensively studied for its upregulation of BMP-2 to promote bone regeneration [187-190]. ISIs have not been investigated for treatment of these diseases, and they traditionally have low porosity and poor

mechanical properties. However, the femoral head is an interesting target tissue for ISIs because it is a naturally constrained geometry, and the network of trabecular bone would require a liquid injection for interpenetration of a scaffold. However, ISIs would require modification of the microarchitectural and material properties in order to be considered as drug delivery scaffolds for these intraosseous applications.

2.4. Significance and Objectives

The PLGA ISIs are approved for clinical use in their simplest form, with a single drug freely mixed into the PLGA phase, and most research has focused on modulating release kinetics by varying PLGA and solvent concentration or chemistry. However, incorporating micro- and nanoparticle additives into the PLGA matrix may be able to influence drug release and mechanical properties without modifying the polymer or solvent. Micro- and nanoparticle additives have been incorporated into pre-formed implants to produce composite scaffolds with a wide range of physical and chemical properties, and this approach allows a material as simple as PLGA to be used as a drug delivery scaffold for soft tissue or orthopedic applications. It is important to note that ISIs are currently considered simply as injectable drug depots, rather than functional scaffolds that can aid in tissue regeneration, because there is very little control over the microstructure or mechanical properties as they solidify. Conceivably, composite ISIs can be considered as drug-delivering scaffolds instead of simply as injectable drug depots. The objective of this research is to develop a modular platform that is easily adapted to different drugs and tissues by varying particulate additives. This research is divided into three separate aims, of which the first two focus on development of a composite PLGA ISI for orthopedic applications, and the last of which seeks to improve the properties of PLGA ISIs used in dental applications.

2.5. Specific Aims

Aim 1: To characterize the drug release and microarchitectural properties of novel orthopedic ISI. These composite PBAE-PLGA-HA ISIs were created by admixing drug-loaded PBAE hydrogel microparticles and HA microparticles into a PLGA solution prior to injection. The potential of PBAE and HA microparticles to modulate release of simvastatin and clodronate was investigated.

Aim 2: To demonstrate the feasibility of the orthopedic ISI from Aim 1 as a mechanically supportive scaffold. The HA content and particle size were varied with the objective of creating a material that is mechanically similar to trabecular bone. Injectability was quantified to ensure that the injectable mixture could be handled in a clinical setting, and as a proof of concept, the mixture was injected *ex vivo* into intact porcine femoral heads.

Aim 3: To develop a composite PBAE-PLGA ISI that is suitable for soft tissue applications such as periodontal drug delivery in gingival tissue. PBAE content was increased compared to Aims 1 and 2, HA not used, and two different molecular weights of PLGA were considered. Co-delivery of doxycycline and simvastatin was investigated. The development of porosity and the preservation of microstructure and mechanical resilience throughout degradation was investigated, and the goal of these experiments was to demonstrate the potential for these ISIs as tissue engineering scaffolds for future studies.

Chapter 3 Improved small molecule drug release from in situ forming poly(lactic-co-glycolic acid) scaffolds incorporating poly(β-amino ester) and hydroxyapatite microparticles

This chapter reproduced from a published manuscript, "Fisher, P.D., P. Palomino, T.A. Milbrandt, J.Z. Hilt, and D.A. Puleo, Improved small molecule drug release from in situ forming poly(lactic-co-glycolic acid) scaffolds incorporating poly(beta-amino ester) and hydroxyapatite microparticles. Journal of Biomaterials Science. Polymer Edition, 2014. 25(11): p. 1174-93."

3.1. Introduction

Controlled drug delivery systems offer a variety of potential advantages over traditional routes of administration, such as oral dosages and intravenous or subcutaneous injection of drug solutions, due to their spatial and temporal control over drug release [191]. Traditional dosage forms result in systemic circulation of drug, and the oral route is also subject to first-pass metabolism [192]. Injections introduce a bolus of drug at high concentrations, and long-term treatment requires repeated dosing, resulting in pulsatile concentration profiles [193]. Implantable drug-loaded scaffolds can be placed at the treatment site to minimize systemic exposure and can be designed to control release kinetics by varying the chemical and physical nature of the carrier [193, 194]. These systems, however, generally require a surgical procedure to implant the device, and in the case of a non-degrading material, require a removal surgery. As a result, significant effort in the drug delivery field has focused on injectable, biodegradable drug carriers, such as *in situ* gelling, polymerizing, or precipitating systems [195, 196]. A space-filling scaffold capable of forming into a biodegradable solid at the treatment site is an appealing option because it can penetrate a tissue network to deliver drugs at a fixed location with minimal invasiveness and no removal surgery.

Poly(lactic-co-glycolic acid) (PLGA) is an attractive material for an *in situ* forming delivery system because it is already present in FDA-approved injectable products (Atridox® and Atrigel® systems), it degrades hydrolytically, and its physical properties can be controlled by varying the lactide:glycolide ratio, molecular weight, and end species [197]. PLGA is dissolved in a water-

miscible solvent and mixed with a pharmaceutical agent prior to injection to form a drug suspension or solution. The resulting mixture is injected into the treatment site, where it precipitates into a solid and gradually releases the drug [198]. These systems have been investigated for protein release [146, 199] as well as small molecule drugs [200], and have demonstrated biocompatibility [147].

Typically, injectable PLGA systems have a large initial burst release followed by sustained release over a period of hours to weeks [195]. The magnitude of this burst release as well as precipitation rate are both governed by the rate of solvent exchange [137, 139]. Therefore, systems with lower initial burst tend to undergo slower solidification due to gradual solvent exchange, while rapid precipitation corresponds to rapid solvent exchange and correspondingly large burst. Release kinetics following the burst are primarily diffusive until degradation of the polymer matrix becomes a contributing factor [139]. The burst can be reduced by increasing polymer content of the solution, increasing polymer molecular weight, or changing to a less water-miscible solvent [138, 195, 201]. However, increasing polymer content increases the viscosity of the solution, slows precipitation, and leads to the formation of a low-porosity “skin” around the scaffold [139, 202]. Increasing polymer molecular weight and/or hydrophobicity increases degradation time [138], and choosing a less water-miscible solvent dramatically slows precipitation [137, 201].

Incorporating drug-loaded microparticles into an injectable PLGA system may provide a secondary means of controlling release kinetics. This concept has been previously investigated by mixing PLGA microspheres containing plasmid DNA into the PLGA solution prior to injection [203]. PLGA microspheres will dissolve in the organic solvents used in the system, however, which confers a time constraint on the mixing process and may be unsuitable for small molecule drugs that can easily escape from partially dissolved microspheres. By instead utilizing crosslinked

microparticles that will not dissolve in NMP but are still hydrolytically degradable, the utility of the *in situ* forming PLGA system may be greatly expanded. Poly(β-amino ester) (PBAE) hydrogels are formed via step growth polymerization of a diacrylate and an amine followed by free radical crosslinking, and degradation time can be modified by changing the monomers to influence crosslink density and hydrophilicity [69]. Recently, PBAE microparticle and nanoparticle systems have been investigated for their drug delivery potential [75, 204, 205]. Incorporation of drug-loaded PBAE microparticles into an injectable PLGA system has the potential advantage of controlling and prolonging drug delivery while reducing initial burst.

Intraosseous injection in particular is a suitable application for an *in situ* forming system due to the interconnected porous network of the trabecular bone that makes placement of pre-formed scaffolds difficult and removal surgery impossible. Injectable PLGA systems can theoretically accommodate filler particles such as hydroxyapatite (HA) to influence microarchitecture, mechanical properties, or osteoconductivity. N-methyl-2-pyrrolidone (NMP), currently used in the FDA-approved Atrigel and Atridox delivery systems, is highly water-miscible and provides rapid solidification. Additionally, NMP has been shown to promote bone morphogenetic protein 2 (BMP-2) dependent alkaline phosphatase activity as well as reduce osteoclast activity [206, 207]. Bisphosphonates, such as clodronate, are used to prevent bone resorption via osteoclast apoptosis or inactivation [189]. Simvastatin is a drug that is primarily used for its inhibition of 3-hydroxy-3-methylglutaryl coenzyme A to treat high cholesterol, but it has recently been investigated for osteogenic applications due to numerous studies reporting that simvastatin promotes bone formation via BMP-2 upregulation [190, 208].

Clodronate and simvastatin are both small molecule drugs, and therefore they are prone to rapid release and high burst in a traditional *in situ* forming PLGA system. It was hypothesized that an *in situ* forming PLGA system containing drug-loaded PBAE microparticles and HA filler

would provide superior simvastatin and clodronate release kinetics compared to existing systems using freely mixed drugs.

3.2. Materials and Methods

3.2.1. Materials

Poly(lactic-co-glycolic acid) (PLGA; 50:50 L:G, acid terminated, inherent viscosity 0.55-0.75 dL/g) was purchased from DURECT, Inc. (Birmingham, AL, USA). Simvastatin was purchased from Haorui Pharma-Chem (Edison, NJ, USA). Clodronate, hydroxyapatite, 2,2-dimethoxy-2-phenylacetophenone (DMPA), and N-methyl-2-pyrrolidone (NMP) were obtained from Sigma-Aldrich (St. Louis, MO, USA).

3.2.2. PBAE polymer synthesis

PBAE macromer was synthesized by reacting diethylene glycol diacrylate and isobutylamine at a 1.2:1 diacrylate:amine molar ratio at 85^{o}C for 16 hours. Macromer was stored in an opaque vial under refrigeration until use. To create crosslinked hydrogels from macromer, 1 wt/wt% DMPA initiator dissolved in 50 wt/wt% ethanol was vortexed with macromer. The mixture was then pipetted between two glass plates with Teflon spacers, sealed and clamped, and then exposed to a UV flood source with an intensity of 12 mW/cm^2 for 5 minutes to form a crosslinked hydrogel slab. These PBAE hydrogel slabs were washed overnight in ethanol to remove unreacted monomer and initiator, and then stored in a desiccator to remain dry until use.

3.2.3. PBAE particle formation and drug loading

PBAE microparticles were formed by grinding dry PBAE slabs with a mortar and pestle, with HA added during the grinding process to coat particles and prevent aggregation. HA content was preliminarily tested at 66 w/w % and 75 w/w % weight ratios, and 75% (50 v/v %) was chosen due to ease of particle fabrication. PBAE particles were sieved to less than 250 μm, and larger

particles were re-ground until all material was collected through the sieve. A Zeiss Evo MA 10 scanning electron microscope (SEM) (Carl Zeiss, Thornwood, NY) at 4 kV accelerating voltage was used to visualize particle morphology, and a Quantax energy-dispersive x-ray spectroscopy (EDS) detector was used for elemental analysis. A series of 10 microscope images of HA and PBAE particles were analyzed using freely available ImageJ software to calculate mean particle size.

Simvastatin was either loaded into PBAE slabs prior to particle formation (pre-loaded) or loaded directly into PBAE microparticles (post-loaded), and each method was assessed for loading efficiency as well as the percentage of drug that was weakly bound to particle surface. Figure 3.1A graphically represents the processing method for creating PBAE microparticles, as well as the differences between pre- and post-loaded particles. Post-loaded particles were prepared by dissolving simvastatin in ethanol at a concentration of 100 mg/mL and pipetting drug solution over particles at a ratio of 2 μL per mg of particles. This ratio allowed particles to swell without excess solution remaining, and expected drug loads were calculated under the assumption that all drug solution was imbibed by the microparticles. Particles were lyophilized overnight, briefly re-ground and sieved to break up aggregates, and stored in a vacuum chamber with desiccant. Pre-loaded microparticles were prepared by immersing PBAE slabs in simvastatin solution, allowing the hydrogel to swell for 24 hours, and then removing the hydrogel and lyophilizing overnight to evaporate ethanol. Drug-loaded PBAE slabs were ground with 75 wt% HA into particles and stored in a vacuum chamber with desiccant. Predicted values for drug loading using the pre-loading method were obtained by calculating swelling of PBAE in solution based on mass increase and assuming drug was homogeneously present in swollen hydrogels as well as surrounding solution. The density and concentration of the drug solution was then used to calculate expected drug loading based on mass change of the PBAE samples. Clodronate was

loaded into separate batches of microparticles using an identical pre-loading technique with a 50 mg/mL clodronate solution in deionized water.

3.2.4. Measurement of drug loading into PBAE

Simvastatin loading into PBAE microparticles was measured by immersing drug-loaded particles in ethanol, vortexing, and allowing the particles to swell for 24 hours. The mixtures containing ethanol and swollen PBAE microparticles were then centrifuged, and supernatants were analyzed using HPLC to detect simvastatin as described in *2.7 Measurement of drug concentrations*. Clodronate loading was measured with an identical technique using 50% ethanol, and was detected by absorbance as described below. A mass balance indicated that all drug was successfully removed from the particles during 24 hours of immersion in ethanol for simvastatin or 50% ethanol solutions for clodronate, and subsequent immersions extracted no additional drug. Loading efficiency was defined as the ratio of the total mass of drug loaded into the particles to the initial mass of drug exposed to the particles.

In addition to loading efficiency, the percentage of drug present on the surface of particles was determined by washing drug-loaded particles with 5 mL ethanol over a filter to remove loosely surface-bound simvastatin or with 5 mL deionized water to remove loosely surface-bound clodronate. The remainder of drug present in the bulk of the microparticles was extracted by immersing particles for 24 hours in ethanol for simvastatin or 50% ethanol for clodronate. Drug detected in the initial wash was deemed loosely bound to the surface of particles, while drug detected after the 24 hour soak was determined to be imbibed into the bulk of the particles.

3.2.5. Formation of injectable scaffold system

PLGA was added to NMP and stirred overnight until fully dissolved to create a 20 wt/wt% PLGA solution. Simvastatin-loaded PBAE microparticles pre-loaded using 100 mg/mL simvastatin were added at 5 wt% and mixed homogeneously prior to injection. HA was also mixed

homogeneously prior to injection to bring the final mixture to 30 wt% HA. Clodronate-loaded PBAE microparticles pre-loaded with 50 mg/mL clodronate were added using an identical technique. Samples without microparticles were prepared by freely mixing 1 wt% simvastatin or clodronate into 20% PLGA solution to simulate a traditional *in situ* forming PLGA system. Figure 3.1B illustrates the differences between the proposed system and a traditional injectable system. Simvastatin and clodronate were measured as described in 3.*2.7. Measurement of drug concentrations*.

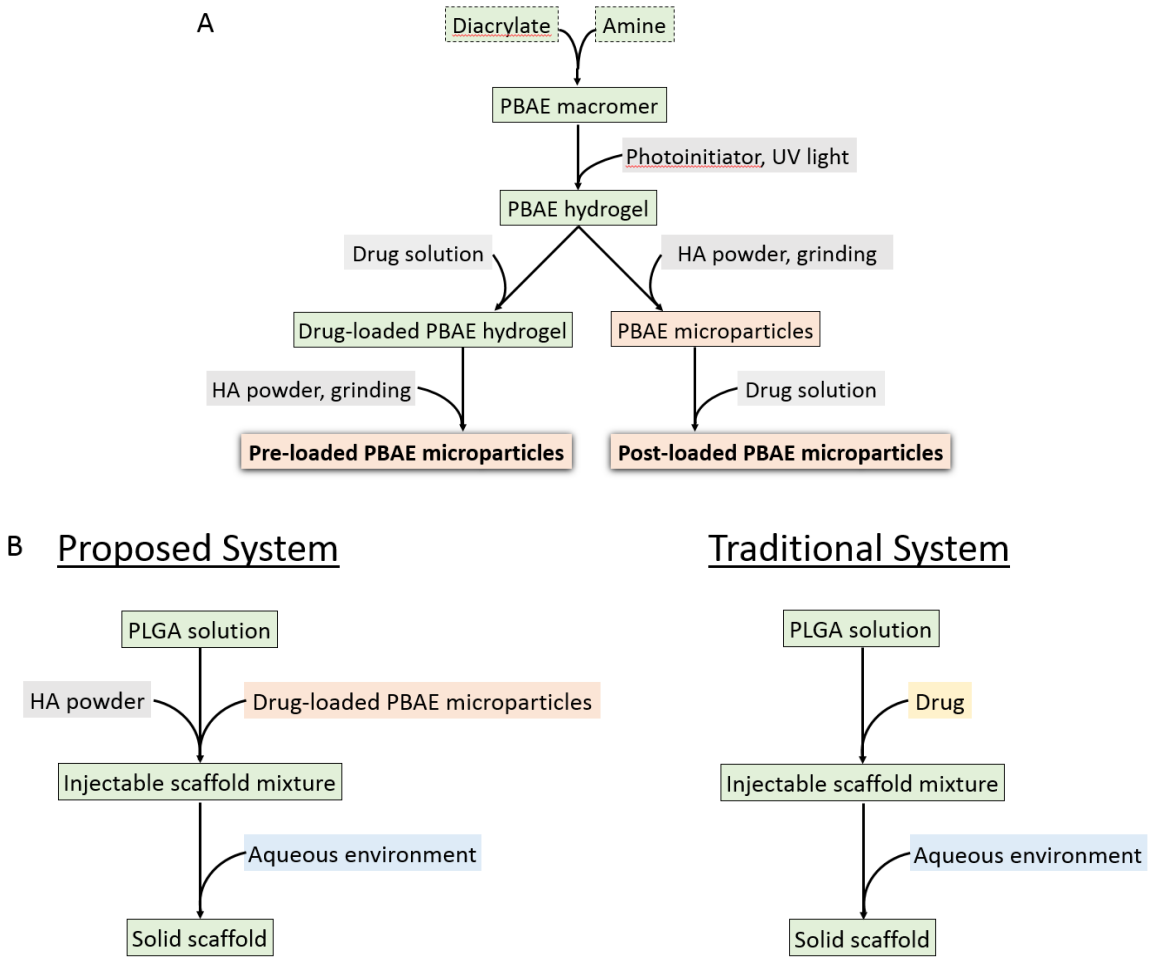

Figure 3.1. PBAE microparticle and injectable scaffold fabrication process. A) Technique for formation of PBAE hydrogels and processing them into drug-containing pre- or post-loaded

microparticles. B) Comparison of a traditional injectable PLGA system (right) to the proposed system (left).

3.2.6. In vitro drug release

The scaffold mixture was injected dropwise through a 16 gauge, blunt-tipped dispensing needle into PBS at 5% wt/vol. Upon contacting PBS, surface PLGA immediately began to precipitate, forming semi-spherical scaffolds approximately 3 mm in diameter that sank to the bottom of the vial. Samples were kept in an incubator at 37°C on a plate shaker for the duration of the study. Supernatant was collected and replaced at each time point, and these samples were preserved at 4^{o}C until analysis. Clodronate release was measured for three loading conditions: freely mixed clodronate without HA filler, freely mixed clodronate with HA filler, and clodronate pre-loaded into PBAE microparticles with HA filler. Because PBAE microparticles were fabricated with HA as a dispersing agent, drug release from loaded particles was not investigated without HA filler. Simvastatin release was measured for three loading conditions: freely mixed simvastatin without HA filler, freely mixed simvastatin with HA filler, and simvastatin pre-loaded into PBAE microparticles with HA filler.

3.2.7. Measurement of drug concentrations

Simvastatin was measured on a Hitachi Primaide HPLC system equipped with a C18 column using a mobile phase composed of 70% acetonitrile and 30% water with 0.1% trifluoroacetic acid at a flow rate of 1 mL/min, and peaks were observed at 240nm. Clodronate from collected supernatants were measured using a Powerwave HT (Biotek; Winooski, VT, USA). *In vitro* release supernatant was pipetted into a UV-grade 96-well plate (Greiner Bio-One, Frickenhausen, Germany), and baseline absorbance was measured at 240 nm. On its own, clodronate does not exhibit a distinct absorption peak, so concentration was measured by mixing

supernatant with a solution of 1.5 mM copper sulfate and 1.5 mM nitric acid at pH 2 to form a clodronate-copper complex that exhibits absorption at 240 nm [209]. A pilot experiment confirmed that HA did not significantly interfere with clodronate readings in the working range.

3.2.8. Characterization of release kinetics

Drug release from polymeric systems is often analyzed using an adaptation of the Higuchi model by Peppas et al., widely known as the power law, to characterize release kinetics [210]:

$$\frac{M_t}{M_\infty} = kt^n \tag{3.1}$$

Here, M_t is the mass of drug at time t, M is the total mass of drug in the system, $\frac{M_t}{M_\infty}$ represents fractional release of drug at time t, k is a constant encompassing scaffold and drug properties, and n is the release exponent used to characterize drug release. In the case of the spherical geometry (consistent with scaffolds formed via dropwise injection), $n = 0.43$ corresponds to pure Fickian diffusion, n =0.85 corresponds to pure case II (polymer relaxation-based) transport, and values in between are combinations of the two, termed anomalous transport [210]. Plots of $\log\frac{M_t}{M_\infty}$ versus $\log t$ were used to determine n for each drug. The power law is applicable when $\frac{M_t}{M_\infty} < 0.6$, so release data were truncated to below 60% cumulative release when calculating n.

3.2.9. Mass loss and degradation

The injectable scaffold system was prepared as described previously, using unloaded microparticles. Non-destructive degradation analysis was performed on hydrated scaffolds in order to observe the mass change of wet samples. Scaffolds were injected dropwise into PBS and incubated at 37°C on a shaker for 80 days. Initial injected mass was recorded for each scaffold. At intervals, scaffolds were removed from PBS, gently blotted dry, and weighed. Destructive analysis of dried samples was used to analyze scaffold dry mass change. Scaffolds were injected dropwise into PBS and incubated at 37ºC on a plate shaker until analysis. At each time point, scaffolds were

lyophilized for 24 hours, and dry weight was measured. Lyophilized scaffolds were also scanned using a Scanco MicroCT 40 (Scanco Medical, Switzerland) at 55 kV and 145 mA with 6 µm voxel size. The built in bone trabecular morphometry tool was used to create 3D reconstructions to visualize microarchitecture and quantify porosity and pore size at various time points during the degradation process.

3.2.10. Statistical analysis

All data are presented as mean ± standard deviation. Release data were analyzed in JMP 10 software, using one-way analysis of variance (ANOVA) to determine differences between release curves followed by Tukey-Kramer mean comparison tests as necessary. Comparisons between individual pairs of samples for loading efficiencies were performed using a student's two-tailed t-test. Differences were considered significant for $p < 0.05$.

3.3. Results

3.3.1. Drug loading into PBAE particles.

Drug loading into PBAE increased linearly with drug solution concentration for simvastatin (Figure 3.2A) and clodronate (Figure 3.2B and 3.2C). Clodronate became insoluble at 20 mg/mL in 50% ethanol, while the drug remained soluble through 100 mg/mL in DI water. At 100 mg/mL clodronate, however, it was observed that hydrogel would swell to a greater degree and fracture upon handling, leading to high variability between samples (Figure 3.2C), so 50 mg/mL clodronate in DI water was used for future experiments. Simvastatin was loaded into gels or particles using a 100 mg/mL solution in 100% ethanol.

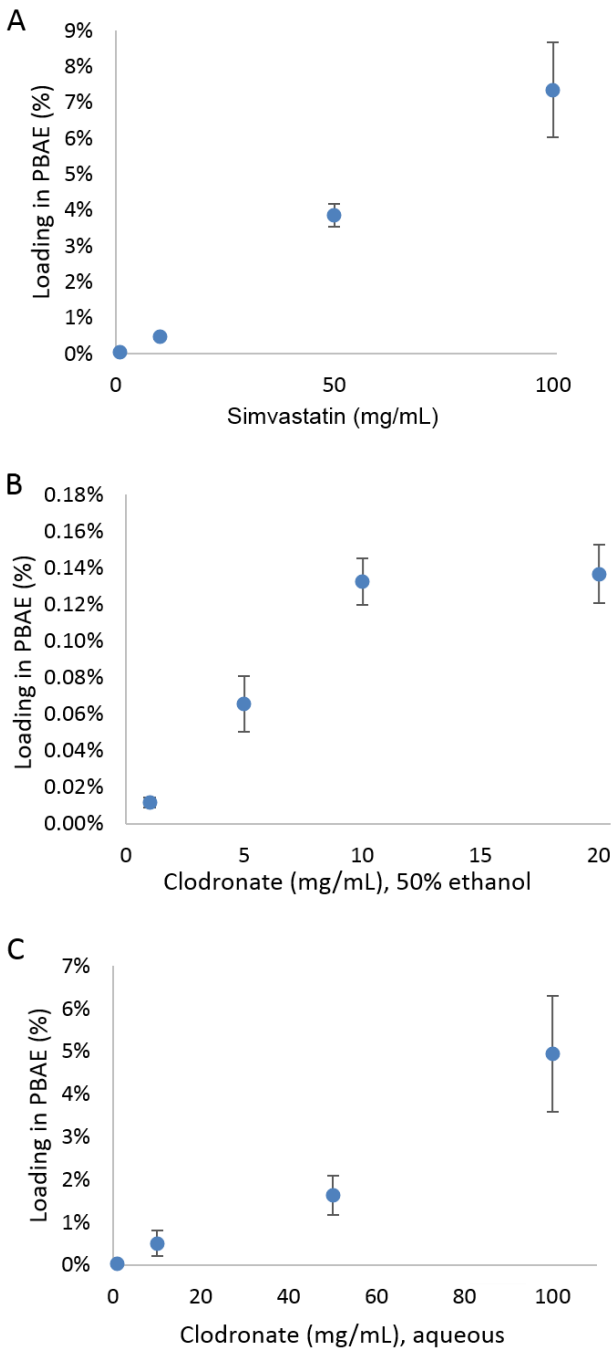

Figure 3.2. Drug loading into PBAE hydrogel. A) Simvastatin loading after soaking in 100% ethanol solutions for 24 hours. B) Loading after soaking in 50% ethanol clodronate solution for 24 hours. C) Loading after immersion in aqueous clodronate solution for 24 hours. Data are mean ± standard deviation (n=3).

HA possessed a mean particle diameter of 10 µm, while the PBAE particles produced by grinding PBAE hydrogels together with HA had a mean diameter of 68 µm. PBAE microparticles exhibited a composite structure consisting of spherical particles consistent with HA sizes embedded in an amorphous material consistent with the hydrogel nature of PBAE (Figure 3.3A). The spherical HA particles exhibited a rough, granular surface morphology, compared to the smooth PBAE component. EDS elemental mapping showed calcium and phosphorous localized to the spherical particles (Figure 3.3B). Point analysis of presumed HA and PBAE regions indicated higher calcium and phosphorous levels in spherical HA particles, and higher carbon and oxygen content in the PBAE region (Figure 3.3C). When these microparticles were immersed in a mixture of 20% PLGA solution in NMP with 30 wt% HA added to simulate pre-injection conditions, they underwent a 47% mass increase due to swelling (Figure 3.3D), with a 28% increase occurring within 5 minutes.

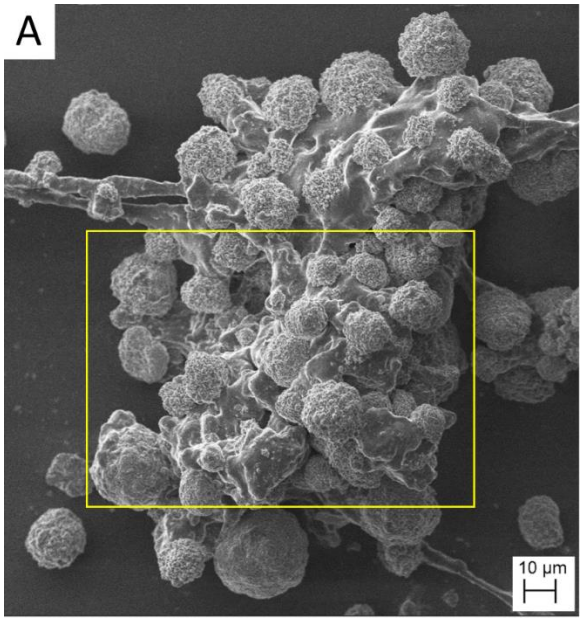
A
10 µm

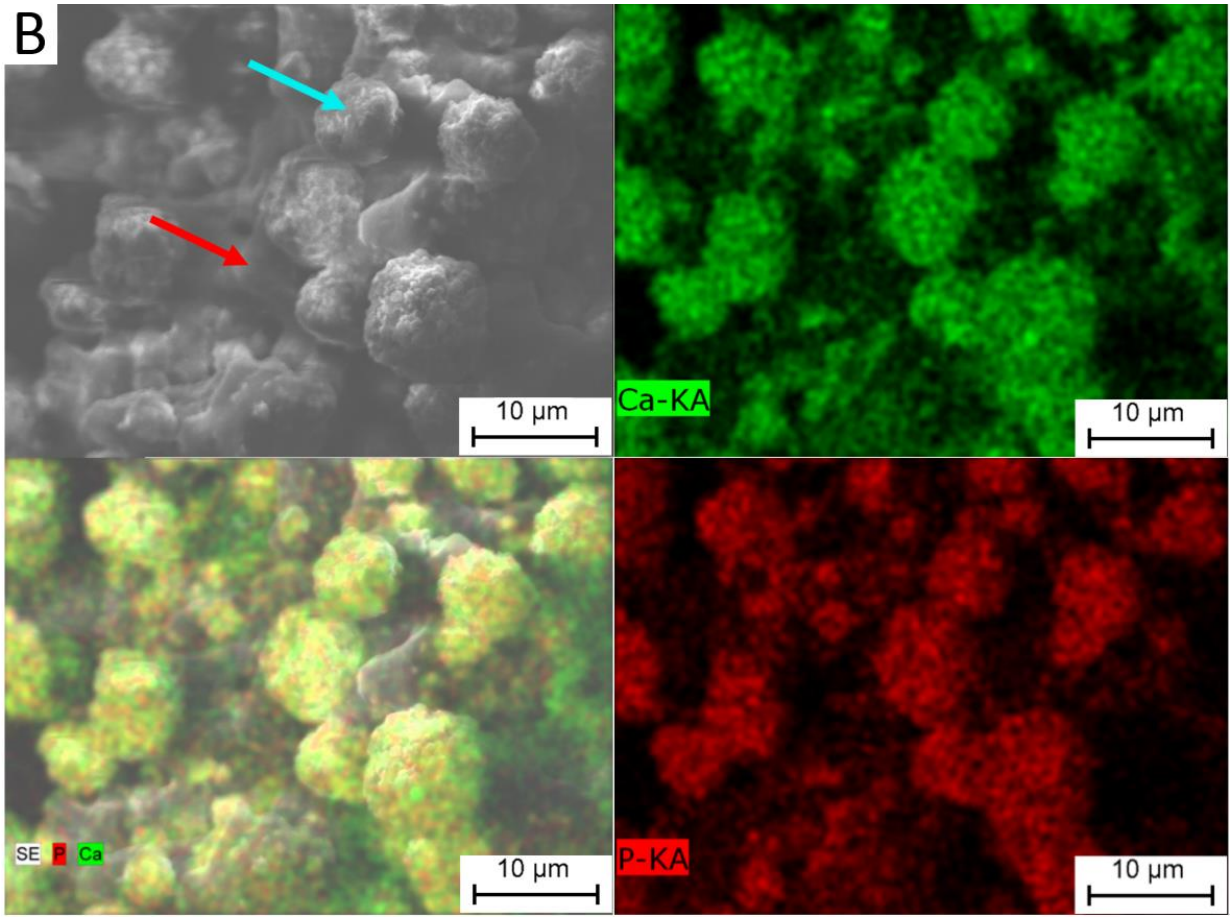
B
10 µm
Ca-KA
10 µm
SE P Ca
10 µm
P-KA
10 µm

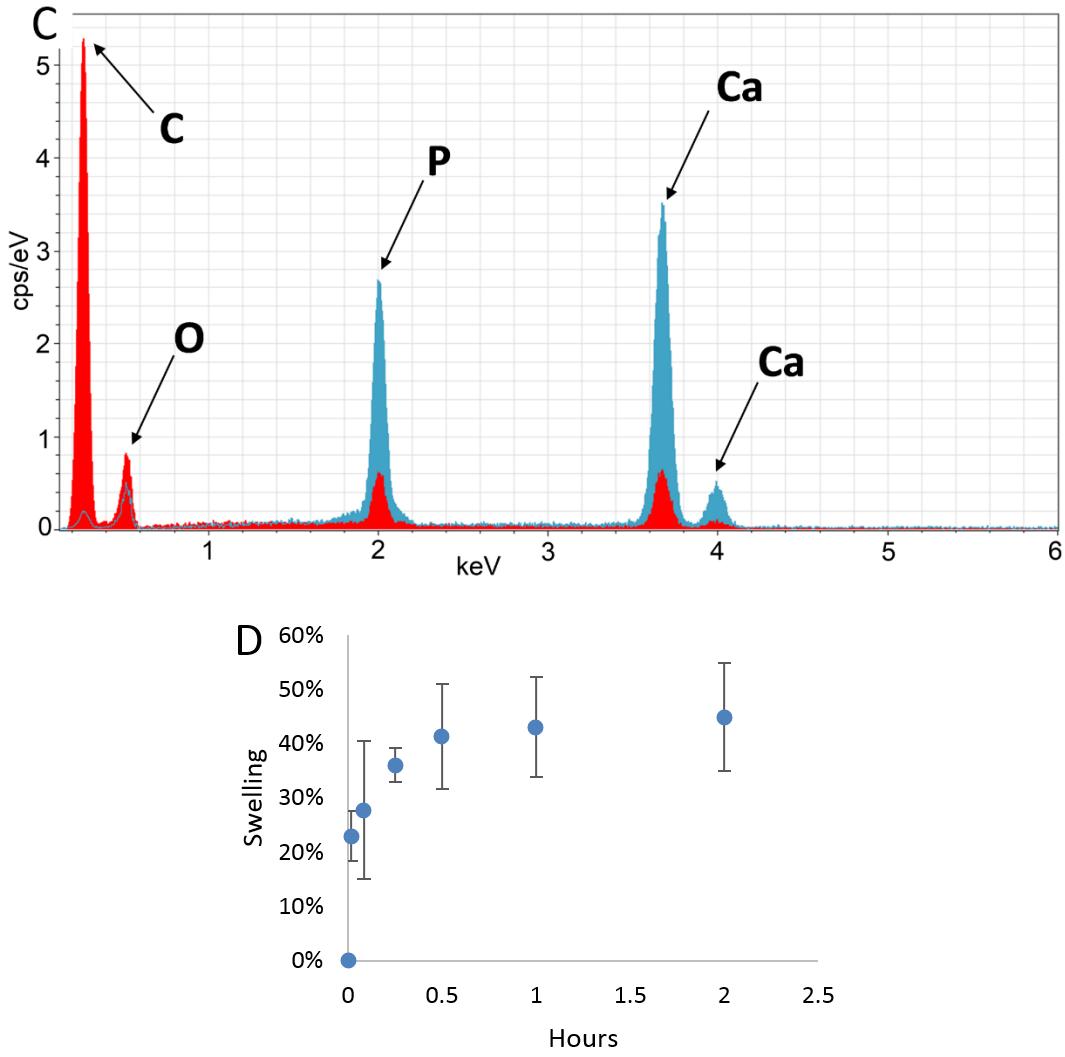

Figure 3.3. Morphology, composition, and swelling of PBAE microparticles. A) SEM image of a PBAE microparticle, with EDS performed on the highlighted portion. B) Top left: Region chosen from (A) for EDS analysis, with arrows indicating points of spectral analysis performed in (C). Bottom left: Composite overlay of calcium and phosphorous on that region. Top right: EDS detection of calcium. Bottom right: EDS detection of phosphorous. B). C) EDS spectra of an HA particle (blue) and PBAE (red). D) PBAE swelling kinetics expressed as a percentage of mass increase in injection mixture (30 wt% HA mixed into 20% PLGA solution). Data are mean ± standard deviation (n=3).

Efficiency of incorporating simvastatin into post-loaded particles ranged from 52% to 77% (Figure 3.4B), and efficiency ranged from 89% to 96% in pre-loaded particles (Figure 3.4D). A surface wash indicated that between 69% and 77% of simvastatin was loosely surface-bound to post-loaded particles, with no differences between simvastatin concentrations (Figure 3.4C). Using the pre-loading technique, a significantly lower amount ($p < .05$), between 46% and 51% of simvastatin, was loosely surface-bound, again with no concentration dependence (Figure 3.4A). Pre-loaded clodronate yielded particles with 74% to 86% of drug loosely surface-bound (Figure 3.4E). Clodronate loading efficiency ranged from 91% to 97% at concentrations up to 50 mg/mL, and dropped to 59% at 100 mg/mL (Figure 3.4F).

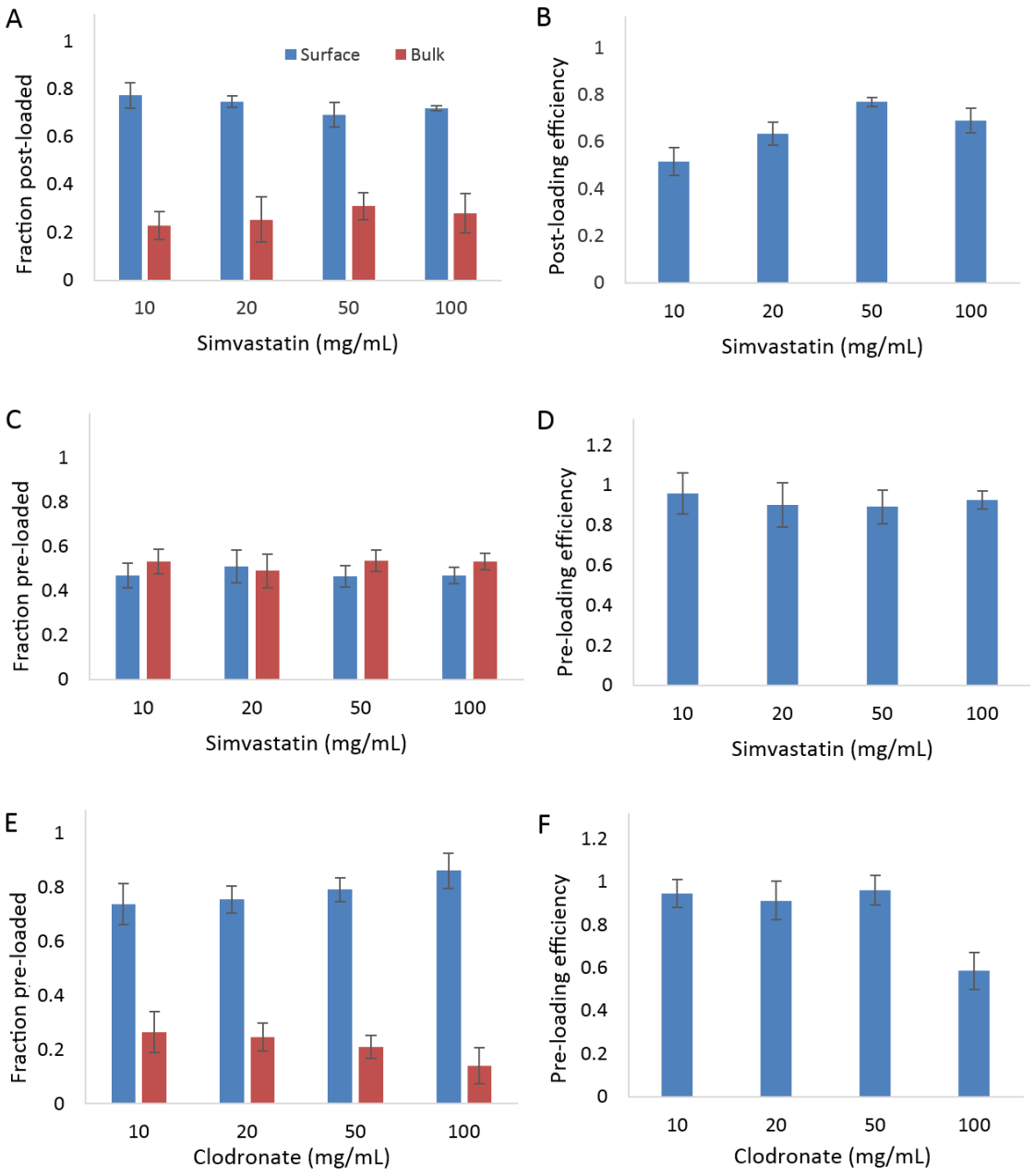

Figure 3.4. Surface vs. bulk loading in microparticles: A) simvastatin post-loaded, C) simvastatin pre-loaded, and E) clodronate pre-loaded. Loading efficiency: B) post-loaded simvastatin, D) pre-loaded simvastatin, and F) pre-loaded clodronate. Data are mean ± standard deviation (n=3).

3.3.2. In vitro release

Freely mixed simvastatin was 81% released within 1 day and 95% released within 10 days, with no difference between scaffolds prepared with or without HA (Figure 3.5A). In both cases, there was a gradual decrease in release rate as fractional release (M_t/M_∞) reached 100%. Pre-loaded simvastatin microparticles mixed into the system reduced the 1 day burst to 39% ($p<0.05$), followed by sustained release of 1.3%/day for 30 days. The sustained release from day 1 through day 30 was roughly linear, with no appreciable decrease in rate until completion of drug release.

Freely mixed clodronate prepared without HA exhibited a 49% burst within one day of release, while both freely mixed and pre-loaded clodronate prepared with HA produced 32% burst ($p<0.05$) (Figure 3.5B). Freely mixed clodronate without HA gradually released at a rate of 0.6%/day through day 19, while clodronate mixed with HA or pre-loaded into microparticles released at 1.3%/day through day 19. By day 20, there was no difference in total clodronate release between each curve. All clodronate release curves showed a distinct increase in release rate to 3%/day at day 20 that continued through day 31, after which nearly all drug was released.

To characterize release kinetics, plots of $\log\frac{M_t}{M_\infty}$ vs $\log t$ were used to calculate n for pre-loaded simvastatin and clodronate through the first day of release. After the first day, release rates tended to be linear and were therefore expressed as a daily release rate. For initial release during the burst, simvastatin and clodronate release exhibited $n = 0.47$ and $n = 0.49$, respectively.

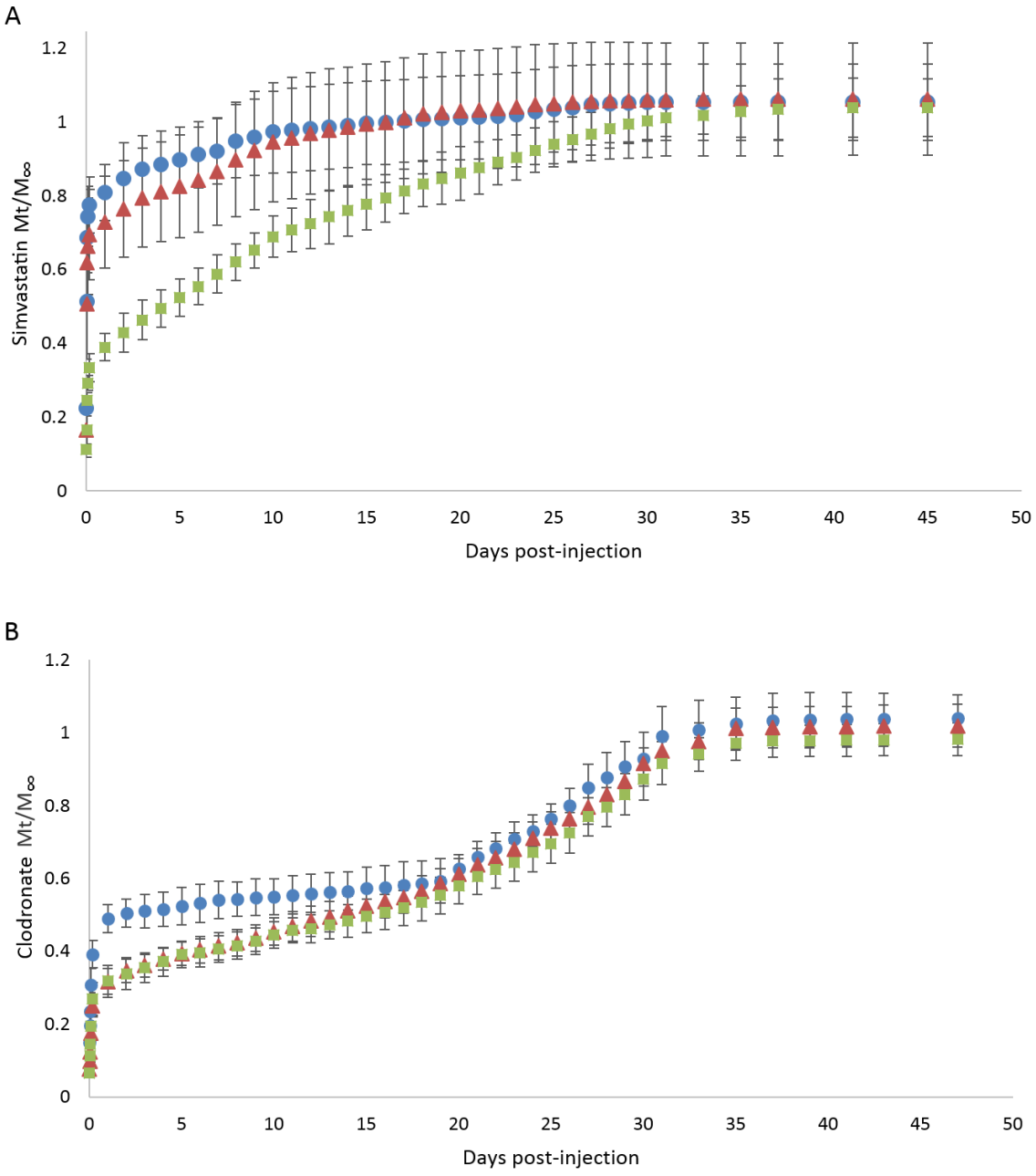

Figure 3.5. Cumulative release profiles. A) Release of simvastatin loaded freely into the PLGA solution with (Δ) or without HA (○), or loaded into PBAE (□) (n=3). B) Release of clodronate freely loaded into PLGA solution with (Δ) or without HA (○), or loaded into PBAE microparticles (□) (n=4). Data are mean ± standard deviation.

3.3.3. Mass loss and degradation

Lyophilized scaffolds exhibited an initial mass loss of 50% in the first hour, followed by an additional gradual decrease of 5% over the first day (Figure 3.6A). Mass fraction remained unchanged at approximately 45% for 15 days, followed by a linear decrease in mass at a rate of 0.2%/day until day 50. Mass fraction did not change significantly after day 50, ranging from 25% to 29% through day 80. Lyophilized samples collected at day 40 and beyond were primarily powder that crumbled upon handling.

Non-destructive mass change of wet scaffolds showed an initial 12% decrease in mass over the first day, followed by a linear increase of 1.4%/day over the next 14 days (Figure 3.6B). At day 15, mass fraction became more variable as some samples began to decrease in mass, while others swelled through day 30. Linear mass loss was observed from day 30 through day 55, when the remaining mass fraction stabilized at 20% until day 80.

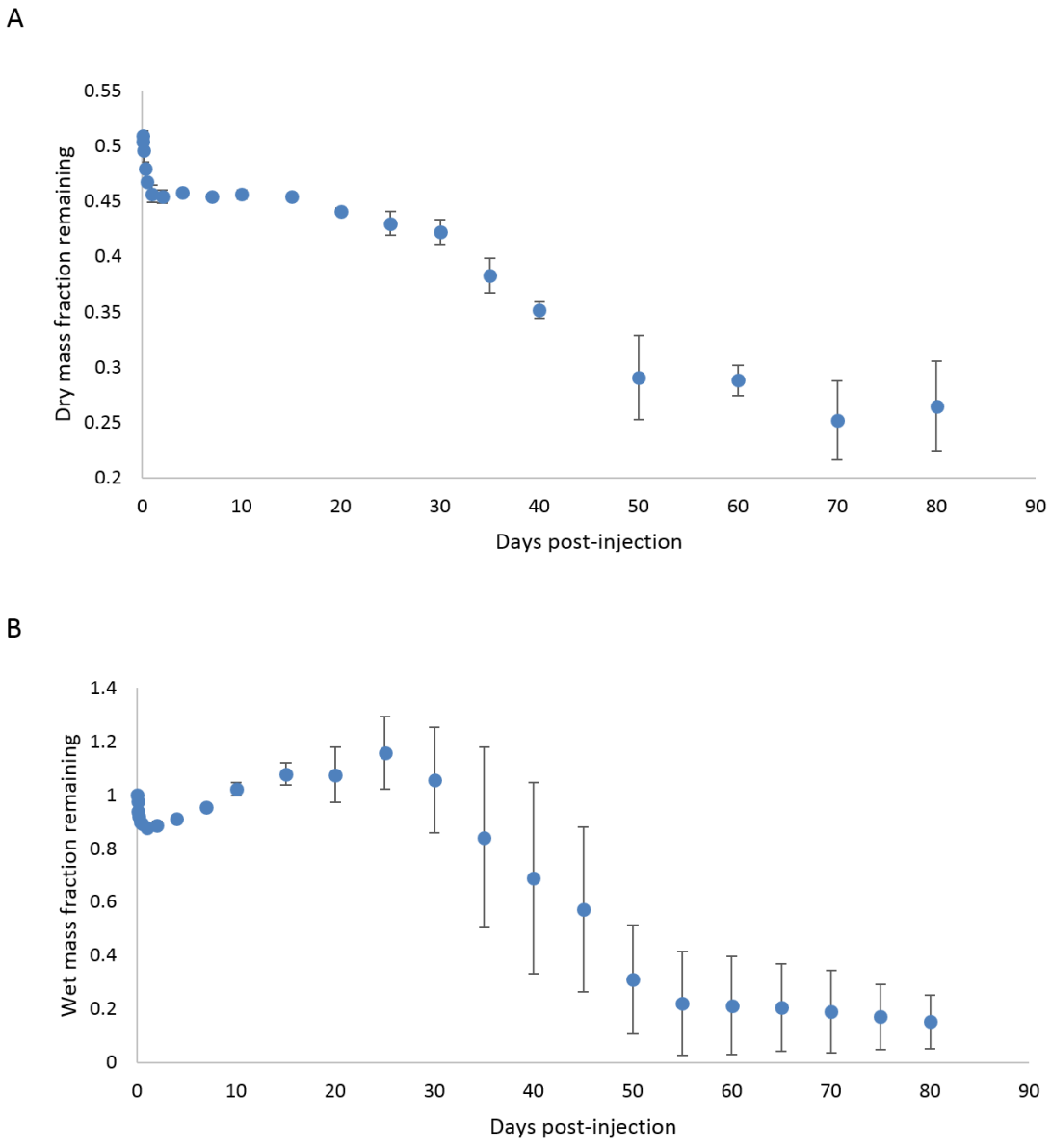

Figure 3.6. Degradation of *in situ* forming PLGA scaffolds. A) Destructive mass loss showing dry mass change expressed as a fraction of pre-injection mass (n=3). B) Non-destructive mass loss showing total hydrated scaffold mass change, expressed as a fraction of pre-injection volume (n=5). Data are mean ± standard deviation

Qualitative assessment of microCT cutplanes roughly bisecting samples revealed a uniformly porous microstructure through day 10 (Figure 3.7). By day 15, denser regions had

developed in the middle and at the edges of scaffolds. By day 20, large macropores were present in the core of the scaffolds. At day 25, scaffold cores appeared more uniformly porous, and the denser regions near the edges of scaffolds had become more porous. The dense regions appeared to migrate towards one side of the scaffold by day 30, and by day 35, scaffolds had significantly decreased in size, leaving behind a uniformly porous pellet. After day 35, scaffolds were too fragile to handle, and a representative sample of residual material collected at day 40 was nonporous. MicroCT morphometry revealed an increase in porosity from 31% through day 20 to 47% by day 30, followed by a return to 30% at day 35 (Figure 3.8A). Average pore size ranged from 40 to 100 µm, except for samples at day 25, which had average pore size of 231 µm (Figure 3.8B).

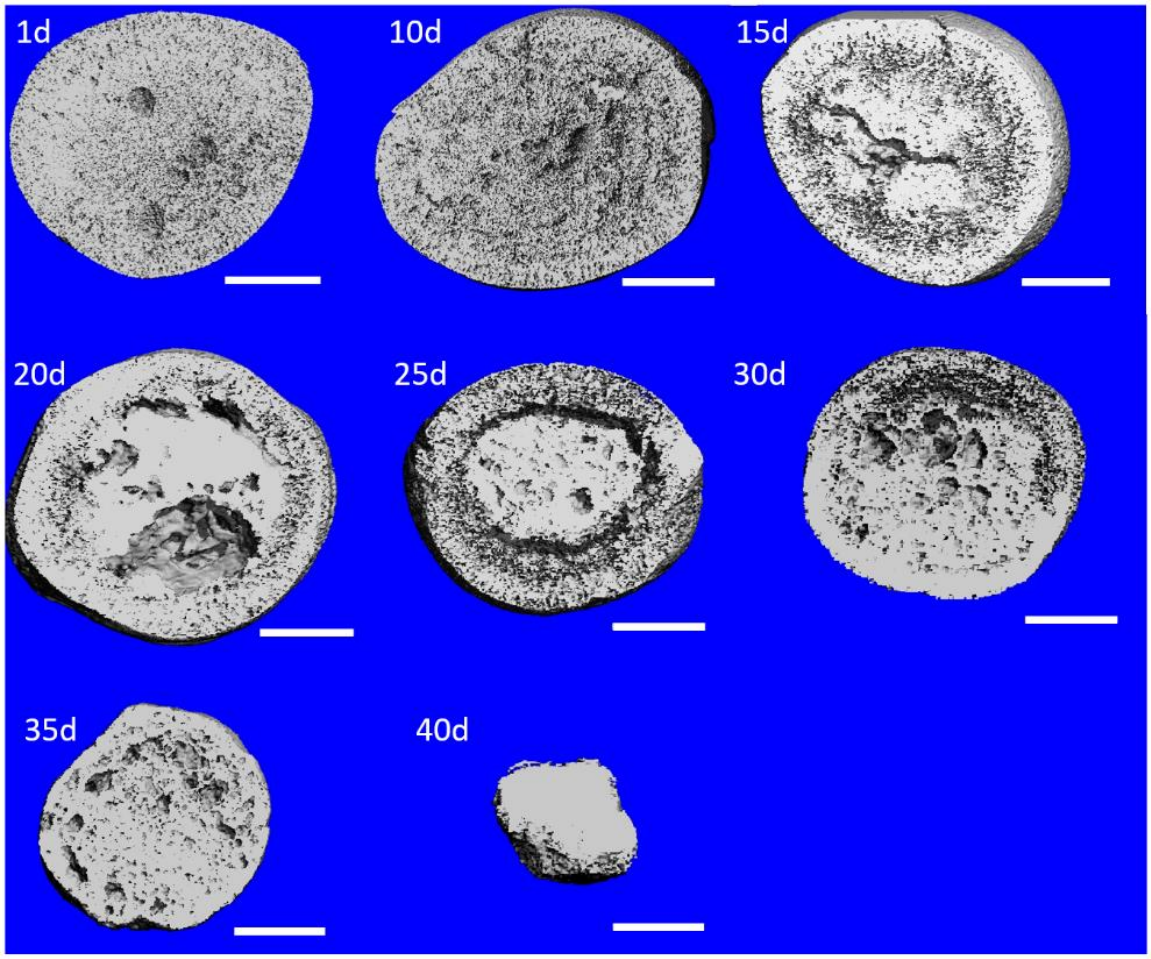

Figure 3.7. Representative microCT cut-plane images of lyophilized scaffolds showing internal microarchitecture throughout the degradation process. Scale bars are 1 mm.

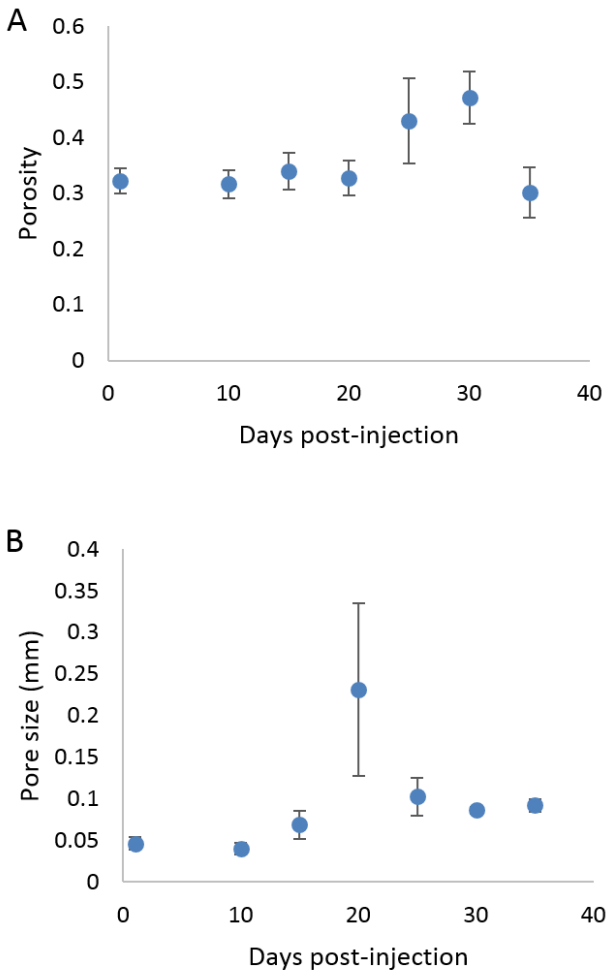

Figure 3.8. Morphometric parameters during degradation. A) Porosity and B) average pore size measured by microCT evaluation of samples through 35 days.

3.4. Discussion

3.4.1. Drug loading

PBAE microparticles were successfully formed by co-grinding PBAE hydrogels with HA, forming individual PBAE particles coated with multiple, smaller HA particles. Elemental analysis confirmed that the smaller, spherical coating consisted of HA, and the underlying particles were hydrogel. Simvastatin pre-loaded into PBAE hydrogels showed both higher loading efficiency and bulk imbibition of drug, which are favorable conditions to prolong drug release relative to freely

mixed drug. Swelling data were found to be an accurate predictor of drug loading into gels at various concentrations, consistent with previous drug loading results with hydrogels [211]. It was determined that processing of particles does not appreciably affect simvastatin loading efficiency using the pre-loading technique while still providing favorable imbibition ratios of surface to bulk drug. A decrease in loading efficiency as well as a higher percentage of simvastatin present loosely bound to the surface of particles using a post-loading technique may be attributable to the free HA powder used to coat the PBAE particles absorbing a percentage of drug solution, preventing its complete penetration into the hydrogel and resulting in a majority of drug sequestered outside the hydrogel microparticles. The high levels of surface drug seen for clodronate pre-loading may be due to the fact that the PBAE used in these experiments swells to a significantly larger degree in ethanol than in water (data not shown), allowing less penetration of drug into the bulk of the gels. Additionally, clodronate was more favorably loaded into PBAEs in aqueous solutions rather than 50% ethanol solutions because its solubility was limited. The swelling kinetics of PBAEs in the injection mixture (30 wt% HA in 20% PLGA solution) suggest that particles swell appreciably due to NMP exposure prior to injection, but the magnitude of swelling is negligible compared to the amount observed in pure NMP (47% at equilibrium vs. 470% in pure NMP). This difference is due to the presence of PLGA, which dissolves readily in NMP [146] and prevents hydrogels from fully swelling as they would in pure NMP. Additionally, the particles may be immersed in PLGA solution for only a matter of minutes before injection, so realistically, particles may swell by only 23% if the system is injected 5 minutes after addition of microparticles to the PLGA solution.

3.4.2. Simvastatin and clodronate release

Simvastatin release was strongly affected by its loading state. A comparison of release kinetics between injectable systems loaded with freely mixed simvastatin and simvastatin-loaded PBAE microparticles indicated that burst release can be significantly reduced and duration of

release can be significantly extended by loading simvastatin into PBAE microparticles. Because simvastatin is soluble in NMP, freely mixed drug presumably was dissolved in NMP and the majority of it exited into the aqueous phase during the solvent exchange process, resulting in a large burst release. The residual 20% of simvastatin was released in a sustained manner over the next 10 days, similar to previous work on such systems using freely mixed drug [212, 213]. PBAE microparticles experience some swelling in the NMP-PLGA solution during the mixing stage prior to injection, but burst is attenuated for pre-loaded PBAE microparticles. The 39% burst release through day 1 using pre-loaded particles may be attributable to loosely surface-bound simvastatin that was likely dissolved by NMP and released during solvent exchange, similarly to freely-mixed simvastatin. Because simvastatin was loaded into PBAE with high efficiency, the release kinetics are likely a combination of the swelling, degradation, and diffusion of drug through the PBAE material as well as the PLGA phase.

Clodronate release appeared to be unaffected by loading state of the drug in PBAE microparticles, but it was instead dependent on the presence of HA in the injection mixture. This can be attributed to the formation of a complex between the bisphosphonate drug and hydroxyapatite, specifically between the two phosphonate groups of clodronate and the divalent calcium cations present in HA crystals [214]. Freely mixed clodronate without HA filler was 49% released within 1 day, compared to 32% for both compositions with HA. Because clodronate is insoluble in NMP, this initial burst is likely due to free clodronate suspended in the PLGA solution being dissolved by water during solvent exchange. The increase in release rate observed around day 20 corresponded to the maximum swelling state of scaffolds, indicating that scaffolds had begun to appreciably degrade and more water could enter the system to promote more rapid clodronate dissolution. Samples prepared with HA had a lower burst and higher release rate between days 1 and 20 due to the clodronate being initially retained in the system by

complexation, after which the drug was released diffusively from the solidified system. Clodronate release kinetics are consistent with the classic 3-stage release profiles observed in rapidly-precipitating systems, in which an initial burst is followed by slow diffusion, and then a more rapid swelling- or degradation-mediated release occurs [215]. Interestingly, the slow diffusion stage was accelerated by the addition of HA, likely because the larger amount of drug retained in the scaffold provided a higher concentration gradient to drive diffusion.

The rapid precipitation implied by the initial burst of clodronate and simvastatin as well as the early mass loss is indicative of rapid NMP exchange, which demonstrates the potential of the system for rapid solidification. Fast precipitation is favorable for quick delivery of NMP for an initial osteogenic stimulus, and rapid formation of a solid drug delivery depot may have advantages over gradually precipitating systems with persistent gel or liquid cores for days or weeks after injection due to NMP retention [213]. Specifically, this has implications for intraosseous injection, where the system can completely precipitate within days while continuing to release drug over a period of weeks to months. In systems with freely suspended or dissolved drug, precipitation rate strongly influences burst release [137, 216], and the addition of drug-loaded PBAE microparticles can allow for prolonged release and decreased burst without prolonging precipitation of the system. The rapid precipitation may also allow filler particles, such as hydroxyapatite, to provide mechanical support in future iterations of the system. After the initial burst, pre-loaded simvastatin exhibited prolonged delivery over the entire 30 day period. The lack of change in simvastatin release kinetics upon addition of 30 wt% HA was expected, because HA should not appreciably interact with statins, which lack the phosphonate groups that provide binding sites for the calcium in HA. The successful demonstration of sustained release of both hydrophilic and hydrophobic small molecule drugs with reduced burst from this system

shows promise for new applications of *in situ* forming PLGA systems where rapid precipitation is required.

By fitting the power law to initial drug release, the release exponent *n* can be used to classify the mechanism of drug release from the system. For simvastatin, *n* of 0.47 indicates primarily Fickian diffusion based on the standard *n* values for a spherical scaffold of *n*=0.43 for pure Fickian diffusion and n=0.85 for pure Case II transport. The slightly higher release exponent compared to the pure Fickian value can be attributed to several factors, including the swelling of the PBAE hydrogel microparticles and minor swelling of the surrounding PLGA matrix. Similarly, *n* of 0.49 for clodronate corresponds to primarily Fickian diffusion as well. Both clodronate and simvastatin are therefore released via diffusive mechanisms prior to their sustained release, which follows a more linear trend. This data supports the idea that the burst was composed of a fraction of the loaded drug dissolved or suspended in NMP, and the rapid solvent exchange was likely responsible for the initial release. The sustained release was likely a combination of diffusion, erosion, and swelling-based mechanisms, and the superposition of these mechanisms produces release curves that are most simply expressed in daily release rates. Because simvastatin is almost insoluble in water but highly soluble in NMP, the larger burst compared to clodronate is unsurprising, as dissolved simvastatin may be transported out of the scaffold during the solvent exchange phase. Future iterations of the system may be able to further reduce burst by reducing access of drug to the NMP phase to limit the initial diffusive component of the system.

3.4.3. Degradation and mass loss

PLGA is a bulk-eroding material that degrades via hydrolysis of ester bonds, resulting in a progressive decrease in molecular weight until monomeric or oligomeric species of sufficiently low molecular weight are generated and cleared when molecular weight drops to approximately 1.5 kDa [217, 218]. The *in situ* forming scaffold has the additional property of a rapid precipitation

event upon injection, and due to the high aqueous miscibility of NMP, a rapid initial dry mass loss was observed within the first hour following injection as NMP entered the aqueous phase and the highly hydrophobic PLGA precipitated. By 24 hours, 46% dry mass remained, corresponding to the loss of the majority of the NMP content that composed 54 wt% of the system. The subsequent lack of dry mass change suggests that hydrolytic degradation was unable to produce small enough molecular weight species to be cleared into the surrounding aqueous environment until day 15. After day 15, the linear decrease in dry mass corresponded to clearance of degradation byproducts until all PLGA was removed from the system. The remaining 29% dry mass can be attributed to remaining HA content that composed 30% of the original mass. For wet scaffolds, the initial 12% decrease in wet mass throughout the first day of degradation supports the replacement of NMP with water due to precipitation of PLGA. The 20% increase in wet mass over the following 14 days indicates swelling of the PLGA matrix. Following this brief swelling, individual sample behavior diverged as swelling reached a maximum between 110-120% between days 20-30. The linear decrease in mass was delayed compared to dry samples because the small losses in polymer degradation byproducts were offset by increased water content as the system swelled. The lack of mass change beyond day 55 was consistent with the complete clearance of PLGA observed in dry mass studies, and the lower mass fraction remaining (20% compared to 29%) was likely due to repeated handling of samples during nondestructive measurements resulting in small amounts of HA being resuspended and removed with supernatant at each time point.

Based on microCT images, it was evident that scaffold microarchitecture underwent dramatic changes throughout the degradation process. The first indicator of change was the development of denser regions in the core and near the edges of scaffold by day 15, which may be attributable to the cessation of NMP release and the hydrophobicity of PLGA causing solid

regions to condense together. At day 20, the highest pore size was observed as large, closed macropores. This phenomenon corresponds to the scaffolds at their maximum swelling state based on wet mass, and was accompanied by further densification of the core and edge regions. At day 25, the core remained dense, but macropores were no longer evident, and the edges of scaffolds were less dense and more porous, which is consistent with reports of PLGA of this molecular weight beginning to lose mass to clearance after 3 weeks [218]. At day 30, it is possible that enough polymer had been lost to allow mobility of HA content through the PLGA, which settled at the bottom of scaffolds during incubation. By day 35, scaffold density and pore distribution appeared more uniform, and scaffolds were noticeably smaller in size due to further degradation of the highly porous regions seen at day 30.

3.4.4. Advantages of the system

In situ forming PLGA systems have been popularized due to their ease of use and unique ability to solidify at the point of injection, forming a drug delivery depot in the tissue of interest. However, because drug release from these systems is highly dependent on solvent exchange and polymer chemistry [137], release of multiple agents with unique release profiles is challenging. Additionally, low molecular weight drugs tend to exit during the solvent exchange, resulting in high initial burst [139]. Multiple drug release platforms for small molecule drugs, therefore, tend to be pre-formed scaffolds or injectable suspensions of micro- or nanoparticles [219-222]. The addition of PBAE microparticles to the *in situ* forming PLGA system combines the ease of use of injectable systems, the controlled release of microparticle systems, and the spatial control of solid scaffolds. Even in a rapidly-solidifying system, PBAE microparticles are capable of prolonging release of both hydrophilic and hydrophobic drugs over a 30 day period with significantly less burst than traditional injectable PLGA systems using freely mixed drug.

3.5. Conclusions

An *in situ* hardening, PLGA-based system offers a unique drug delivery platform due to its injectability and space-filling properties, and the addition of drug-loaded microparticles introduces the possibility for tunable release profiles for multiple pharmaceutical agents. In addition to the potential for multiple release profiles, the addition of drug-loaded PBAE microparticles enables the sustained release of water-soluble, small molecule drugs, such as clodronate, as well as lipophilic drugs, such as simvastatin, independent of PLGA precipitation. The biodegradability of the system makes this a favorable candidate for applications where a secondary surgery to remove the depleted scaffold is undesirable or impossible. Release kinetics can be multiphasic simply by loading drug freely into the PLGA solution for burst release, or into PBAE microparticles for sustained release with reduced burst. This injectable scaffold provides the simplicity of a targeted injection with the utility of an implantable drug delivery scaffold without compromising desirable release kinetics.

Chapter 4 Hydroxyapatite-Reinforced in Situ Forming PLGA Systems for Intraosseous Injection

4.1. Introduction

In situ forming poly(lactic-co-glycolic acid) (PLGA) implants have been investigated primarily for injection into soft tissue for sustained drug delivery [195]. These systems were conceived due to the phase separation observed when a hydrophobic polymer dissolved in a water-miscible organic solvent is introduced to an aqueous environment, resulting in solidification of the polymer matrix [198]. By mixing drugs into the polymer phase prior to injection, a drug-loaded, solid depot can form upon injection into the body. Such systems are available in FDA-approved formulations, such as Atridox®, for delivery of doxycycline into gum tissue, and Atrigel®, which is approved for delivery of leuprolide acetate for treatment of prostate cancer. These systems provide prolonged drug release, with an initial burst dependent on drug and solvent properties and a release period dependent on drug and polymer properties [139]. As such, these injectable systems avoid the additional trauma that would be needed for implantation of large, solid dosage forms. Furthermore, PLGA is hydrolytically degradable, so there is no secondary surgery required to remove an implant after drug delivery is complete [218]. Because the systems are locally injectable and space-filling, they should theoretically be able to infiltrate and conform to complex geometries, such as a network of trabecular bone.

Most research on *in situ* forming PLGA systems to date has focused on modifying release kinetics by changing solvent or polymer chemistry or concentrations [137, 200, 201]. There has been little focus, however, on the capability of these systems to accommodate filler particles to modify mechanical properties [223]. Recently, it was shown that hydroxyapatite (HA) and poly(β-amino ester) (PBAE) additives can improve bisphosphonate and simvastatin release, respectively, from *in situ* forming PLGA systems [81]. HA has also been demonstrated to improve the osteoconductive and mechanical properties of pre-formed polymeric scaffolds for orthopedic

applications [224-226], although to date there has been no published research on the mechanical effects of HA additives in *in situ* forming PLGA scaffolds, to the authors' knowledge.

Many orthopedic conditions result in structurally compromised bone that would benefit from both pharmaceutical treatments and mechanical support. For example, avascular necrosis and osteoporosis reduce both bone quality and quantity, and can ultimately lead to structural collapse [227-229]. Trabecular bone is composed of a high-porosity, interconnected network of bone, and the inter-trabecular space houses marrow, adipose tissue, blood vessels, and interstitial fluid. This trabecular network is a potential target for intraosseous injection of an *in situ* forming system, allowing a scaffold to form a network complementary to trabecular bone. From a mechanical standpoint, it is beneficial to surround weakened or necrotic bone with a structurally supportive material to prevent collapse, especially if that material can promote repair of the compromised tissue. To this end, the previously described injectable HA-PLGA-PBAE system was investigated for its mechanical benefits in trabecular bone.

A necessary step in designing such a system is characterizing the mechanical effects that HA has on an *in situ* forming PLGA system. Scaffolds need to be considered both for their intrinsic material properties and for their ability to augment the structural properties of trabecular bone. Another consideration is the injectability of the system, which encompasses both force required to extrude the mixture as well as the potential for the injection to penetrate the trabecular bone network and solidify. The present studies investigated the mechanical and microarchitectural properties of composite HA-PLGA-PBAE injectable scaffolds, as well their space-filling and reinforcement effects on trabecular bone.

4.2. Materials and Methods

4.2.1. Synthesis of PBAE microparticles

PBAE hydrogel slabs were synthesized as described previously [69, 70]. Briefly, macromer was created by reacting diethylene glycol diacrylate with isobutylamine at 85°C for 16 hours at a 1.2:1 molar ratio. This macromer was then photopolymerized between two glass plates with 1% w/w DMPA initiator and a 1:1 weight ratio of macromer to microparticulate hydroxyapatite (MHA) (Sigma-Aldrich, St. Louis, MO, USA) to form a PBAE hydrogel slab. PBAE hydrogels were previously loaded with drug for use as delivery vehicles, but were left unloaded for these experiments. Microparticles were formed by grinding PBAE slabs and sieving until all collected particles were 250 μm or less in size.

4.2.2. NHA synthesis

Nanoparticulate HA (NHA; nGimat, Lexington, KY, USA) was produced at nGimat LLC's facility in Lexington, KY, using a solution combustion process called NanoSpray Combustion ^{SM}. This scalable process is capable of producing synthetic bone minerals, such as HA, tricalcium phosphate (TCP), and amorphous calcium phosphate (ACP), using cost-effective precursor materials. To produce NHA, a calcium carboxylate precursor and an alkyl phosphate precursor of appropriate proportions were dissolved in an organic solvent system, the solution was converted to an ultrafine spray (referred to as a NanoSpray) using a device called a Nanomiser®, and the spray was combusted under a controlled atmosphere. The average particle size for the NHA was <200 nm, as estimated by BET. X-ray diffraction confirmed the presence of the HA phase ($Ca_5(OH)(PO_4)_3$), and X-ray fluorescence spectroscopy showed that the Ca:P ratio was close to 5:3.

4.2.3. Formation of cylindrical scaffolds

PLGA (50:50 L:G, acid terminated, inherent viscosity 0.55-0.75 dL/g) was obtained from DURECT, Inc. (Birmingham, AL, USA). All experiments used a polymer solution of 30% w/w PLGA in NMP (Sigma-Aldrich, St. Louis, MO, USA). PBAE microparticles and MHA or NHA were mixed homogeneously into the polymer solution using a spatula. The scaffold mixture was loaded into a syringe and injected through a 16 gauge needle into a cylindrical agarose mold, where the system was allowed to solidify in phosphate-buffered saline (PBS). Scaffolds contained different concentrations of MHA or NHA, ranging from 0% to 50% w/w. All scaffolds contained 5% w/w PBAE microparticles to mimic prior drug release study conditions, unless otherwise indicated. PBS was replaced daily to prevent accumulation of NMP or low molecular weight species that were cleared from the scaffolds.

4.2.4. Mechanical properties of cylindrical scaffolds

All compression tests were performed using a Bose ELF 3300 mechanical testing instrument. Modulus was calculated as the slope of the initial linear region of the stress-strain curve (approximately the first 5-10% strain). Yield stress was determined as the stress at which the stress-strain curve became nonlinear. To first identify any strain rate-dependence of mechanical properties, scaffolds prepared with increasing MHA content were tested in unconstrained compression to 50% strain at displacement rates of 0.006, 0.06, and 0.6 mm/s (strain rates of 0.001, 0.01, and 0.01 s^{-1}, respectively). The contribution of PBAE microparticles to mechanical properties was quantified by increasing PBAE content from 1% to 15% w/w in scaffolds prepared with 30% NHA.

To determine the effects of NHA versus MHA on scaffold properties, a comparison of mechanical properties for scaffolds containing different amounts of MHA and NHA was performed at a displacement rate of 1 mm/min (0.0167 mm/s, or a strain rate of 0.0028 s^{-1}) to

50% strain. Total HA content ranged from 0 to 50% in intervals of 10%. Scaffolds were prepared with either pure MHA, pure NHA, or different ratios of the two.

4.2.5. Injectability

To quantify injectability, scaffold mixtures containing 30% w/w NHA and 5, 10, or 15% w/w PBAE microparticles were loaded into a 3 mL syringe affixed with a 1.5 inch, 16 gauge needle. The loaded syringe was suspended by its flanges in a 15 mL centrifuge tube to collect the injected mixture, with the end of the tube in contact with the load cell and the plunger of the syringe in contact with the axial mover. The plunger was subjected to a series of sustained loads to simulate injection force, and the resulting displacement of the plunger was recorded. Injectability was quantified by plotting the time to inject 0.5 mL as a function of the injection force. Rational limits of 60 second injection time and 50 N injection force were set as the limits of injectability based on consultation with an orthopedic surgeon (T.A.M.).

4.2.6. Microarchitecture

Effects of HA on microarchitecture were analyzed by preparing scaffolds with increasing NHA and MHA content, as well as a variety of NHA/MHA mixtures totaling 30% HA, lyophilizing these scaffolds after they had solidified in PBS for 3 days, and then scanning them with a SCANCO MicroCT 40 (SCANCO Medical AG, Switzerland) at 55 kV and 145 mA and 6 μm voxel size. Microarchitecture was quantified by porosity and material density. Scanning electron microscopy (SEM) was used to visualize micro- and nanoarchitecture of scaffolds containing 30% w/w NHA. Samples were freeze-fractured, coated with gold-palladium alloy, and imaged with a Hitachi S-4300 scanning electron microscope at 3 kV accelerating voltage.

4.2.7. Ex vivo scaffold injections

Humeral heads were harvested from 10 week old male piglets euthanized in a separate study, and were kept frozen until use, without chemical fixation or removal of marrow. Using a 16-gauge, 2.5-inch bone biopsy needle inserted through the growth plate into the proximal humeral epiphysis, two humeral heads each received 3 mL *ex vivo* injections of 30% NHA / 5% PBAE scaffolds. Two humeral heads were used as untreated controls. All humeral heads were scanned using microCT prior to injection, immersed in PBS for 5 days to allow scaffolds to fully solidify, and then scanned again to quantify scaffold infiltration. After 5 days in PBS, a 3 mm diameter cylindrical punch was used to remove tissue samples in the mediolateral direction, with the punch approaching through the articular cartilage and penetrating through the growth plate, for a total of 7 samples each for treatment and control groups. These cylindrical samples were trimmed to 6 mm in length, using only trabecular bone tissue between the growth plate and the articular cartilage. All samples were stored in PBS and tested the same day in unconstrained compression at a rate of 1 mm/min.

4.3. Results

4.3.1. Strain rate and MHA content

Scaffolds prepared with different MHA contents were compressed at strain rates spanning three orders of magnitude. At strain rates of 0.001, 0.01, and 0.1 s^{-1} (corresponding to displacement rates of 0.006, 0.06, and 0.6 mm/s), modulus increased with MHA content (Figure 4.1A). The highest modulus increased from 64 to 82 to 96 MPa for each respective strain rate, and overall, moduli ranged from 9 to 96 MPa. The lowest recorded modulus for any scaffold containing HA was 29 MPa (10% MHA, 0.001 s^{-1}), while scaffolds without any HA ranged from 9 to 30 MPa, increasing with strain rate. At 0.001 s^{-1}, significant increases in modulus occurred between 0-10% ($p<0.01$) and 30-50% MHA ($p<0.01$). At 0.01 s^{-1}, significant increases occurred between 0-20%

($p<0.05$) and 20-50% MHA ($p<0.0001$). At the highest strain rate of 0.1 s^{-1}, modulus increased between 0-10% ($p<0.01$), 10-30% ($p<0.001$), and 30-40% MHA ($p<0.001$). For equivalent scaffold formulations, average modulus increased with increasing strain rate in every case, and this trend was significant at 40% MHA between 0.01 and 0.1 s-1 ($p<0.0001$) and at 50% w/w MHA between 0.001 and 0.01 s-1 ($p<0.05$).

Yield stress followed a similar trend to modulus, however the differences between scaffold formulations and between strain rates were less pronounced (Figure 4.1B). Yield stresses ranged from 1.1 to 7 MPa, and the highest yield stresses at the three strain rates of 0.001, 0.01, and 0.1 s^{-1} were 4.4, 5, and 7 MPa, respectively. Addition of 10% MHA to scaffolds led to a threefold increase in yield stress at a strain rate of 0.001 s^{-1} (from 1.1 to 3.3 MPa) and a twofold increase in yield stress at 0.01 s^{-1} (from 2 to 4.2 MPa), while 10% MHA scaffolds experienced only a 13% increase (from 4.5 to 5.1 MPa) at a strain rate of 0.1 s-1. At 0.001 s^{-1}, significant increases in yield stress occurred between 0-10% ($p<0.0001$) and 40-50% MHA ($p<0.01$). At 0.01 s^{-1}, yield stress significantly increased at 0-10% ($p<0.0001$) and 10-30% MHA ($p<0.01$). At the highest strain rate of 0.1 s^{-1}, yield stress increased from 0-20% ($p<0.05$) and 20-50% MHA ($p<0.05$). Similar to modulus, average yield stress for equivalent scaffold formulations increased at every strain rate. Increasing strain rate from 0.001 to 0.01 s^{-1} led to an increase in yield stress for 20% ($p<0.001$), 30% ($p<0.01$), and 40% MHA scaffolds ($p<0.001$). Further increasing strain rate from 0.01 to 0.1 s^{-1} resulted in significantly increased yield stress for 0% ($p<0.0001$), 30% ($p<0.01$), 40% ($p<0.01$), and 50% MHA scaffolds ($p<0.0001$).

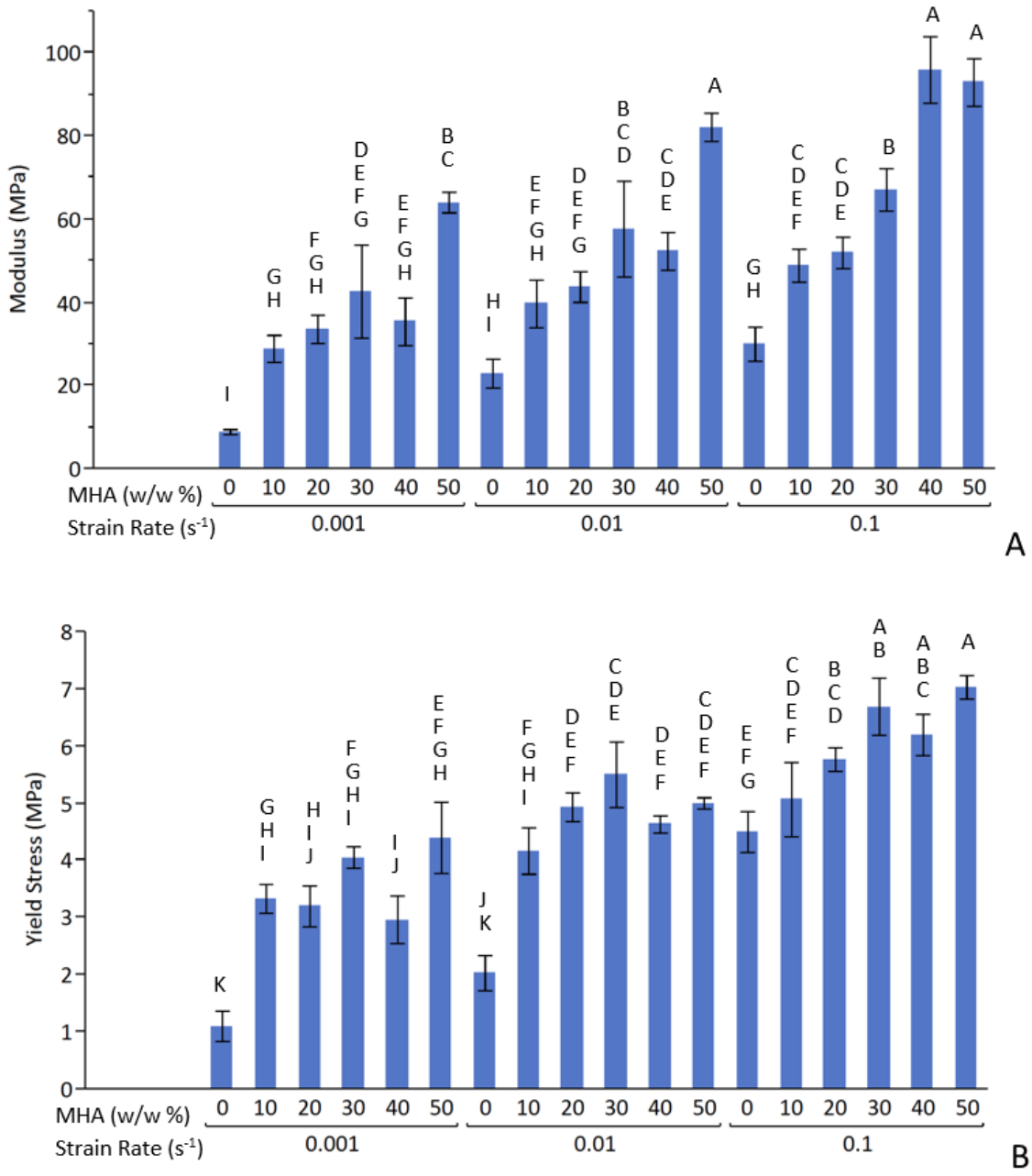

Figure 4.1. Mechanical properties of cylindrical scaffolds prepared with different MHA content and tested at multiple strain rates. A) Compressive modulus. B) Yield stress. Data are grouped by displacement rate and ordered by increasing MHA content. Shared letters denote statistical similarity, and columns without a single shared letter are significantly different. Data are mean ± standard deviation (n=3).

4.3.2. PBAE content

Scaffolds prepared with 30 w/w% NHA and different PBAE microparticle contents were compressed at 1 mm/min (0.0028 s^{-1}). PBAE microparticle content did not significantly affect 30% NHA scaffold mechanical properties for PBAE content ranging from 1 to 10 w/w %. Moduli ranging from 96-120 MPa (Figure 4.2A) and yield stresses from 4.3-4.9 MPa (Figure 4.2B) were recorded in these PBAE content ranges, with the highest modulus occurring at 10% PBAE and the highest yield stress occurring at 1% PBAE. Increasing PBAE content from 10 to 15% led to a significant decrease in modulus from 120 to 84 MPa ($p<0.05$). Average yield stress of 15% PBAE scaffolds was 3.6 MPa, significantly lower than 1% PBAE scaffolds ($p<0.05$), which had an average yield stress of 4.9 MPa. Samples became more viscous and difficult to inject into molds as PBAE content was increased. Beyond 15% PBAE, the mixture could still be injected, but the scaffold began precipitating before it could flow and fill the cylindrical mold, resulting in inconsistent morphology and unreliable mechanical properties.

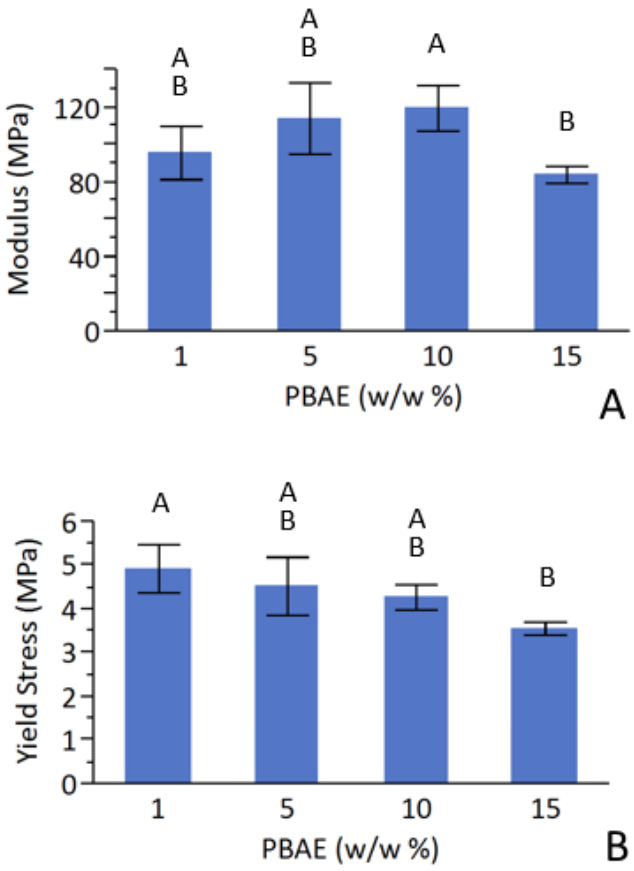

Figure 4.2. Mechanical properties of 30 w/w % NHA scaffolds prepared with increasing PBAE microparticle content. A) Compressive modulus. B) Yield stress. Shared letters denote statistical similarity, and columns without a single shared letter are significantly different. Data are mean ± standard deviation (n=3).

4.3.3. Ratio of MHA to NHA

Scaffolds prepared with different amounts of MHA and NHA were compressed at 1 mm/min (0.0028 s^{-1}). All scaffolds generally increased in modulus up to 30% w/w total HA content (Figure 4.3A). In scaffolds prepared with only MHA, a linear increase in modulus from 33 to 68 MPa was observed from 10% through 30% MHA, although no significant difference was observed between groups. Modulus was significantly different between 10% and 50% MHA scaffolds ($p<0.05$). Scaffolds prepared with only NHA exhibited a large and significant increase in modulus,

from 53 to 141 MPa, between 20% and 30% NHA ($p<0.0001$). Scaffolds prepared with equal amounts of NHA and MHA possessed moduli similar to 30% NHA scaffolds, with 15:15, 20:20, and 25:25 NHA:MHA scaffolds all exhibiting moduli between 128 and 151 MPa. Other scaffolds with similarly high moduli included mixed NHA and MHA scaffolds with total HA concentrations of 50% (10:40, 20:30, and 30:20 NHA:MHA). Notably, 20:10 scaffolds exhibited significantly lower modulus than 15:15 and 30:0 NHA:MHA scaffolds ($p<0.0001$). Scaffolds with 40% and 50% total had the highest modulus at a 1:1 NHA:MHA ratio, which decreased when the NHA:MHA ratio was changed in either direction.

Yield stress followed trends similar to modulus, however the magnitude of these differences was lower (Figure 4.3B). For example, out of all scaffolds prepared with 30% total HA, only 30:0 and 10:20 NHA:MHA samples were significantly different ($p<0.01$). Scaffolds made with 40% pure MHA or 40% pure NHA had significantly lower yield stresses than scaffolds prepared with a mixture of NHA and MHA ($p<0.01$). At 50% total HA, scaffolds with 30% or higher NHA content possessed lower yield stresses than scaffolds composed of 25:25, 20:30, or 10:40 NHA:MHA ($p<0.01$).

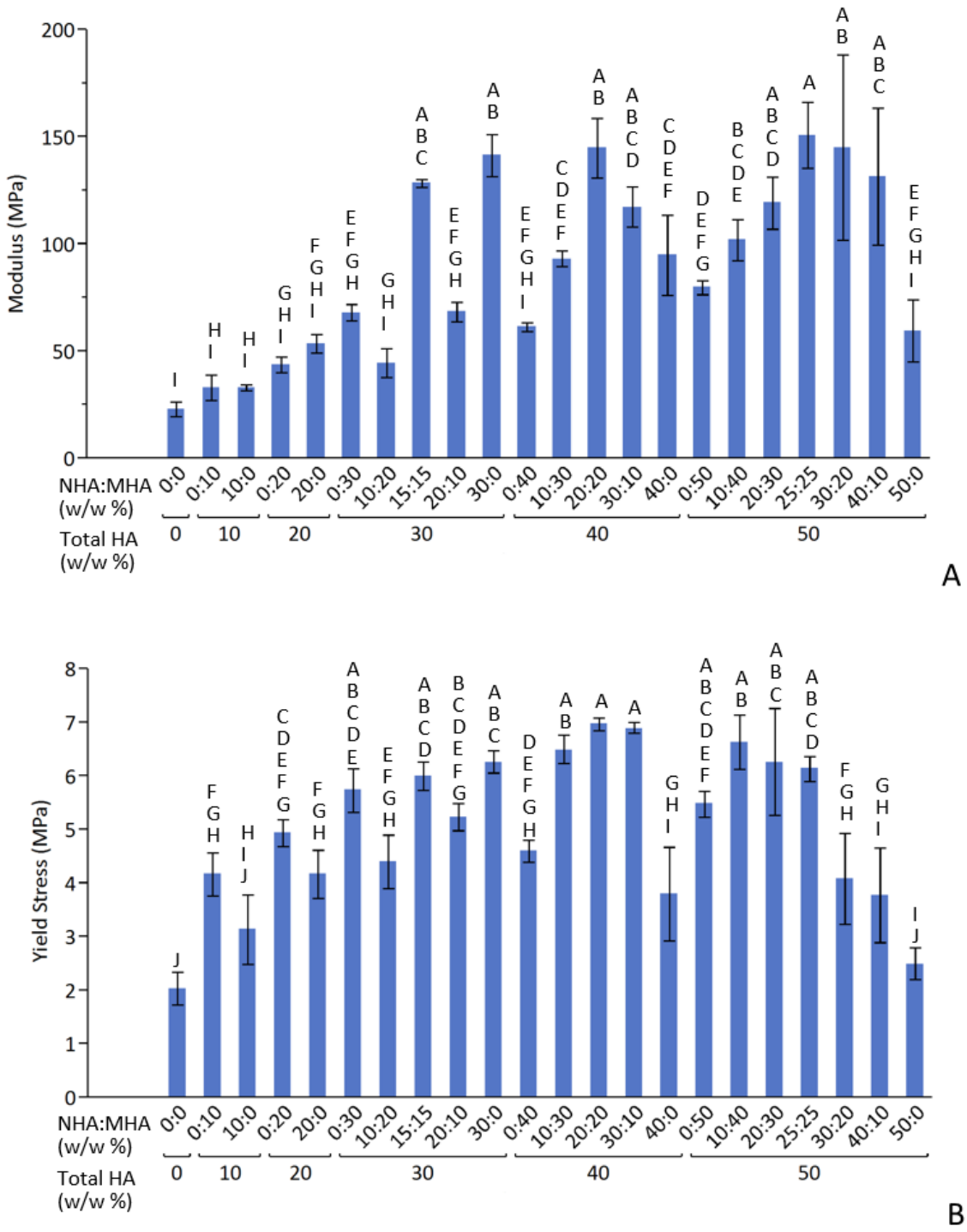

Figure 4.3. Mechanical properties of scaffolds prepared with different MHA:NHA ratios, grouped by increasing total HA content (w/w %) and subsequently ordered by increasing MHA content (w/w %). A) Compressive modulus. B) Yield stress. Shared letters denote statistical similarity, and

columns without a single shared letter are significantly different. Data are mean ± standard deviation (n=3).

4.3.4. Injectability

Injectable scaffold mixtures containing 5, 10, or 15 w/w% PBAE microparticle content were injected through a 16 gauge, 1.5 inch needle with a series of increasing injection forces. For each injection, the displacement of the plunger initially increased rapidly due to compression of the rubber plunger, the scaffold mixture, and any air bubbles, before reaching a period of linear displacement where flow rate was constant, followed by a relaxation period as force was removed (Figure 4.4A). The linear portion of the displacement curve was used to calculate displacement rate of the syringe plunger, and the internal diameter of the syringe barrel was used to calculate volumetric flow rate. The time required to inject 0.5 mL of each mixture increased with increasing PBAE content, and it decreased with increasing injection force (Figure 4.4B). Scaffolds were considered injectable if a 0.5 mL injection could be performed in 60 seconds or less, which is indicated by the horizontal dashed line in Figure 4B. The 5% PBAE scaffolds were injectable for injection forces greater than 16 N, 10% PBAE scaffolds became injectable at 40 N, and 15% PBAE scaffolds became injectable at 75 N. The vertical dotted line at 50 N in Figure 4B indicates the limit for a reasonable injection force, beyond which sustained forces may be uncomfortable or cause fatigue for the surgeon performing the procedure. For each scaffold composition, a logarithmic transformation of both injection force and injection time resulted in the best fit.

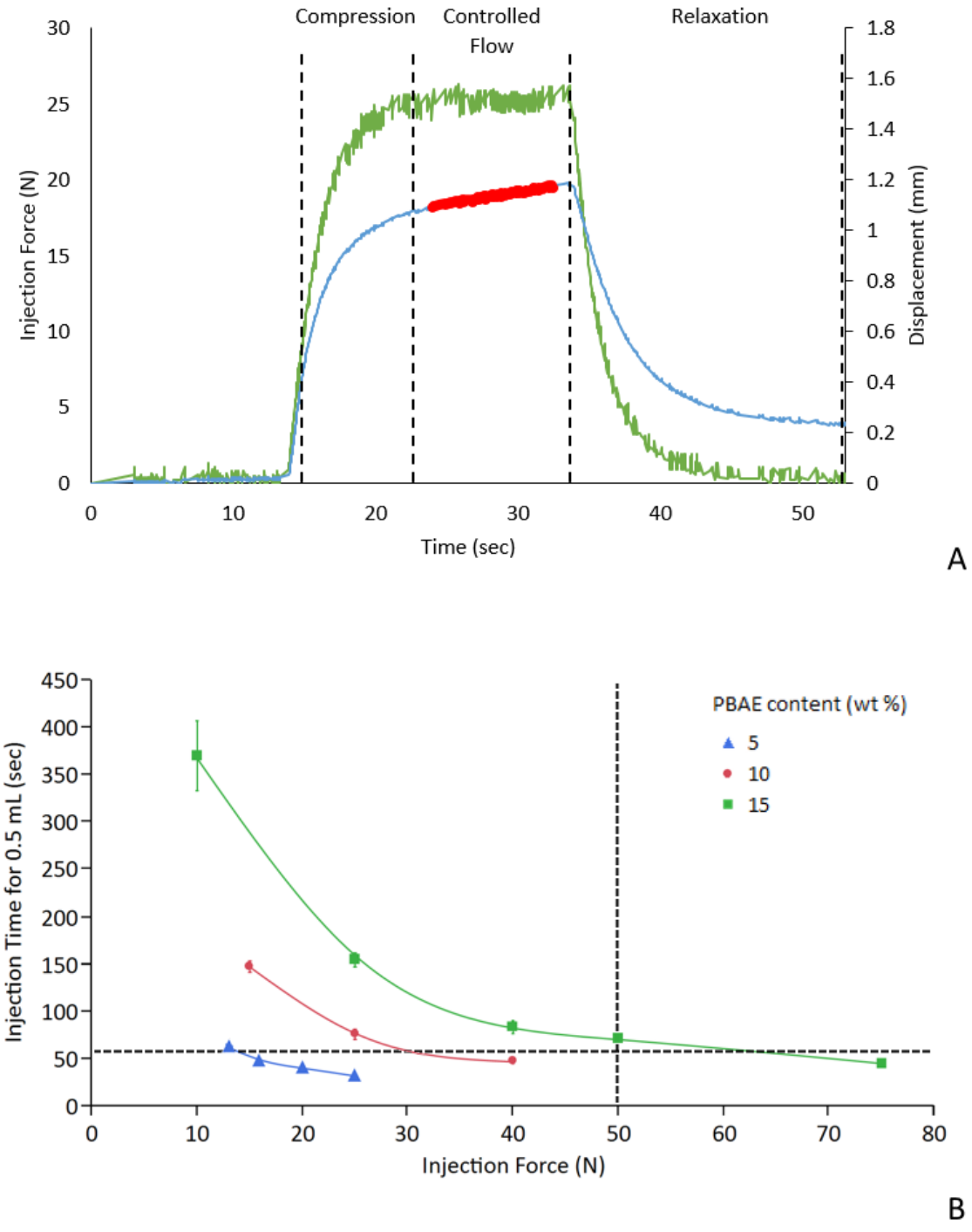

Figure 4.4. Injectability of 30% NHA scaffold mixtures prepared with varying PBAE microparticle content. A) Representative graph of collected force (green curve, left axis) and displacement (blue curve, right axis) data, with the highlighted linear portion of the displacement used to calculate

volumetric flow rate. B) Time required to inject 0.5 mL from a 16 gauge needle for various injection forces and PBAE microparticle contents. The dotted lines indicate reasonable limits for injection time for 0.5 mL (60 sec) and injection force (50 N). Data are mean ± standard deviation (n=3).

4.3.5. Microarchitecture

Visualizing the microarchitecture of scaffolds prepared with 30% w/w NHA and 5% w/w PBAE microparticles revealed two distinct levels of porosity, with NHA and PBAE particles trapped within the solid PLGA matrix. Macroscopic pores on the order of 100 μm in diameter were scattered throughout the scaffold (Figure 4.5A), and the solid PLGA matrix was primarily composed of a microporous, honeycomb-like structure with pore sizes on the order of 10 μm (Figure 4.5B). Elongated pores were observed at the scaffold surface (Figure 4.5C). HA nanoparticles, with spherical morphology and diameters on the order of 50 nm, were present in the PLGA walls of the micropores (Figure 4.5D). These particles were densely packed in 30% w/w NHA scaffolds.

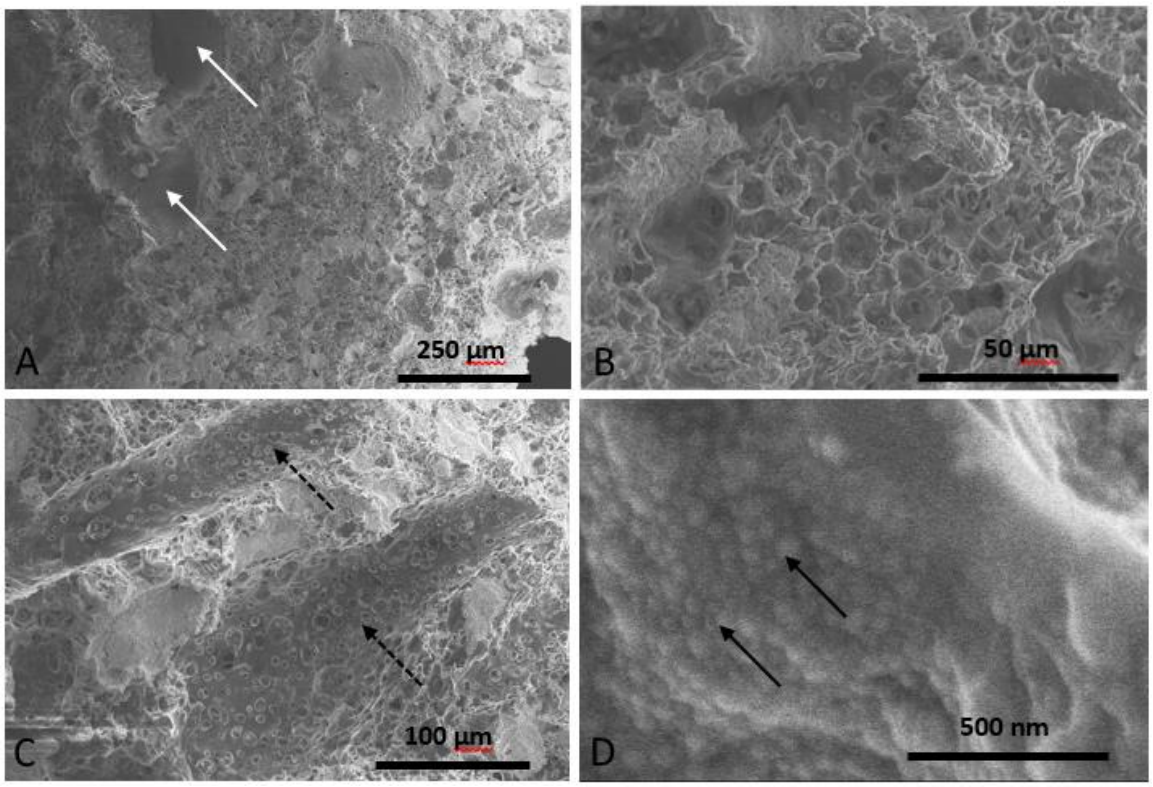

Figure 4.5. SEM images of 30% w/w NHA scaffold microarchitecture, showing A) macropores on the order of 100 µm (white arrows), B) microporous PLGA substructure, C) elongated pores perpendicular to the surface (dotted arrows), and D) NHA nanoparticles embedded in the PLGA matrix (black arrows).

MicroCT analysis allowed for quantification of microarchitectural parameters such as porosity and material density. Porosity generally decreased with increasing total HA content, and this trend was most pronounced in samples prepared with only MHA, which possessed porosities ranging from 2.4 to 48.1%, while samples prepared with only NHA had a porosity range of 13 to 22.5% (Figure 4.6A). MHA-only samples experienced a significant decrease in porosity from 10-20% ($p<0.001$) and 30-40% ($p<0.05$), and NHA-only samples had a significant decrease in porosity from 10-30% ($p<0.05$). Samples with 30% total HA prepared with different mixtures of MHA and NHA did not exhibit significantly different porosity from each other. At equivalent weight percentages, samples prepared with pure NHA had significantly lower porosity than those

prepared with MHA at 10% ($p<0.0001$), 20% ($p<0.001$), and 30% ($p<0.05$), while porosity between the two groups was not different at 40% and 50% w/w.

Material density increased with total HA content, and scaffolds prepared with NHA experienced a larger increase in density at each 10% increment of HA content (Figure 4.6B). MHA scaffolds exhibited significantly higher density than NHA scaffolds at 10% ($p<0.0001$) and 20% ($p<0.01$), but due to the smaller rate of increase, they exhibited lower density than NHA scaffolds at 30%, 40%, and 50% w/w ($p<0.0001$). The 30% HA scaffolds prepared with a mixture of NHA and MHA had lower density at 10:20 NHA:MHA formulations than scaffolds prepared with 15:15 and 20:10 NHA:MHA ($p<0.0001$).

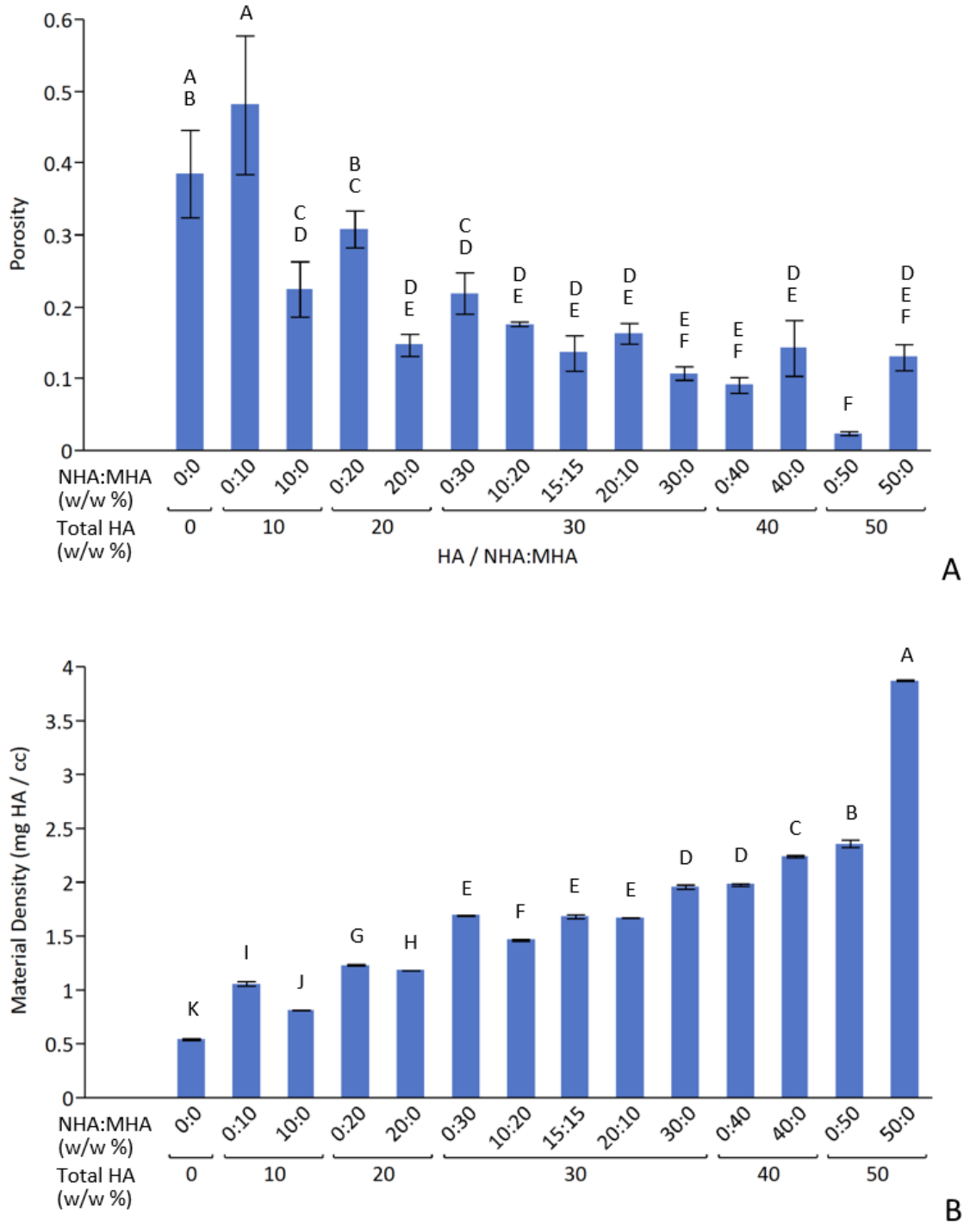

Figure 4.6. MicroCT analysis of scaffolds prepared with varying NHA and MHA content, showing A) porosity and B) material density of cylindrical samples. Data are grouped by total HA content, and ordered by increasing NHA content. Shared letters denote statistical similarity, and columns

without a single shared letter are significantly different. Data are mean ±- standard deviation (n=3).

4.3.6. Ex vivo scaffold injections

During the injection of scaffolds into the humeral heads, fluid was observed leaking out of bone near the growth plate, indicating that the scaffold was displacing marrow and filling the intertrabecular space. After the 3 mL injection into two humeral heads, there was an average reduction in free volume of 2.8 mL, corresponding to a 58% filling of the intertrabecular volume (data not shown). A comparison of cutplanes from a 3D reconstruction of the humeral heads showed scaffold material distributed throughout the bone volume, with small (sub-millimeter) regions of that were unfilled (Figure 4.7A). During removal of the cylindrical cores from injected bones, it was observed that scaffold material was constrained by the articular cartilage and growth plate (Figure 4.7B). Cylindrical samples of injected bone possessed a mean compressive modulus of 180 MPa, compared to 81 MPa for controls ($p<0.001$) (Figure 4.7C). Yield stress was also significantly higher for injected bone, with a yield stress of 5.9 MPa for injected samples compared to 3.5 MPa for controls ($p<0.01$) (Figure 4.7D).

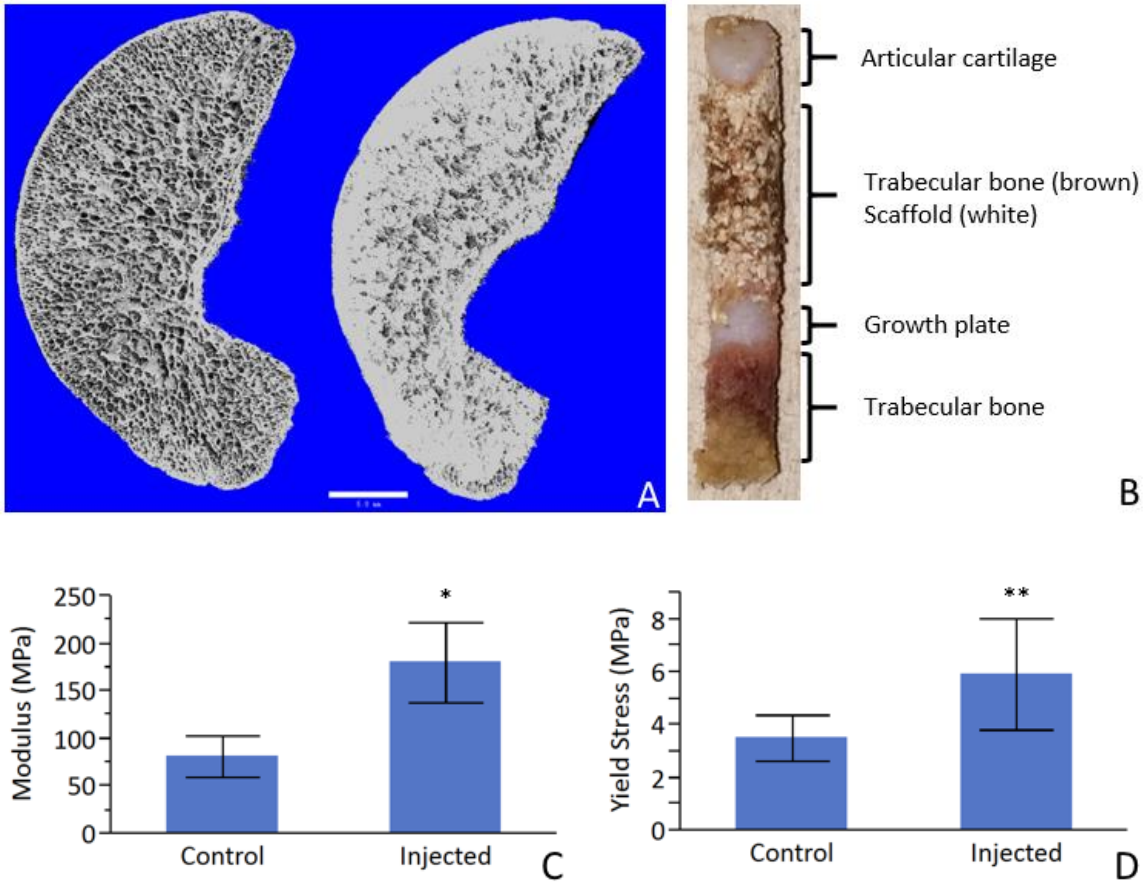

Figure 4.7. Microstructural and mechanical properties of trabecular bone samples from porcine humeral heads with or without injection of 30% NHA / 5% PBAE scaffolds. A) MicroCT cutplane of humeral head prior to injection (left) and post-injection (right). B) Cylindrical bone sample containing solidified scaffold. C) Compressive modulus. D) Yield stress. Data are mean ±- standard deviation (n=7). *Significantly different from Control ($p<0.001$). **Significantly different from Control ($p<0.01$). Scale bar is 5 mm.

4.4. Discussion

4.4.1. Mechanical properties

The general effects of HA additives on *in situ* forming PLGA scaffolds were consistent with existing research on preformed, implantable scaffolds [224, 230-232], with HA additives providing mechanical reinforcement, as evidenced by both compressive modulus and yield stress. As HA

content was increased beyond a certain point (generally around 30% w/w, depending on the specific MHA and NHA content), mechanical properties either plateaued, in the case of MHA, or decreased, in the case of NHA. This effect can be attributed to the total surface area of HA relative to the volume of PLGA, which results in maximal scaffold mechanical properties when sufficient PLGA is present to bind HA together tightly without excess HA or PLGA. SEM images of the 30% NHA scaffolds showed dense packing of NHA nanoparticles embedded in the PLGA phase, which may explain why further increasing NHA content was not beneficial since particles were already in close proximity at this loading. MHA scaffolds were mechanically inferior to NHA at equivalent concentrations, likely due to the lower surface area to volume ratio of MHA, which allowed fewer PLGA:HA and HA:HA interfaces to form, and thus led to a more loosely packed HA microstructure. Additionally, there may exist a critical threshold for particle size, below which significant mechanical benefits occur in a composite [233]. Scaffolds with a higher NHA and MHA packing capacity could potentially be created by increasing PLGA concentration in the PLGA/NMP solution [232], however, this would also increase the viscosity of the injectable mixture [234].

Interestingly, scaffolds prepared with equal amounts of NHA and MHA tended to possess comparable mechanical properties to scaffolds prepared with pure NHA or pure MHA. This similarity may be due to the tight packing of NHA in the spaces between MHA particles, resulting in scaffolds that are effectively identical to tightly packed NHA when compressed. Ultimately, the similarity between pure NHA and equally mixed NHA/MHA scaffolds is probably the result of two factors: 1) HA should be present at sufficient concentrations so that load is primarily being transmitted between tightly packed HA particles, and 2) enough PLGA should be present so that it can bind all the HA particles together. For a system intended for intraosseous injection, however, 30% NHA provides the highest mechanical properties at the lowest total HA concentration, and was therefore the most appealing formulation in terms of injectability.

Native trabecular bone in human femoral heads has a wide range of mechanical properties, with compressive moduli ranging from 100-600 MPa and yield strength ranging from 1-9 MPa [227, 235]. For conditions that may be candidates for an injectable, intraosseous treatment, these values may be reduced by 24% (yield stress) and 20% (modulus) in osteoporotic patients [227], or 50% (yield stress) and 72% (modulus) in osteonecrosis patients [235]. Scaffolds with material properties similar to trabecular bone can aid load-bearing while the drug delivery component of the scaffold exerts its effect [236]. The average modulus of scaffolds prepared with 30% NHA was 141 MPa, and the average yield stress was 6.2 MPa, which are both within the range of trabecular bone. Although *in situ* forming PLGA systems have not been extensively investigated for their mechanical properties, the strength of these scaffolds is 10-fold higher than a similar system containing 33% α-tricalcium phosphate and PLGA of a lower molecular weight [223]. Furthermore, the yield stress was on the higher end of healthy trabecular bone, so even if scaffolds are slightly less stiff than the native bone tissue, they can withstand similar stresses to healthy bone before beginning to collapse. It is important to consider these scaffolds as a means for temporary augmentation that can acutely preserve bone while treatment occurs, not as a replacement for healthy bone tissue. For this purpose, the material properties of the 30% NHA system are sufficient.

4.4.2. Injectability

Injectability is a unique concern for *in situ* forming scaffolds, because both HA and PBAE particle additives increase viscosity. Becaue prior injectable PLGA systems were not intended for mechanical support, and drug is usually mixed freely into the polymer solution, viscosity has not been a limiting factor when designing these systems. However, injectable bone cements and fillers have encountered issues with injectability because they are composed of a liquid phase containing high concentrations of suspended particles [237, 238]. For example, decreasing the

liquid to powder ratio increases the required injection force and decreases the extruded fraction [237, 239], which is roughly analogous to increasing HA content in an injectable PLGA system. Various additives have been investigated to decrease the required injection force [240]. Injectability will likely be a persistent, nontrivial issue for *in situ* forming PLGA systems containing mechanical filler. Setting NHA content to a constant 30% and varying PBAE microparticle content revealed that there is a clear limit on PBAE microparticle content (and, therefore, drug loading) beyond which the system cannot be injected without exceeding limits of injection force or injection time. Longer-duration injections may be complicated by the precipitation of PLGA into a solid [241], leading to increased backpressure and a loss of injectability, while injections requiring large sustained force may be uncomfortable for the surgeon performing the procedure. The injection force limit may be circumvented by the use of an injection gun, which would improve injection time and greatly increase the injection force limit.

4.4.3. *Ex vivo* injections

The space-filling and mechanical reinforcement potential of an injectable system is likely to differ *in situ* from simulated tests, due to the presence of a constrained geometry filled with marrow and bordered by anatomical features such as articular cartilage, cortical bone, and the growth plate. The incomplete filling of free volume by the scaffold suggests that the material establishes flow channels of low resistance, resulting in small pockets of unfilled bone. MicroCT images and cylindrical tissue samples, however, show that these unfilled regions are distributed throughout the bony network, and the scaffold was capable of filling the bone tissue in all directions. Furthermore, injected bone tissue was significantly stronger and stiffer than native tissue, suggesting that the 58% filling that was achieved is sufficient to greatly improve mechanical properties of trabecular bone.

4.4.4. Advantages of the system

An *in situ* forming HA-PLGA-PBAE implant offers several advantages over traditional orthopedic injectables, such as poly(methyl methacrylate) (PMMA) bone cement. The heat of free radical polymerization of PMMA *in situ* can lead to protein denaturation and tissue necrosis [242], whereas *in situ* forming PLGA scaffolds are formed via solvent exchange at ambient temperature. PMMA is not biodegradable, while PLGA degrades hydrolytically over a time period dependent on its chemical properties [218]. Biodegradation is important for a drug delivery scaffold embedded in a trabecular network, where removal surgery is impossible and a permanent implant is not ideal. Finally, the mechanical properties of PMMA are a better match for cortical bone than a trabecular bone network, while PLGA is a less stiff material that may be appropriately augmented to match trabecular bone via addition of HA filler [236, 243]. An implant that acutely reinforces compromised bone, controls drug release, and gradually degrades to allow regeneration of native tissue can provide a comprehensive treatment in a single injection.

4.5. Conclusions

The present study demonstrated the feasibility of an injectable PLGA scaffold containing PBAE and HA particles as a mechanically supportive, *in situ* forming scaffold. Injectable scaffold mixtures are capable of being injected through a standard bone biopsy needle, infiltrating trabecular bone, then solidifying to produce scaffolds with mechanical properties comparable to those of trabecular bone. This injectable scaffold offers a promising treatment platform for ailments requiring both drug delivery and mechanical reinforcement of trabecular bone, and it has the advantage of being easily injectable and fully resorbable. This particular system was optimized to accommodate NHA mechanical filler and PBAE microparticles for drug delivery, with the goal of an intraosseous injection into the femoral head. *In situ* forming PLGA systems have

traditionally been viewed purely as drug delivery devices, but this study clearly demonstrates the potential for a mechanical component to these systems as well.

Chapter 5 Poly(β-amino ester) hydrogel microparticles to improve *in situ* forming delivery systems for periodontitis

5.1. Introduction

Periodontitis is a complex oral infection, in which bacteria colonize below the gum line, leading to the destruction of multiple tissues, including the gingiva, alveolar bone, and periodontal ligament [151]. Beyond the progressive deterioration of oral health leading to tooth loss, periodontitis has also been implicated in systemic conditions such as cardiovascular and cerebrovascular disease, and diabetes [153, 154]. Traditionally, periodontitis is treated with mechanical removal of bacteria from tissue surfaces in a process called scaling, followed by smoothing of the tooth surface, called root planing [157]. In many cases, scaling and root planing are accompanied by local or systemic delivery of antibiotics to treat difficult infections and to prevent recurrence [158]. However, systemic antibiotics can lead to adverse side effects due to the relatively high dosage required to provide sufficient concentration in oral tissues, and simple local delivery, such as rinses, needs to be repeated frequently to maintain appropriate antibiotic concentrations. Therefore, local delivery systems have been developed to maintain antibiotic dosages within the periodontal pocket [244-246]. In advanced cases of periodontitis, significant alveolar bone loss occurs, and augmentation procedures involving implanted grafts or scaffolds may be used to promote bone regrowth after the infection has been cleared [151, 247].

A single, injectable therapy, containing both antibiotic and osteogenic components in a biodegradable scaffold, can potentially provide an all-encompassing, minimally invasive treatment for this condition. The commercially available Atridox® system is an injectable formulation of poly(lactic-co-glycolic acid) (PLGA) containing doxycycline, an antibiotic, and has been shown to maintain local doxycycline concentrations above the minimum inhibitory

concentration for over 1 week. Recently, a similar system containing particulate additives for orthopedic applications was investigated for delivery of simvastatin, which has osteogenic and anti-inflammatory properties [81].

Historically, little focus has been placed on these *in situ* forming implants (ISIs) for their potential as scaffolds for new tissue growth. This is due to the dense, solid microstructure, which is not conducive to cellular infiltration [248], as well as the tendency of these implants to loosen within the periodontal pocket, which can also lead to fragments of polymer breaking off and dislodging.[246] Incorporation of degradable or soluble porogen particles into delivery systems improves the microstructure of these scaffolds [248], and incorporation of bioadhesive polymers and plasticizers was shown to improve adhesive properties [249]. The mechanical properties of ISIs, as well as the physical changes (i.e., swelling and microarchitectural changes), are important for periodontal applications, because the periodontal pocket presents a constrained geometry that is subject to cyclical stresses from chewing, and compared to the gingiva, PLGA is a stiff material prone to plastic deformation. Conceivably, a highly porous material that swells to fill the pocket and releases both antibiotic and osteogenic stimuli may be beneficial for future consideration as a scaffold for tissue regeneration. Biodegradable poly(β-amino ester) (PBAE) hydrogel microparticles have been used previously to modulate both drug release and microarchitecture of PLGA ISIs designed for orthopedic applications [81]. A first step towards testing adapting PBAE-loaded PLGA ISIs for periodontitis is to quantify the drug release and material changes due to these additives. Therefore, the aim of this study was to demonstrate acute antibiotic delivery accompanied by co-delivery of an antibiotic and an osteogenic agent from PBAE-containing PLGA ISIs, and to quantify the effects of these PBAE additives on swelling, degradation, microarchitecture, and mechanical properties.

5.2. Materials and Methods

5.2.1. Materials

Diethylene glycol diacrylate and poly(ethylene glycol) 400 diacrylate (PEG400DA) were bought from Polysciences, Inc. (Warrington, PA). 2,2-Dimethoxy-2-phenylacetophenone (DMPA), high molecular weight PLGA (HMW PLGA; 50:50 lactide:glycolide, 0.55-0.75 dL/g in hexafluoroisopropanol, carboxylate-terminated), low molecular weight PLGA (LMW PLGA; 50:50 lactide:glycolide, 0.15-0.25 dL/g in hexafluoroisopropanol, carboxylate terminated) were purchased from DURECT (Birmingham, AL). N-methyl-2-pyrrolidone (NMP), gelatin (from porcine skin, type A), glutaraldehyde (25%, grade I), agarose, trifluoroacetic acid (TFA), doxycycline hyclate, and glycine were obtained from Sigma Aldrich (St. Louis, MO). Simvastatin was from Haorui Pharma-Chem (Edison, NJ).

5.2.2. PBAE hydrogel preparation

PBAE macromer was created by reacting a diacrylate with isobutylamine at 85°C for 48 hours. Macromers were named according to the classification system from Anderson et al., in which the letter corresponds to a specific diacrylate and the number corresponds to a specific amine [69]. Thus, macromer made by reacting PEG400DA with isobutylamine for 48 hours was termed H6. A macromer containing a 2:1 molar ratio of diethylene glycol diacrylate:PEG400DA was also created, and will subsequently be referred to as AH6.

PBAE hydrogels were formed by adding 0.1% w/w DMPA, dissolved in ethanol, to the macromer, pipetting this mixture between two parallel glass plates, and exposing the mixture to a 365 nm UV flood source for 5 minutes to crosslink the macromer. The resulting hydrogels were washed overnight in ethanol to remove residual DMPA and unreacted monomers, and were stored in a desiccator until use.

PBAE microparticles were made by swelling PBAE hydrogels in ethanol for 1 hour and then grinding them with a mortar and pestle. The slurry was passed through a 250 µm sieve using an ethanol wash, and any larger particles were re-ground until 100% of the hydrogel was sieved. The microparticle slurry was lyophilized, and the resulting microparticles were stored in a desiccator.

5.2.3. Injectable mixture formulations

A PLGA solution was formed by dissolving 30% or 40% w/w of either HMW or LMW PLGA in NMP overnight. PBAE microparticles (H6, AH6, or a mixture of the two) were added to the PLGA solution at 10% w/w and stirred until the mixture was homogeneous. 2% w/w simvastatin or doxycycline (or 2% w/w each for co-delivery) were added to the PLGA-PBAE-NMP suspension and mixed thoroughly. Alternatively, doxycycline was pre-loaded into AH6 microparticles by swelling the microparticles with a 3 mg/mL doxycycline solution in acetone at a ratio of 100 mg AH6 to 500 µL of solution. These swollen particles were lyophilized for 24 hours, resulting in doxycycline pre-loaded into AH6 microparticles. Pre-loaded AH6 microparticles at 10% w/w in PLGA solutions were then used in drug release studies. HMW formulations containing simvastatin were tested first, and the most promising mixtures were used in subsequent tests with doxycycline and/or LMW PLGA. Table 5.1 contains a list of all scaffold formulations that were examined for these drug release studies.

Table 5.1. Scaffold formulations investigated for drug release. S = simvastatin. D = doxycycline. HMW = high molecular weight PLGA. LMW = low molecular weight PLGA. (Pre) indicates drug was pre-loaded into PBAE microparticles. "+" indicates co-delivery from the same scaffold.

Scaffold Name	PLGA	PLGA %	PBAE	Drugs
HMW-AH	HMW	30	AH6	S / D / S+D / D(Pre)
HMW-H	HMW	30	H6	S
HMW-H/AH	HMW	30	AH6+H6	S
HMW-Control	HMW	30	None	S / D
LMW-AH	LMW	30	AH6	S / D / S+D
LMW-Control	LMW	30	None	S / D / S+D
40LMW-AH	LMW	40	AH6	S / D / S+D / D(Pre)
40LMW-Control	LMW	40	None	S / D / S+D / D(Pre)

5.2.4. Microstructure and mass change

To observe changes in ISI mass and microstructure, the following drug-free formulations were prepared: HMW-AH, HMW-H, HMW-H/AH, HMW-Control, LMW-AH, and LMW-Control (Table 5.1). In a 96-well plate, approximately 10 mg of injectable scaffold mixture was injected dropwise from an 18-gauge needle into 300 µL PBS. The syringe was weighed after each injection to calculate the mass of each scaffold. PBS was replaced daily to prevent buildup of degradation byproducts. At each time point, 3 scaffolds from each group were removed, dabbed dry, and weighed to measure the wet mass. For HMW scaffolds, scaffolds were collected at 1 day and 5 days following the injection, and for every 5 days thereafter. For LMW scaffolds, scaffolds were collected at 1 day, 2 days, and every other day thereafter. All collected ISIs were lyophilized for 24 hours and weighed again to determine dry mass. HMW scaffolds were then scanned using a SCANCO MicroCT 40 (SCANCO Medical AG, Switzerland) with X-ray parameters of 55 kV and 145 mA, and a 6 µm voxel size. A built-in bone trabecular morphometry analysis tool was used to create 3-D reconstructions, and measurements of porosity, mean pore size, and material density were conducted. To quantify accessible volume and surface area,

simulated mercury intrusion porosimetry was run on the 3-D reconstructions using an included script. At select time points, samples were freeze-fractured, and a Hitachi S-4300 scanning electron microscope (SEM) at 4 kV accelerating voltage was used to visualize the microarchitecture of scaffolds.

5.2.5. Mechanical tests

All mechanical tests were performed with a Bose ELF 3300 system. Gelatin slabs (20%) measuring 8 mm thick was prepared, and were crosslinked by immersing overnight in 5 mM glutaraldehyde. The aldehyde groups were quenched by immersing crosslinked gelatin slabs in a 50 mM glycine solution for 2 hours and washing serially in deionized water. Cylindrical samples (4 mm in diameter) were punched out of the slabs, and their mechanical properties were characterized by compressing these cylindrical samples to 10% strain at a frequency of 1 Hz for 30 seconds to mimic chewing conditions [250]. The slabs containing cylindrical holes were used as molds to inject HMW-Control and HMW-AH scaffolds measuring 8 mm length by 4 mm diameter. After injection, the molds were capped with 2% agarose slabs, clamped shut lightly to prevent extrusion of material due to swelling, and immersed in PBS. After 3, 6, 9, 12, or 15 days, the solidified samples within the molds were subjected to a displacement rate of 0.5 mm/sec. The interfacial shear strength required for push-out was calculated by dividing the maximum push-out force by the scaffold surface area in contact with the mold. Cylindrical scaffolds that had been pushed out of their molds were tested for their compressive properties under 1% strain triangular waves applied at a frequency of 1 Hz for 60 seconds. The initial modulus was determined from the first compression cycle, and the equilibrium modulus was measured during the final cycle. Resilience was calculated by integrating the linear region of the stress-strain curve.

5.2.6. Drug release

Approximately 100 mg of each mixture (Table 5.1) was injected dropwise into 1 mL PBS (n=3), where the PLGA rapidly solidified into droplet-shaped scaffolds. At each time point, supernatant was entirely removed, stored in a refrigerator, and replaced with fresh PBS. A Hitachi Primaide HPLC system with a C18 column was run isocractically at 1 mL/min with a mobile phase composed of 70% acetonitrile / 30% water + 0.1% TFA to detect simvastatin at 240 nm. Collected supernatant was mixed with ethanol at a 2:1 supernatant:ethanol ratio to dissolve any precipitated simvastatin prior to HPLC analysis. Doxycycline was assayed using a mobile phase composed of 30% acetonitrile / 70% water + 0.1% TFA running at 1 mL/min and with detection at 350 nm.

5.3. Results

5.3.1. Mass change

HMW-Controls exhibited little dry mass change through the first 15 days of degradation, after which a linear decrease in mass of 4.8%/day occurred through day 30 (Figure 1A). A significant ($p<0.05$) decrease in mass was observed at each time point from day 20 and onward. Over the first 5 days, the wet mass of these scaffolds decreased significantly ($p<0.05$) at a rate of 9.4%/day, then increased slightly between days 10 and 20, before gradually declining through day 35, although none of these later changes was significant (Figure 1B). Both HMW-AH and HMW-H/AH scaffolds exhibited a small wet mass loss in the first day, followed by a relatively linear 6.5%/day wet mass increase through day 30 to a maximum of 273% of original mass. At day 35, scaffolds fell apart upon handling and measurable mass decreased to 93% of the initial. HMW-H scaffolds had a larger wet mass loss of 37% ($p<0.05$) after 1 day, and between days 5 and 25, an 8.6%/day mass increase occurred. A plateau was reached between days 25 and 30 prior to a large decrease in mass at day 35. After a 1-day dry mass loss of 12%, HMW-AH

scaffolds lost mass at a rate of 1.7%/day until day 10. Mass loss resumed at day 15 and continued at a rate of 0.87%/day until day 30. HMW-H/AH scaffolds had a dry mass loss of 26% after day 1, and no significant mass change followed through day 30. Similarly, HMW-H scaffolds exhibited a large initial dry mass loss of 38% after 1 day, and no significant subsequent mass loss occurred until day 30 ($p<0.05$).

LMW-Controls exhibited a gradual dry mass decrease to 89% after 8 days, after which the mass decreased linearly at a rate of 3%/day through day 30 (Figure 5.1C). LMW-Control wet mass rapidly increased to 193% through the first 5 days, then sharply declined and fluctuated around 150% through day 16 (Figure 5.1D). Beyond day 16, a linear mass loss of 7%/day occurred through day 30. LMW-AH scaffolds decreased steadily in dry mass at a rate of 5%/day for the first 8 days, followed by a brief plateau through 12 days, and terminating with a linear mass loss of 2%/day through day 30. LMW-AH wet mass increased for the first 5 days and plateaued, fluctuating around 150% through day 16. After day 16, a mass loss of 7%/day occurred through day 30.

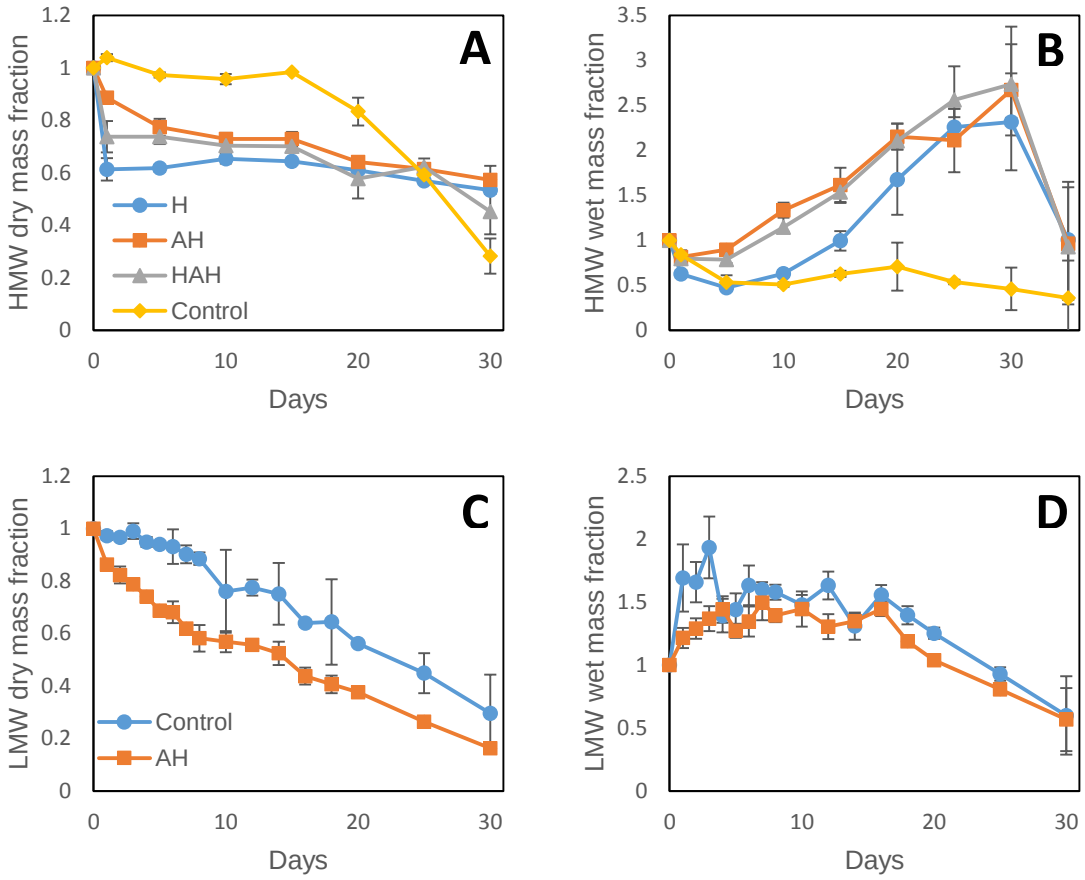

Figure 5.1. Mass loss of ISIs. Remaining dry mass of A) HMW scaffolds and C) LMW scaffolds. Remaining wet mass of B) HMW scaffolds and D) LMW scaffolds. Data are mean +/- standard deviation (n=3).

5.3.2. Microarchitecture

The microarchitecture of HMW-Controls changed dramatically throughout the first 15 days of degradation, leading to collapse, while HMW ISIs containing PBAE additives possessed a more uniform pore structure and swelled visibly throughout the 15 day period (Figure 5.2). After 1 day, HMW-Controls were composed of a dense solid phase with large, homogeneously distributed spherical pores. By day 5, some large pores remained in the core of the scaffold, while most were present near the edges and were oriented radially. By day 10, the radial pores were more numerous, surrounding the dense core, and by day 15, the scaffolds had collapsed.

HMW-H scaffolds possessed a uniformly porous microstructure by day 1, and there were little microstructural changes until day 15, when noticeable swelling had occurred. HMW-AH and HMW-H/AH scaffolds both initially possessed porous networks with radiopaque regions inside these pores, which is indicative of non-degraded PBAE material (Figure 2, arrows). By day 5, scaffolds were noticeably swollen, and there was little evidence of non-degraded PBAE material, resulting in a uniformly porous microstructure; the swelling increased progressively through day 15. None of the scaffolds containing PBAE additives collapsed within the 15-day period.

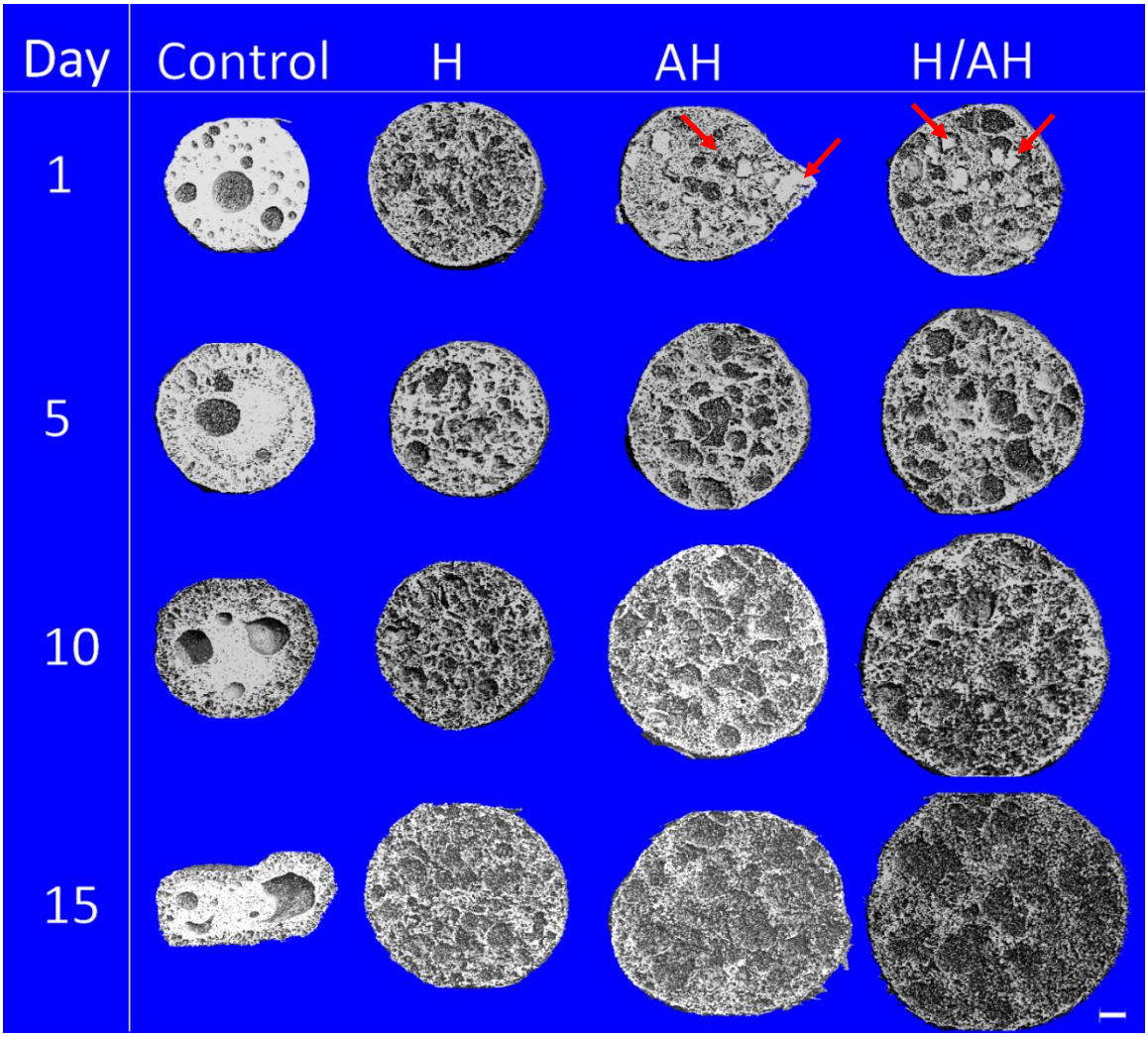

Figure 5.2. 3-D micro CT reconstructions, bisected, of HMW ISIs containing no additives (Control) or 10% PBAE particles (H, AH, or H/AH). White indicates material present in the cut plane. Arrows indicate solid material within pores

HMW ISIs generally increased in both porosity (Figure 5.3A) and volume (Figure 5.3B) as they degraded. Specifically, HMW-Controls initially possessed 24% porosity, which increased to a maximum of 54% at day 10, and then declined slightly to 46% by day 15. All PBAE-containing scaffolds steadily increased throughout the 15-day period, with initial porosities ranging from 42% (HMW-AH) to 55% (HMW-H). All PBAE-containing ISIs possessed significantly higher

porosities than HMW-Controls at all time points ($p<0.001$). Among PBAE-containing ISIs, only HMW-AH at day 1 differed significantly in porosity from others. Scaffold volume, normalized to initial mass, showed that HMW-Controls increased slightly in volume by day 5 before gradually declining (Figure 3B), and had significantly lower volume than all PBAE groups throughout degradation ($p<0.01$). HMW-H exhibited an initial decrease in scaffold volume between days 1 and 5, followed by a linear increase beyond the initial volume by day 15. Both HMW-AH and HMW-H/AH generally increased in volume throughout the 15 day period.

Accessible volume was measured for various simulated penetrating sphere diameters ranging from 12 μm to 120 μm, and the volume accessible by a 24 μm sphere was compared between groups over 15 days (Figure 5.3C). This diameter approximates the size of the progenitor cells that may migrate into these pores [251, 252]. At day 1, HMW-Control and HMW-AH possessed significantly lower accessible volume than HMW-H and HMW-AH samples ($p<0.01$). At day 5 and beyond, all PBAE-containing ISIs possessed similar accessible volumes, which increased from 34-38% at day 5 to 65-78% by day 15. From days 5 through 15, controls had significantly lower accessible volume ($p<0.001$). Accessible surface area was normalized to initial scaffold mass, and measured using the same 24 μm penetrating sphere size (Figure 5.3D). The trends for accessible surface area were similar to accessible volume, with HMW-Control and HMW-AH initially possessing significantly lower values than HMW-H and HMW-AH ($p<0.01$). Controls remained significantly lower than all other groups for each subsequent time point ($p<0.001$). HMW-AH increased linearly in accessible surface area through day 15 before plateauing, while both HMW-H/AH steadily increased in accessible surface area throughout degradation. HMW-H remained relatively unchanged between days 1-5 before increasing linearly through day 15.

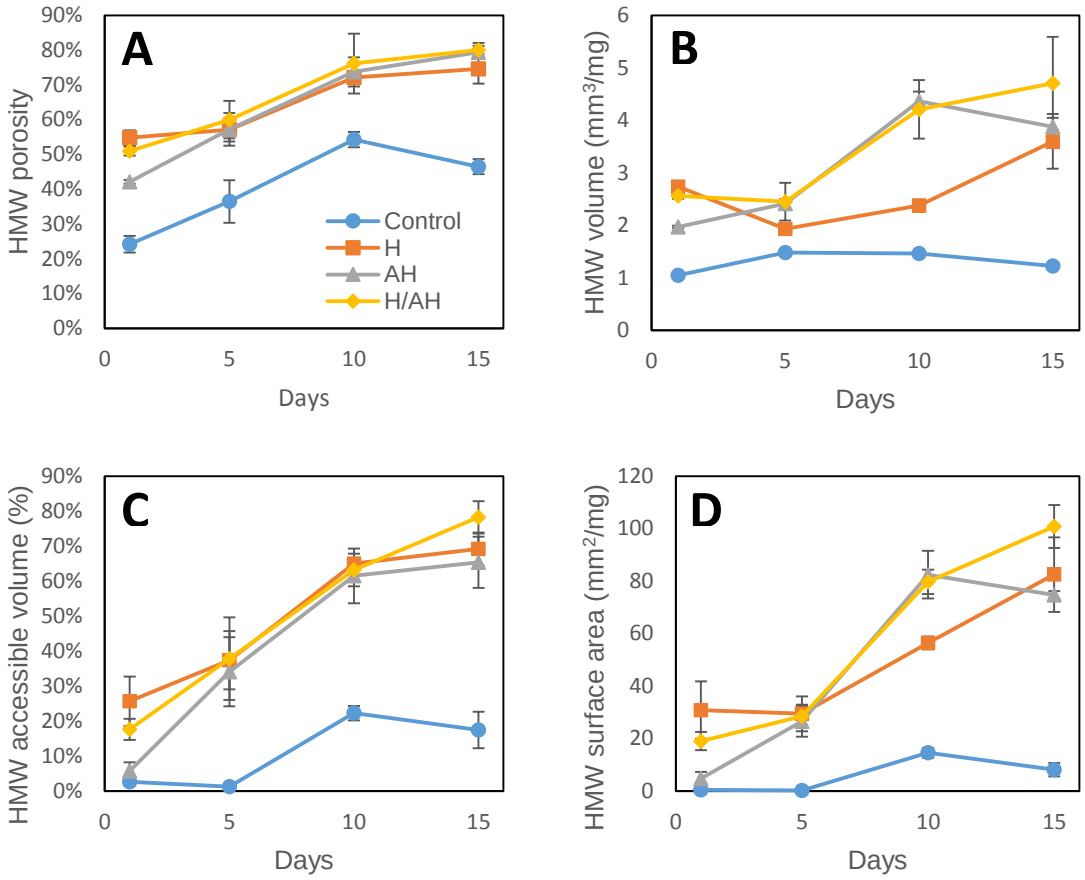

Figure 5.3. Microarchitecture of HMW scaffolds throughout degradation. A) Porosity and B) mass-normalized volume of scaffolds, evaluated using micro CT. Accessibility of C) scaffold volume and D) mass-normalized surface area to a simulated 24 µm sphere. Data are mean ± standard deviation (n=3).

5.3.3. Interfacial strength and mechanical properties

The interfacial strength in cylindrical gelatin molds, as measured by maximum push-out force, decreased over 15 days for HMW-Controls and increased over the same period for HMW-AH (Figure 5.4). For HMW-Controls, at 3 days, the interfacial strength was 1.2 kPa, and decreased relatively linearly until it was significantly reduced to 0.5 kPa by day 12 ($p<0.05$). The interfacial strength of HMW-AH samples increased significantly from 4.7 kPa at day 3 to 8.8 at day 6 ($p<0.01$), and the interfacial strength continued to increase, although not significantly, to

11 kPa by day 15. At every time point, the interfacial strength of HMW-AH significantly exceeded that of HMW-Controls ($p<0.001$).

LMW samples exhibited a less dramatic difference between AH and Control groups (Figure 5.4). LMW-Controls remained significantly higher than HMW-Controls and lower than HMW-AH at all time points ($p<0.01$), with interfacial strengths ranging from 2.7 to 5 kPa. LMW-AH interfacial strength increased from 5.2 at day 3 to 8.7 by day 9, then decreased down to 5.3 by day 15. LMW-AH samples possessed significantly higher interfacial strength than LMW-Controls for the first 12 days tested ($p<0.005$), and the interface remained similar to HMW-AH samples until days 12 and 14, which were both significantly lower than corresponding HMW-AH interfacial strengths ($p<0.01$).

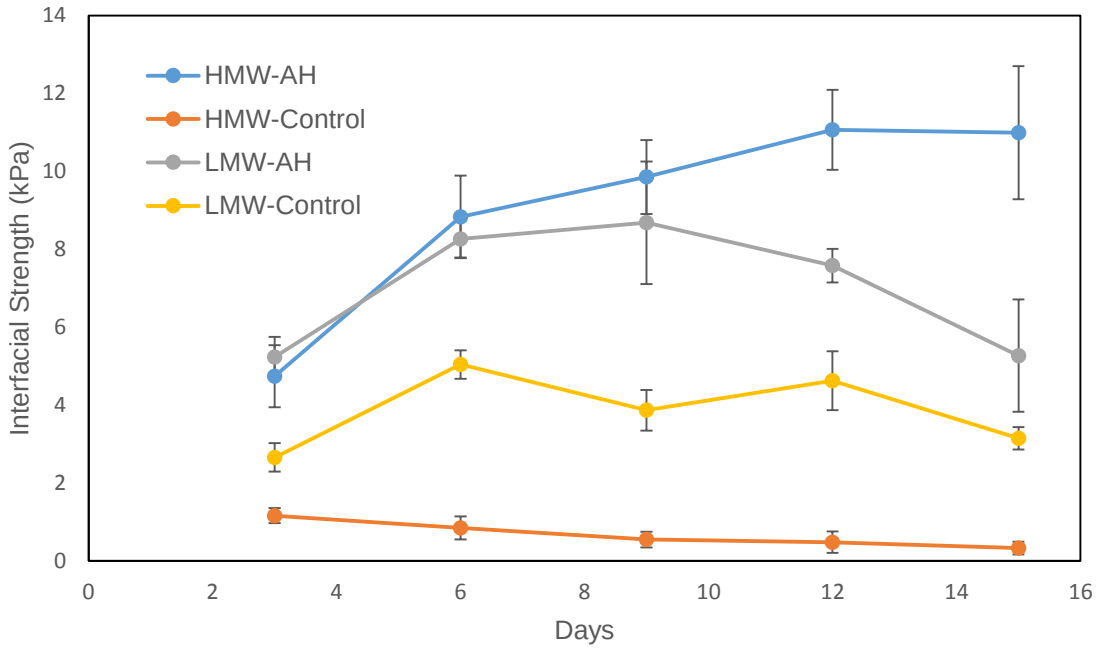

Figure 5.4. Interfacial strength measured from push-out tests on cylindrical samples within gelatin molds. Data are mean ± standard deviation (n=3).

Both HMW-Control and HMW-AH cylindrical samples exhibited initial and 30-cycle compressive moduli that remained unchanged through the first 9 days, followed by a decrease

through day 15 (Figure 5.5A). For HMW-Controls, initial modulus ranged between 48 and 61 MPa through the first 12 days, and then a significant decrease to 25 MPa occurred ($p<0.01$). Significant changes in HMW-AH samples were detected only between day 15 and days 6 or 9 ($p<0.05$), and over the 15-day period, these moduli ranged from a minimum of 14 MPa at day 15 to 29 MPa at day 9. The 30-cycle modulus did not change in HMW-Controls for the first 9 days, with moduli ranging from 94 to 102 MPa. Significant decreases occurred at day 12, to 58 MPa, and at day 15, to 17 MPa ($p<0.0001$). Modulus ranged from 24 MPa at day 3 to 34 MPa by day 9, and then decreased significantly to 14 MPa by day 15 ($p<0.001$). The ratio of the initial to the 30-cycle modulus did not change significantly throughout the 15 day period in HMW-AH samples, and it ranged from 0.95 at day 15 to 1.16 at day 9 (Figure 5.5B). In HMW-Controls, the modulus ratio ranged from 1.67 to 1.88 over the first 9 days, and then decreased significantly to 1.2 by day 12 and 0.7 by day 15 ($p<0.01$).

HMW-Controls and HMW-AH samples increased in resilience between days 3 and 6 before declining through day 15, and HMW-Controls exhibited the highest initial resilience and the lowest 30-cycle resilience (Figure 5.5C). Resilience from the initial compression cycle of HMW-Controls increased significantly from 1 J/m^3 at day 3 to 3.1 J/m^3 at day 6 ($p<0.0001$), and then decreased significantly at day 12 to 0.97 J/m^3 ($p<0.0001$). The 30-cycle resilience followed the same trend, with 0.35 J/m^3 at day 3, which increased significantly to 0.9 J/m^3 by day 6, then dropped significantly to 0.25 J/m^3 by day 12 ($p<0.001$). The ratio of the initial to the 30-cycle resilience through the first 12 days ranged from 0.26 to 0.33, and a significant decrease occurred between days 9 and 15, down to 0.15 ($p<0.05$) (Figure 5.5D). HMW-AH initial resilience increased significantly between days 3 and 6, from 0.73 to 1.7 J/m^3 ($p<0.001$). The resilience did not change until day 15, when a significant decrease occurred from 1.53 J/m^3 at day 9 to 0.79 J/m^3 at day 15 ($p<0.01$). The 30-cycle modulus of HMW-AH samples increased significantly from

0.46 J/m^3 at day 3 to 1.28 J/m^3 at day 6 ($p<0.0001$), with subsequent significant decreases at day 12, to 0.83 J/m^3 ($p<0.01$), and at day 15, to 0.52 J/$m^3$3 ($p<0.05$). The ratio of these two resilience values for HMW-AH samples did not change significantly throughout the 15 day period.

LMW-Controls possessed uniformly higher ratios of initial to 30-cycle modulus at each time point compared to LMW-AH, though this difference was only significant at days 3 and 12 ($p<0.05$) (Figure 5.5F). Similar to HMW samples, LMW-AH samples exhibited an initial to 30-cycle modulus ratio ranging from 0.94 to 1.13. While LMW-Control initial modulus increased steadily from 3.2 to 8.6 MPa between days 3 and 12, LMW-AH initial modulus fluctuated from 3.7 to 12 MPa, with a maximum at 9 days and a minimum at 12 days, resulting in no clear trend (Figure 5.5E). The initial resilience of both LMW-AH and LMW-Control was highest at day 12, and in all cases, the 30-cycle resilience was lower than the initial value for both LMW-AH and LMW-Control (Figure 5.5G). However, the ratio of initial to 30-cycle resilience of LMW-AH, ranging from 0.46 to 0.56, was significantly higher at every time point than the same ratio for LMW-Control ($p<0.05$), which ranged from 0.15 to 0.33 (Figure 5.5H).

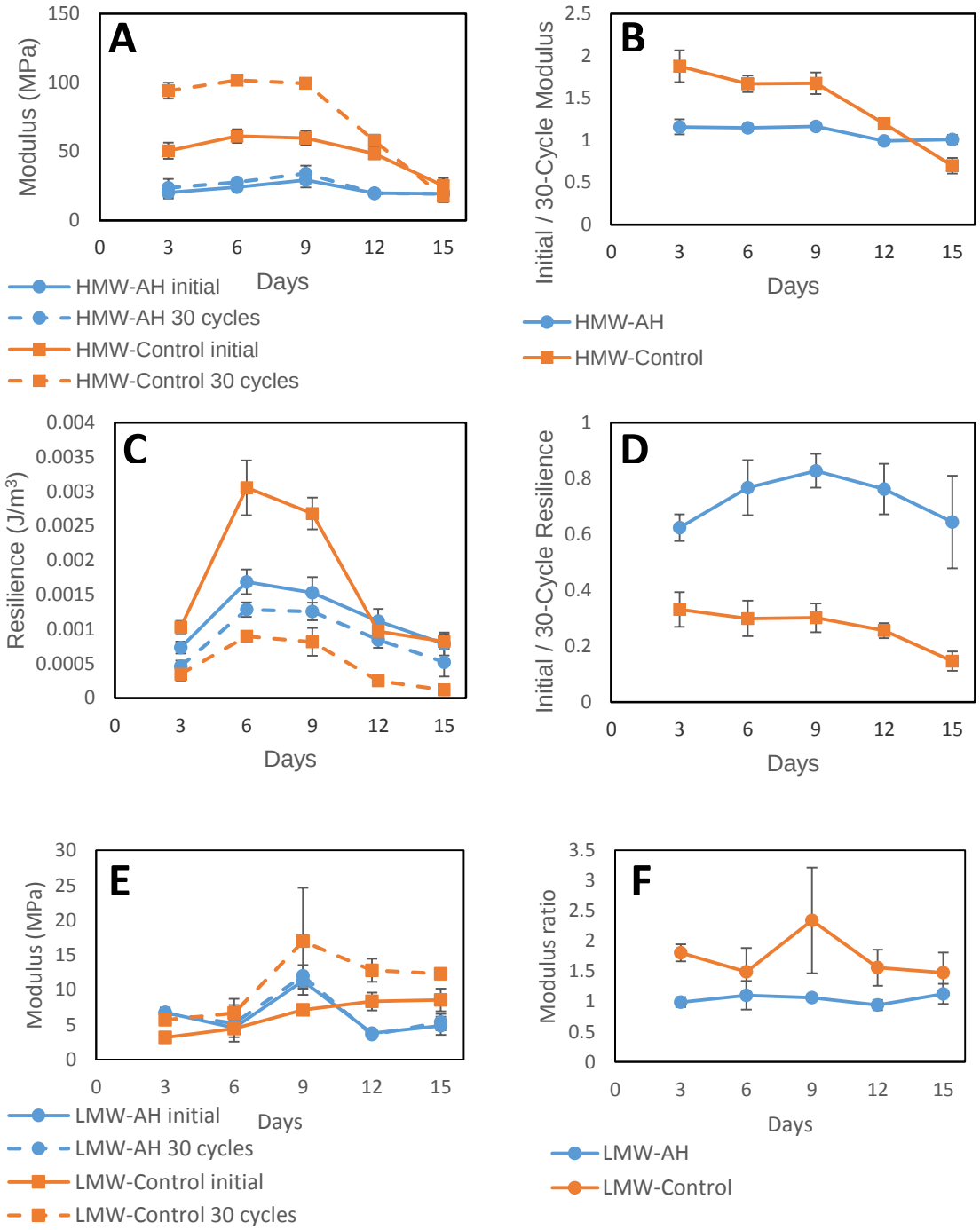
A
Modulus (MPa)
150
100
50
0
0
3
6
9
12
15
Days
HMW-AH initial
HMW-AH 30 cycles
HMW-Control initial
HMW-Control 30 cycles
B
Initial / 30-Cycle Modulus
2.5
2
1.5
1
0.5
0
Days
HMW-AH
HMW-Control
C
Resilience (J/m3)
0.004
0.0035
0.003
0.0025
0.002
0.0015
0.001
0.0005
0
Days
D
Initial / 30-Cycle Resilience
1
0.8
0.6
0.4
0.2
0
Days
E
Modulus (MPa)
30
25
20
15
10
5
0
Days
LMW-AH initial
LMW-AH 30 cycles
LMW-Control initial
LMW-Control 30 cycles
F
Modulus ratio
3.5
3
2.5
2
1.5
1
0.5
0
Days
LMW-AH
LMW-Control

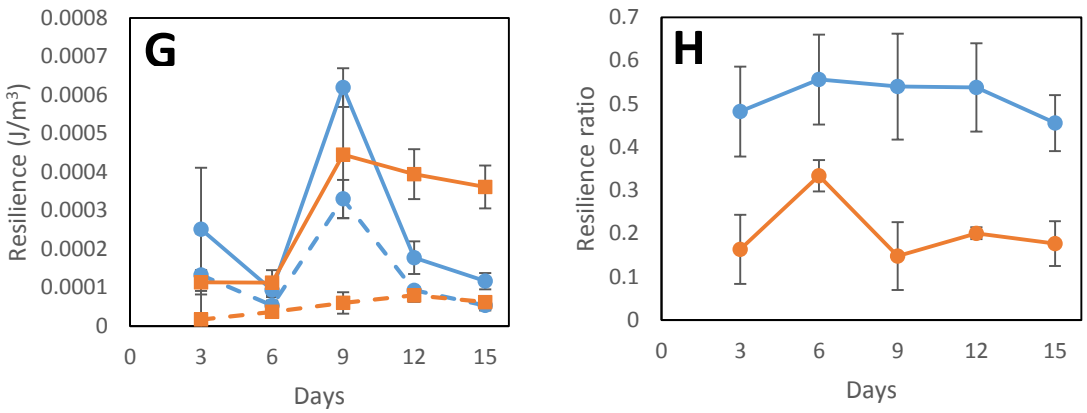

Figure 5.5. Mechanical properties of HMW (A-D) and LMW (E-H) cylindrical implants subjected to 30 cycles of 1% compressive strain at 1 Hz. A,E) Initial and 30-cycle modulus. B,F) Ratio of initial to 30-cycle modulus. C,G) Initial and 30-cycle resilience. D,H) Ratio of initial to 30-cycle resilience. Data are mean ± standard deviation (n=3).

5.3.4. Drug Release

HMW scaffolds loaded with simvastatin released simvastatin over 90 days, and scaffolds containing PBAE microparticles produced release profiles with distinct regions of different release rates (Figure 5.6A). HMW-Controls exhibited a significantly higher 1-day burst of 36% ($p<0.001$), compared to all PBAE-containing groups, which all had a burst of 6% or less. HMW-Controls exhibited a declining daily release rate over the course of 40 days, with residual simvastatin released over the last 40 days as scaffolds completely degraded. HMW-H exhibited a relatively linear release rate of 1%/day through day 30, followed by a period of minimal release through day 60. HMW-AH had a release rate of 2.8%/day for the first 13 days, followed by a period of 1%/day through day 30 and then 0.25%/day through day 50. HMW-H/AH had release rates of 2.1%/day through day 13, 1%/day through day 30, and then 0.2%/day through day 50. Beyond day 60, the remaining drug was released through day 90 as scaffolds completely degraded.

LMW scaffolds released simvastatin through 30 days, and AH6 microparticle additives reduced burst for each formulation (Figure 5.6B). LMW-Controls had 47% burst followed by a roughly linear release rate of 2.1%/day through day 30. The burst was reduced to 21% for 40LMW-Controls, after which the release rate steadily declined through day 30. There was no difference in simvastatin release kinetics between LMW-AH scaffolds containing simvastatin alone or doxycycline and simvastatin together. Both LMW-AH and 40LMW-AH scaffolds had no appreciable burst, and linear release rates ranged from 2.3 to 2.5%/day through days 24 and 26, respectively. At day 24 or 26, the release rate increased to 10%/day until all drug was released.

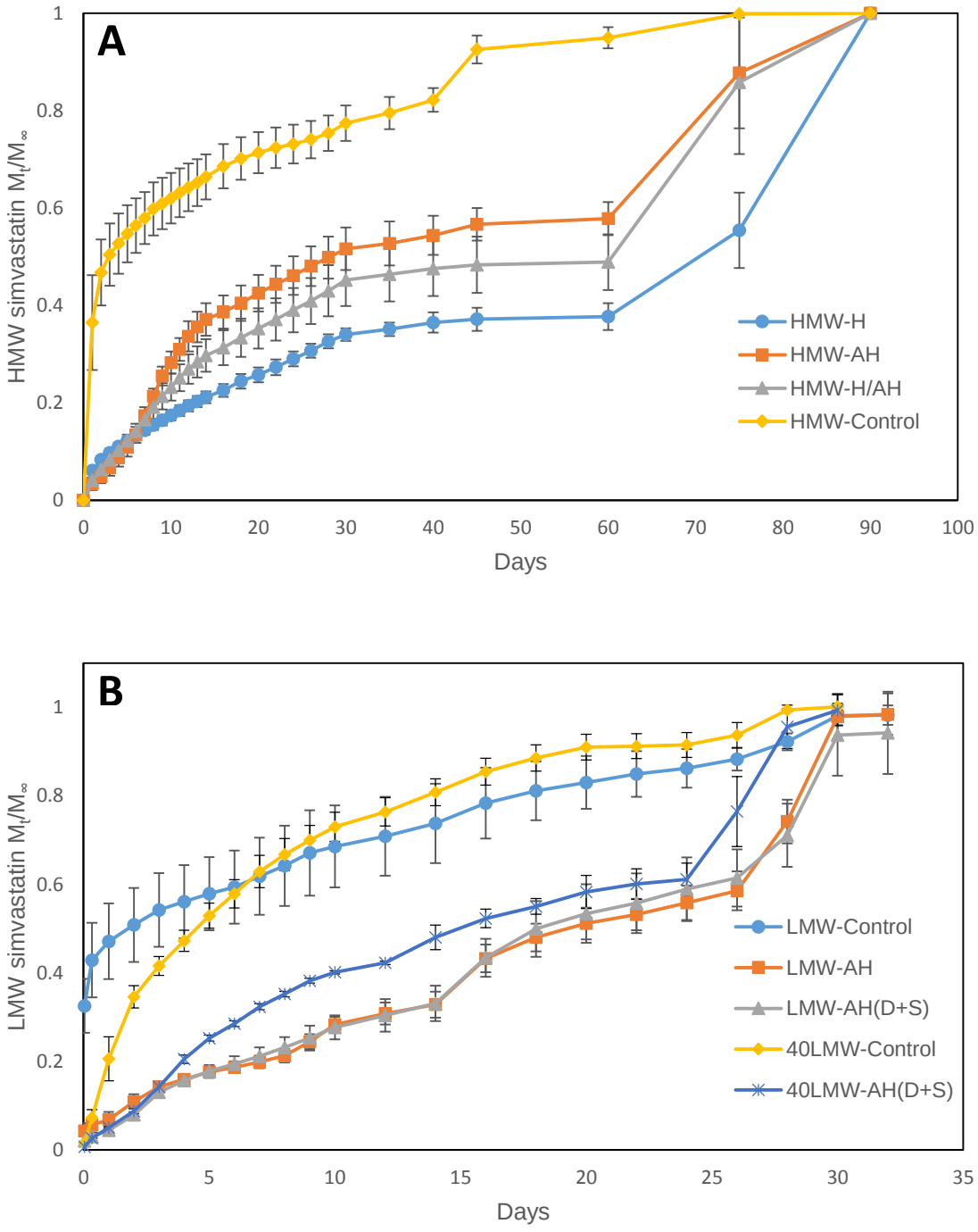

Figure 5.6. Simvastatin release from A) HMW and B) LMW scaffolds. D+S indicates that scaffolds were co-loaded with simvastatin and doxycycline. Data are mean ± standard deviation (n=3).

Doxycycline exhibited similar release patterns from both HMW (Figure 5.7A) and LMW ISIs (Figure 5.7B), with no difference observed between PBAE-containing scaffolds and controls. Pre-loading doxycycline into PBAE microparticles resulted in a 1-day burst similar to controls, but with significantly more drug released over the remainder of the week. In all cases where the antibiotic was not pre-loaded into AH6 microparticles, the release plateaued within one or two days, and drug was released incrementally for the remainder of the monitored period. In all HMW ISIs tested, release plateaued at approximately 70% of total drug, and pre-loaded doxycycline released an additional 28% over the following 6 days. In LMW ISIs, the plateau ranged from 86-95% for 30% PLGA and from 63-74% in 40% PLGA. 40% LMW PLGA ISIs were tested with pre-loaded doxycycline, and after an initial 63% burst, release continued up to 87% by day 7.

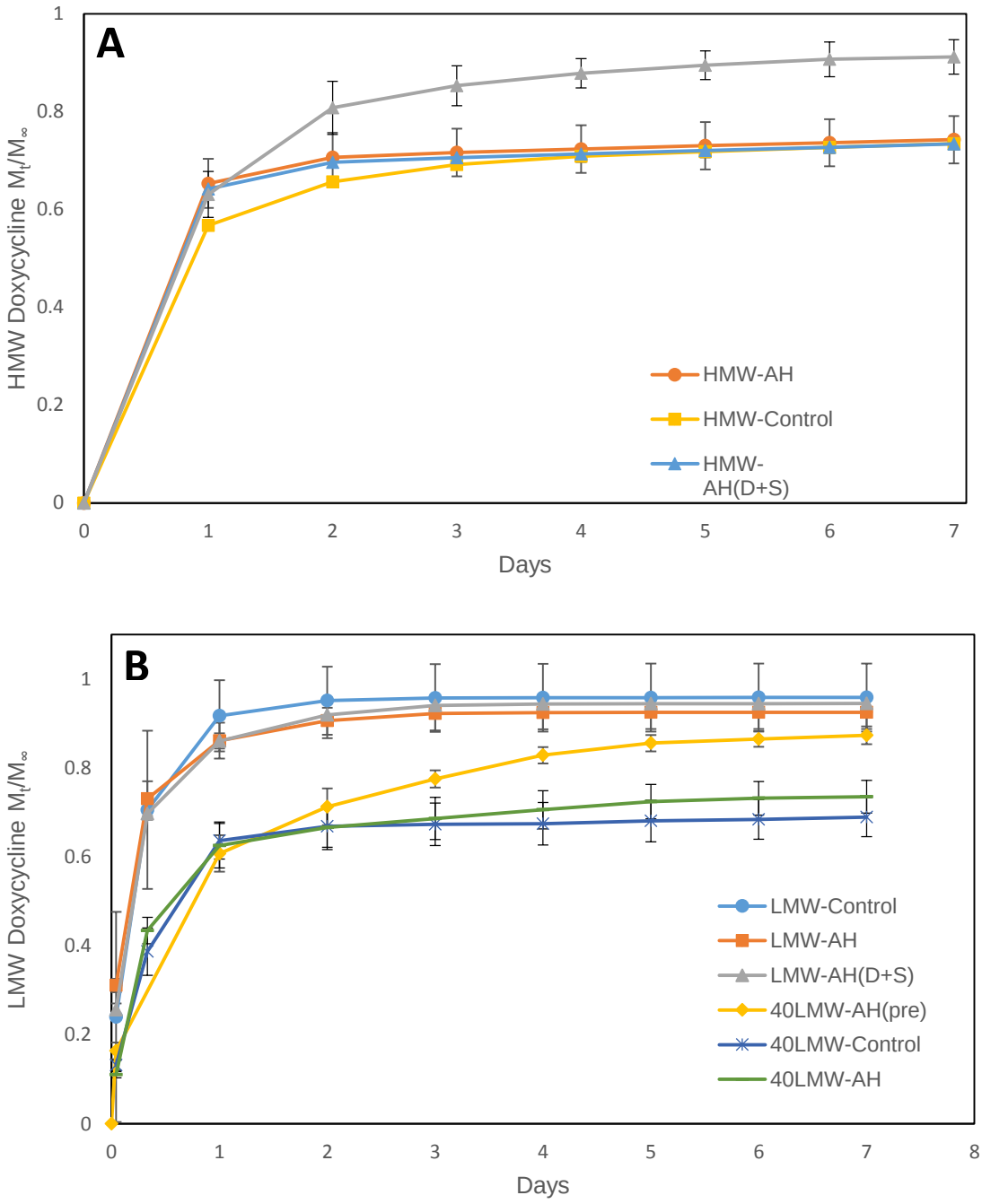

Figure 5.7. Doxycycline release from A) HMW and B) LMW ISIs. D+S indicates that scaffolds were co-loaded with simvastatin and doxycycline. Data are mean ± standard deviation (n=3).

5.4. Discussion

PBAE additives act as both porogens and drug delivery vehicles within the solid PLGA ISI matrix. As porogens,the 1-day mass loss of HMW-H and HMW-H/AH scaffolds indicated complete degradation of H6, which has an expected degradation time of 4-8 hours [70], while both HMW-AH and LMW-AH scaffolds exhibited a gradual mass loss through 10 days, which is twice the 5 day *in vitro* degradation time of AH6 PBAEs [253]. The difference is probably due to the PLGA matrix both limiting the accessibility of water to the embedded PBAE microparticles and physically restraining them from swelling, thus slowing degradation [80, 254]. There is evidence that PBAE swelling is restricted by comparing the microCT cutplanes and implant volumes between groups, in which HMW-H, which contains the most hydrophilic PBAE, swelled more gradually and to a smaller degree than HMW-H and HMW-H/AH formulations. Theoretically, H6 should achieve greater maximum swelling than AH6, and the maximum swelling point should occur at 4 hours and 36 hours, respectively [255]. HMW-H scaffolds likely had delayed degradation of the PBAE as well, however, the daily sampling frequency would not detect a difference unless the degradation period of H6, which typically degrades in 4-8 hours [70], was prolonged beyond 24 hours. The failure of HMW-Controls to swell beyond their initial mass suggests that the loss of NMP during precipitation exceeded the water uptake of the scaffolds. Conversely, LMW-Controls were capable of entrapping water in the core of the scaffolds due to their less hydrophobic nature, and the rapid decrease in wet mass after day 3 was caused by the fragile PLGA skin rupturing, allowing the entrapped buffer to leak out. Interestingly, all HMW scaffolds containing PBAE microparticles swelled up to 250% of their original mass over a period of 30 days, while comparable LMW scaffolds swelled to a maximum of 150%. Again, LMW scaffolds were prone to rupture, which would allow water to escape, while the HMW scaffolds remained structurally sound as they swelled, and therefore

maintained a larger water capacity. Prior research on similar systems containing porogens such as sucrose or sodium chloride did not show such a dramatic mass changes [248], which suggests that the swelling behavior of PBAE hydrogel particles has a more profound effect on water uptake and retention than traditional porogens.

PBAE microparticles also influence macro- and microstructural changes of ISIs as they degrade. HMW-Controls possessed surface-adjacent smaller pores and centrally-located macropores, which is typical of these implants because PLGA at the surface tends to precipitate rapidly, while the interior precipitates more gradually, allowing voids to coalesce [141]. PBAE microparticles caused the ISIs to adopt a porous network with no difference between surface or central pore sizes, because the homogeneous distribution of hydrogel microparticles acted as a template for a uniform PLGA microstructure. This hypothesis is supported by the rapid swelling and increase in accessible volume observed in all PBAE-containing ISIs. The lack of collapse in HMW-AH, -H, or H/AH implants implies that these homogeneously distributed hydrogel particles also play a role in stabilizing the implant structurally. In HMW-Controls, the largest pores collapsed, whereas in PBAE-containing scaffolds, with their uniform microstructures, were able to distribute stresses throughout the PLGA matrix and did not collapse. It has been previously demonstrated that varying the size and distribution of pores can dramatically alter mechanical properties of materials [256, 257]. The lattice-like PLGA network of PBAE-containing implants may also help explain the sustained mechanical resilience observed in HMW-AH implants even after the degradation period of the PBAE had passed. The increased porosity and accessible surface area of PBAE-containing ISIs offers many advantages when considering PLGA ISIs as potential scaffolds rather than simply drug delivery devices. In pre-formed PLGA scaffolds, larger accessible volume and surface area provides more opportunity for tissue ingrowth, and it is anticipated that PLGA ISIs will behave similarly in future cell culture or *in vivo* testing.

A persistent issue with antibiotic-releasing implants in periodontal applications is that the implant is not secure inside the periodontal pocket, which can lead to small pieces breaking off as the implant moves within the space [258]. Here, push-out forces were used to measure the interfacial strength between the implant surface and a simulated tissue pocket. The opposing trends observed in push-out force for HMW-Control compared to HMW-AH samples indicate that swelling of AH hydrogels can improve space-filling and pocket retention of implants. Even at the initial 3-day measurement, HMW-AH samples had significantly higher interfacial strength than controls, and this difference became even more pronounced as the incubation period increased. Although HMW PLGA does swell to a small degree as it degrades, this behavior is offset by the shrinkage of the implant during the precipitation phase, and the net result is that the interfacial strength remains negligible. On the other hand, AH hydrogels were observed to swell beyond 200% of their initial mass within 2 days in PBS (data not shown), and although this effect is probably muted due to the physical constraint within the PLGA matrix, there is enough of an effect to provide 4 to 10-fold higher interfacial strength than controls. Preliminary studies also showed no measurable adhesion between the gelatin surface and the implants (data not shown), so any differences in interfacial strength should be solely a result of the superior space-filling due to swelling of HMW-AH implants. LMW-AH scaffolds exhibited a similar benefit compared to LMW-Controls, though this difference was less pronounced due to the natural swelling behavior of LMW-Controls, which increased interfacial strength, and the rapid degradation of material, which caused both LMW-Controls and LMW-AH to decrease in strength over the 15 day period. A scaffold that expands to fill its injection site as it solidifies is less likely to cause irritation due to movement within the pocket. Furthermore, more contact area between the implant and the tissue means that the released drug has a shorter path to enter the gingival tissue, and it has a smaller likelihood of being washed away

due to fluid exchange in the crevicular fluid. Unfortunately, little information is available on the magnitude of stresses experienced within gingival soft tissue, although it is widely reported that the periodontal ligament is the soft tissue responsible for transmitting chewing force between the tooth and the underlying alveolar bone [259, 260]. Measurements of the stress in oral mucosal tissues under typical bite forces of denture wearers suggested that these tissues experiences compressive stresses ranging from 5 to 40 kPa during chewing [261]. According to these values, HMW-AH ISIs have initial interfacial strengths within that range, and within 6 days the interfacial strength exceeds the stress generated by a soft bite. HMW-Controls at every time point possessed interfacial strengths 1-2 orders of magnitude lower than these stress ranges. This data suggests that patients receiving HMW-AH ISIs may be able to chew food shortly after receiving treatment without danger of loosening the implant, while controls, which approximate clinically available treatments, are easily loosened and dislodged. This swelling-based, space-filling approach is an alternative to other avenues that seek to reduce detachment by improving the adhesion between the polymer surface and surrounding tissue [249]. While the bioadhesion approach was observed in the first several hours following implantation, the PBAE-containing ISIs were demonstrated to improve pocket retention through a 15-day period. An interesting approach for future studies may be to incorporate both bioadhesive and swelling additives in order to provide acute attachment followed by prolonged space-filling.

Although these periodontal ISIs are not designed as load-bearing structures, they are subject to stresses, primarily due to chewing, which typically occurs at frequencies between 0.1 and 1 Hz in humans [262]. The gelatin molds used in push-out studies had similar compressive modulus compared to gingival tissues in order to simulate a periodontal pocket (data not shown) [250]. It has been proposed that less stiff implants may reduce irritation due to the presence of material within the periodontal pocket [263]. PLGA deformed plastically and

became stiffer under compression even at low strains and only 30 compression cycles, while the modulus of HMW-AH and LMW-AH samples remained unchanged, indicating that PBAE additives preserve elasticity. In the commercially available Atridox® system, a dressing or adhesive is used to keep the implant in place, but there is also the concern that repeated compression cycles can cause the implants to break apart, allowing pieces of material to cause local irritation, or escape the periodontal pocket [264, 265]. Therefore, flossing and brushing are discouraged for up to a week following implantation, and patients are told to expect small pieces of material to break off [265]. Although neither control nor PBAE-containing ISIs broke apart during the timeframe or compression cycles observed, the 30-cycle modulus of HMW-Controls was reduced dramatically between 9 and 15 days, and this difference would likely become more pronounced as time or compression cycles increased. HMW-AH and LMW-AH samples were less stiff and retained their modulus throughout cyclic compression, which suggests they are more suitable to withstand the dynamic mechanical environment of the periodontal tissue. HMW-Controls and LMW-Controls were more resilient during the initial compression cycle, yet they were consistently less resilient than corresponding AH-containing implants after 30 cycles, indicating that the PBAE hydrogel component helps preserve resilience. The lack of change for both modulus and resilience after cyclic loading is promising for the development of more mechanically suitable implants for the periodontal pocket. Dynamic mechanical analysis is required to assess viscoelastic properties for full lifespan of the implant, but this short-term cyclic compression data suggests that the addition of only 10% hydrogel particles can greatly improve the durability of these implants. As mentioned previously, the addition of PBAE microparticles led to a lattice-like PLGA microstructure, which should theoretically provide more resilience than the heterogeneous structure of the controls because there are no macropores, which appear to be the source of collapse in controls. Oral soft tissues

have compressive moduli ranging from 0.2 to 8 MPa [250, 266], and typical dental materials used to fill these soft tissues after extractions or other procedures have moduli on the order of 1-20 MPa [267], which are both similar to the compressive properties of ISIs developed here.

Simvastatin release kinetics from both HMW and LMW ISIs were highly dependent on PBAE microparticle content. The larger burst in controls can be attributed to simvastatin dissolved in the NMP phase being rapidly lost during solvent exchange, which has been previously reported [81]. Because PBAEs swell even more freely in organic solvents, such as NMP, acetone, and ethanol, than in water, PBAE microparticles become swollen with NMP and simvastatin during the mixing phase prior to injection. These swollen microparticles act as an additional diffusive barrier to reduce initial burst, and once the initial hardening of the scaffold surface has occurred, simvastatin release is governed by both diffusion and PBAE degradation. The degradation profile of AH6 microparticles is reflected in the accelerated release rate of AH and H/AH scaffolds through day 13. The release profile of HMW-H/AH closely approximates the average of the HMW-H and HMW-AH curves, which suggests that the two hydrogels contribute independently to simvastatin release kinetics, and the results of their contributions are additive. Simvastatin release kinetics were more strongly affected by PBAE microparticle content in 30% LMW PLGA scaffolds than in 40% LMW PLGA scaffolds, and this difference is attributable to multiple factors. First, the higher PLGA content formulation is more viscous, which allows more rapid formation of a protective “skin” that slows solvent exchange and thus burst release. Second, 40% LMW ISIs contain more PLGA for equivalent injected masses when compared to 30% LMW ISIs, which provides more polymer volume to entrap simvastatin, further limiting burst. Interestingly, AH6 degradation did not appear to accelerate simvastatin release in LMW scaffolds as dramatically as it did in HMW scaffolds for the first 10 days. This may be due to the

faster degradation time and relatively higher hydrophilicity of LMW PLGA, which allows faster simvastatin release from the PLGA phase and masks the contribution of AH6-mediated release.

Release kinetics of freely-mixed doxycycline from HMW and LMW ISIs were unaffected by the addition of PBAE microparticles, however pre-loading doxycycline into AH6 microparticles provided a measure of control. The lack of additional doxycycline release after the initial burst in freely-mixed cases is probably due to the entrapment of remaining drug in the PLGA phase, and because doxycycline is substantially more hydrophilic than simvastatin, it has low mobility through the hydrophobic PLGA matrix. This plateau effect is undesirable for antibiotic delivery, because bacteria surviving the initial burst will be free to re-colonize. By pre-loading doxycycline into AH6 PBAE microparticles, the initial burst was followed by continuous release of remaining drug through 1 week, which is consistent with systemic doxycycline regimens of 1 week following scaling and root planing.

5.5. Conclusions

PLGA ISIs formulated with PBAE microparticle additives provide multiple advantages over existing periodontal ISIs. These composite ISIs are more resilient and are retained more firmly in simulated gingival tissue than PLGA alone, so there will be a lower risk of the implant deforming, loosening, and breaking apart prematurely, which is a concern with existing systems. Additionally, PBAE microparticles offer a secondary means of controlling drug release kinetics, and multiple drugs with independent release profiles can be delivered, instead of the single-drug systems that are currently available. Future studies will focus on the potential of these PBAE-containing ISIS to act as scaffolds for tissue regeneration, because the high porosity and open pore network is suitable for tissue ingrowth.

Chapter 6 Summary and Conclusions

In this dissertation, hydrogel and hydroxyapatite additives were used to improve the properties of PLGA ISIs, and provide an early proof of concept that these materials can also serve a role as scaffolds rather than pure drug delivery devices.

First, the orthopedic potential of composite PLGA/PBAE/HA ISIs was investigated. Both simvastatin and clodronate were released with reduced burst compared to controls, which demonstrated that drug release can be controlled independently of traditional techniques that modify the precipitation rate. These results suggest that a modular system can be developed, where a single PLGA solution can be easily modified to provide tailored release kinetics simply through the addition of HA and drug-loaded PBAE microparticles. Hydroxyapatite was then shown to control mechanical properties of these ISIs, and this information was used to develop a formulation that was mechanically similar to healthy trabecular bone. Importantly, the proposed system would be locally injectable into the intertrabecular space within the femoral head, which eliminates the need for invasive surgery and removal of tissue. Instead, the *ex vivo* injections showed the feasibility of this system to mechanically support bone within the femoral head while the drug release component takes effect. The orthopedic scaffolds developed in Chapters 3 and 4 have the potential to fill an important role in the treatment of osteonecrosis, because existing techniques are invasive and have limited effectiveness once the disease has weakened the bone enough to cause collapse.

PBAE hydrogel microparticles were also shown to improve PLGA ISIs for soft tissue applications, specifically in the oral gingiva. ISIs capable of co-delivery of doxycycline for 1 week and simvastatin for 30 to 90 days were developed, which has implications in cases of advanced periodontitis where extensive bone loss has occurred. Additionally, the PBAE additives improved interfacial strength in a simulated periodontal pocket due to swelling, and were responsible for

reducing stiffness and increasing durability of solidified ISIs. Ultimately, the PBAE-containing ISIs are a more suitable match for soft tissue, and also provide dramatically more accessible volume and porosity, which is advantageous for tissue ingrowth.

From a tissue engineering perspective, current PLGA ISIs are nonfunctional as scaffolds, with closed pores, a heterogeneous microarchitecture, and poor mechanical properties. In preformed, implantable PLGA scaffolds, additives are frequently used as porogens or to facilitate drug delivery, and that approach was employed here to improve numerous properties of PLGA ISIs. The resulting PBAE-containing ISIs are a versatile drug delivery platform with tremendous potential as “all in one” treatments that can be adapted to different tissues simply by modifying the additives.

References

1. Williams, D.F., *On the nature of biomaterials.* Biomaterials, 2009. **30**(30): p. 5897-5909.
2. Kulkarni, R.K., E.G. Moore, A.F. Hegyeli, and F. Leonard, *Biodegradable poly(lactic acid) polymers.* Journal of Biomedical Materials Research, 1971. **5**(3): p. 169-181.
3. Schindler, A., R. Jeffcoat, G.L. Kimmel, C.G. Pitt, M.E. Wall, and R. Zweidinger, *Biodegradable Polymers for Sustained Drug Delivery*, in *Contemporary Topics in Polymer Science*, E. Pearce and J. Schaefgen, Editors. 1977, Springer US. p. 251-289.
4. Pitt, C.G., A.R. Jeffcoat, R.A. Zweidinger, and A. Schindler, *Sustained drug delivery systems. I. The permeability of poly(epsilon-caprolactone), poly(DL-lactic acid), and their copolymers.* Journal of biomedical materials research, 1979. **13**(3): p. 497-507.
5. Pitt, C.G., M.M. Gratzl, A.R. Jeffcoat, R. Zweidinger, and A. Schindler, *Sustained drug delivery systems II: Factors affecting release rates from poly(ε-caprolactone) and related biodegradable polyesters.* Journal of Pharmaceutical Sciences, 1979. **68**(12): p. 1534-1538.
6. Graham, N.B., *Polymeric Inserts and Implants for the Controlled Release of Drugs.* British Polymer Journal, 1978. **10**(4): p. 260-266.
7. Benagiano, G. and H.L. Gabelnick, *Biodegradable systems for the sustained release of fertility-regulating agents.* Journal of Steroid Biochemistry, 1979. **11**(1, Part 2): p. 449-455.
8. Beck, L.R., D.R. Cowsar, D.H. Lewis, R.J. Cosgrove, C.T. Riddle, S.L. Lowry, and T. Epperly, *A new long-acting injectable microcapsule system for the administration of progesterone.* Fertility and sterility, 1979. **31**(5): p. 545-551.
9. Angelova, N. and D. Hunkeler, *Rationalizing the design of polymeric biomaterials.* Trends in Biotechnology, 1999. **17**(10): p. 409-421.
10. Leong, K.W., B.C. Brott, and R. Langer, *Bioerodible polyanhydrides as drug-carrier matrices. I: Characterization, degradation, and release characteristics.* J Biomed Mater Res, 1985. **19**(8): p. 941-55.
11. Göpferich, A. and J. Tessmar, *Polyanhydride degradation and erosion.* Advanced Drug Delivery Reviews, 2002. **54**(7): p. 911-931.
12. Rosen, H.B., J. Chang, G.E. Wnek, R.J. Linhardt, and R. Langer, *Bioerodible polyanhydrides for controlled drug delivery.* Biomaterials, 1983. **4**(2): p. 131-133.
13. Göpferich, A. and R. Langer, *The influence of microstructure and monomer properties on the erosion mechanism of a class of polyanhydrides.* Journal of Polymer Science Part A: Polymer Chemistry, 1993. **31**(10): p. 2445-2458.
14. Akbari, H., A. D'Emanuele, and D. Attwood, *Effect of geometry on the erosion characteristics of polyanhydride matrices.* International Journal of Pharmaceutics, 1998. **160**(1): p. 83-89.
15. Jiang, H.L. and K.J. Zhu, *Preparation, characterization and degradation characteristics of polyanhydrides containing poly(ethylene glycol).* Polymer International, 1999. **48**(1): p. 47-52.
16. Shieh, L., J. Tamada, I. Chen, J. Pang, A. Domb, and R. Langer, *Erosion of a new family of biodegradable polyanhydrides.* J Biomed Mater Res, 1994. **28**(12): p. 1465-75.
17. Torres, M.P., B.M. Vogel, B. Narasimhan, and S.K. Mallapragada, *Synthesis and characterization of novel polyanhydrides with tailored erosion mechanisms.* Journal of biomedical materials research. Part A, 2006. **76A**(1): p. 102-110.

18. Uhrich, K.E., A. Gupta, T.T. Thomas, C.T. Laurencin, and R. Langer, *Synthesis and Characterization of Degradable Poly(anhydride-co-imides).* Macromolecules, 1995. **28**(7): p. 2184-2193.
19. Muggli, D.S., A.K. Burkoth, and K.S. Anseth, *Crosslinked polyanhydrides for use in orthopedic applications: degradation behavior and mechanics.* J Biomed Mater Res, 1999. **46**(2): p. 271-8.
20. Li, H., Y. Chen, and Y. Xie, *Photo-crosslinking polymerization to prepare polyanhydride/needle-like hydroxyapatite biodegradable nanocomposite for orthopedic application.* Materials Letters, 2003. **57**(19): p. 2848-2854.
21. Lai, P.-L., D.-W. Hong, I.M. Chu, W.-J. Chen, L.-H. Chen, C.-C. Niu, T.-S. Fu, T.-T. Tsai, and J.-C. Liao, *Polyanhydride copolymer and bioceramic composites as bone substitutes.* Formosan Journal of Musculoskeletal Disorders, 2013. **4**(1): p. 6-10.
22. Leong, K.W., P. D'Amore, M. Marletta, and R. Langer, *Bioerodible polyanhydrides as drug-carrier matrices. II. Biocompatibility and chemical reactivity.* Journal of Biomedical Materials Research, 1986. **20**(1): p. 51-64.
23. Brem, H., A. Kader, J.I. Epstein, R.J. Tamargo, A. Domb, R. Langer, and K.W. Leong, *Biocompatibility of a biodegradable, controlled-release polymer in the rabbit brain.* Sel Cancer Ther, 1989. **5**(2): p. 55-65.
24. Tamargo, R.J., J.I. Epstein, C.S. Reinhard, M. Chasin, and H. Brem, *Brain biocompatibility of a biodegradable, controlled-release polymer in rats.* J Biomed Mater Res, 1989. **23**(2): p. 253-66.
25. Laurencin, C., A. Domb, C. Morris, V. Brown, M. Chasin, R. McConnell, N. Lange, and R. Langer, *Poly(anhydride) administration in high doses in vivo: studies of biocompatibility and toxicology.* J Biomed Mater Res, 1990. **24**(11): p. 1463-81.
26. Woodland, J.H.R., S. Yolles, D.A. Blake, M. Helrich, and F.J. Meyer, *Long-acting delivery systems for narcotic antagonists. 1.* Journal of Medicinal Chemistry, 1973. **16**(8): p. 897-901.
27. Martin, W.R. and V.L. Sandquist, *A sustained release depot for narcotic antagonists.* Archives of General Psychiatry, 1974. **30**(1): p. 31-33.
28. Pitt, C.G., T.A. Marks, and A. Schindler, *Biodegradable drug delivery systems based on aliphatic polyesters: application to contraceptives and narcotic antagonists.* NIDA Res Monogr, 1981. **28**: p. 232-53.
29. Reed, A.M. and D.K. Gilding, *Biodegradable polymers for use in surgery — poly(glycolic)/poly(lactic acid) homo and copolymers: 2. In vitro degradation.* Polymer, 1981. **22**(4): p. 494-498.
30. Lu, L., C.A. Garcia, and A.G. Mikos, *In vitro degradation of thin poly(DL-lactic-co-glycolic acid) films.* J Biomed Mater Res, 1999. **46**(2): p. 236-44.
31. Lu, L., S.J. Peter, M. D. Lyman, H.-L. Lai, S.M. Leite, J.A. Tamada, S. Uyama, J.P. Vacanti, L. Robert, and A.G. Mikos, *In vitro and in vivo degradation of porous poly(dl-lactic-co-glycolic acid) foams.* Biomaterials, 2000. **21**(18): p. 1837-1845.
32. Anderson, J.M. and M.S. Shive, *Biodegradation and biocompatibility of PLA and PLGA microspheres.* Advanced Drug Delivery Reviews, 2012. **64, Supplement**(0): p. 72-82.
33. Park, T.G., *Degradation of poly(lactic-co-glycolic acid) microspheres: effect of copolymer composition.* Biomaterials, 1995. **16**(15): p. 1123-1130.
34. Wiggins, J.S., M.K. Hassan, K.A. Mauritz, and R.F. Storey, *Hydrolytic degradation of poly(d,l-lactide) as a function of end group: Carboxylic acid vs. hydroxyl.* Polymer, 2006. **47**(6): p. 1960-1969.

35. Fu, K., D.W. Pack, A.M. Klibanov, and R. Langer, *Visual evidence of acidic environment within degrading poly(lactic-co-glycolic acid) (PLGA) microspheres.* Pharm Res, 2000. **17**(1): p. 100-6.
36. Vert, M., S. Li, and H. Garreau, *More about the degradation of LA/GA-derived matrices in aqueous media.* Journal of Controlled Release, 1991. **16**(1–2): p. 15-26.
37. Pitt, C.G., A.R. Jeffcoat, R.A. Zweidinger, and A. Schindler, *Sustained drug delivery systems. I. The permeability of poly(epsilon-caprolactone), poly(DL-lactic acid), and their copolymers.* J Biomed Mater Res, 1979. **13**(3): p. 497-507.
38. Pitt, C.G., F.I. Chasalow, Y.M. Hibionada, D.M. Klimas, and A. Schindler, *Aliphatic polyesters. I. The degradation of poly(ε-caprolactone) in vivo.* Journal of Applied Polymer Science, 1981. **26**(11): p. 3779-3787.
39. Pitt, G.G., M.M. Gratzl, G.L. Kimmel, J. Surles, and A. Sohindler, *Aliphatic polyesters II. The degradation of poly (DL-lactide), poly (ε-caprolactone), and their copolymers in vivo.* Biomaterials, 1981. **2**(4): p. 215-220.
40. Broström, J., A. Boss, and I.S. Chronakis, *Biodegradable Films of Partly Branched Poly(l-lactide)-co-poly(ε-caprolactone) Copolymer: Modulation of Phase Morphology, Plasticization Properties and Thermal Depolymerization.* Biomacromolecules, 2004. **5**(3): p. 1124-1134.
41. Lee, H.Y., H.M. Jeong, J.S. Lee, and B.K. Kim, *Study on the Shape Memory Polyamides. Synthesis and Thermomechanical Properties of Polycaprolactone-Polyamide Block Copolymer.* Polym J, 2000. **32**(1): p. 23-28.
42. Shen, Y., W. Sun, K.J. Zhu, and Z. Shen, *Regulation of biodegradability and drug release behavior of aliphatic polyesters by blending.* J Biomed Mater Res, 2000. **50**(4): p. 528-35.
43. Ma, G. and C. Song, *PCL/poloxamer 188 blend microsphere for paclitaxel delivery: Influence of poloxamer 188 on morphology and drug release.* Journal of Applied Polymer Science, 2007. **104**(3): p. 1895-1899.
44. Engelberg, I. and J. Kohn, *Physico-mechanical properties of degradable polymers used in medical applications: A comparative study.* Biomaterials, 1991. **12**(3): p. 292-304.
45. Koleske, J.V. and R.D. Lundberg, *Lactone polymers. I. Glass transition temperature of poly-ε-caprolactone by means on compatible polymer mixtures.* Journal of Polymer Science Part A-2: Polymer Physics, 1969. **7**(5): p. 795-807.
46. Cohn, D. and A. Hotovely Salomon, *Designing biodegradable multiblock PCL/PLA thermoplastic elastomers.* Biomaterials, 2005. **26**(15): p. 2297-2305.
47. Temple, J.P., D.L. Hutton, B.P. Hung, P.Y. Huri, C.A. Cook, R. Kondragunta, X. Jia, and W.L. Grayson, *Engineering anatomically shaped vascularized bone grafts with hASCs and 3D-printed PCL scaffolds.* Journal of biomedical materials research. Part A, 2014.
48. Wang, F., L. Shor, A. Darling, S. Khalil, W. Sun, S. Güçeri, and A. Lau, *Precision extruding deposition and characterization of cellular poly-ε-caprolactone tissue scaffolds.* Rapid Prototyping Journal, 2004. **10**(1): p. 42-49.
49. Park, S., S. Lee, and W. Kim, *Fabrication of porous polycaprolactone/hydroxyapatite (PCL/HA) blend scaffolds using a 3D plotting system for bone tissue engineering.* Bioprocess and Biosystems Engineering, 2011. **34**(4): p. 505-513.
50. Hoque, M.E., W.Y. San, F. Wei, S. Li, M.H. Huang, M. Vert, and D.W. Hutmacher, *Processing of polycaprolactone and polycaprolactone-based copolymers into 3D scaffolds, and their cellular responses.* Tissue Eng Part A, 2009. **15**(10): p. 3013-24.
51. Allen, C., Y. Yu, D. Maysinger, and A. Eisenberg, *Polycaprolactone-b-poly(ethylene Oxide) Block Copolymer Micelles as a Novel Drug Delivery Vehicle for Neurotrophic Agents FK506 and L-685,818.* Bioconjugate Chemistry, 1998. **9**(5): p. 564-572.

52. Wang, F., T.K. Bronich, A.V. Kabanov, R.D. Rauh, and J. Roovers, *Synthesis and Evaluation of a Star Amphiphilic Block Copolymer from Poly(ε-caprolactone) and Poly(ethylene glycol) as a Potential Drug Delivery Carrier.* Bioconjugate Chemistry, 2005. **16**(2): p. 397-405.
53. Zhou, S., X. Deng, and H. Yang, *Biodegradable poly(ε-caprolactone)-poly(ethylene glycol) block copolymers: characterization and their use as drug carriers for a controlled delivery system.* Biomaterials, 2003. **24**(20): p. 3563-3570.
54. Causa, F., P.A. Netti, L. Ambrosio, G. Ciapetti, N. Baldini, S. Pagani, D. Martini, and A. Giunti, *Poly-ϵ-caprolactone/hydroxyapatite composites for bone regeneration: In vitro characterization and human osteoblast response.* Journal of biomedical materials research. Part A, 2006. **76A**(1): p. 151-162.
55. Fujihara, K., M. Kotaki, and S. Ramakrishna, *Guided bone regeneration membrane made of polycaprolactone/calcium carbonate composite nano-fibers.* Biomaterials, 2005. **26**(19): p. 4139-4147.
56. Rai, B., M.E. Oest, K.M. Dupont, K.H. Ho, S.H. Teoh, and R.E. Guldberg, *Combination of platelet-rich plasma with polycaprolactone-tricalcium phosphate scaffolds for segmental bone defect repair.* Journal of biomedical materials research. Part A, 2007. **81A**(4): p. 888-899.
57. Wutticharoenmongkol, P., N. Sanchavanakit, P. Pavasant, and P. Supaphol, *Preparation and Characterization of Novel Bone Scaffolds Based on Electrospun Polycaprolactone Fibers Filled with Nanoparticles.* Macromolecular Bioscience, 2006. **6**(1): p. 70-77.
58. Heller, J., *Controlled drug release from poly(ortho esters) — A surface eroding polymer.* Journal of Controlled Release, 1985. **2**(0): p. 167-177.
59. Shih, C., T. Higuchi, and K.J. Himmelstein, *Drug delivery from catalysed erodible polymeric matrices of poly(ortho ester)s.* Biomaterials, 1984. **5**(4): p. 237-240.
60. Tue Huu, N., H. Takeru, and K.J. Himmelstein, *Erosion characteristics of catalyzed poly(ortho ester) matrices.* Journal of Controlled Release, 1987. **5**(1): p. 1-12.
61. Ng, S.Y., T. Vandamme, M.S. Taylor, and J. Heller, *Synthesis and Erosion Studies of Self-Catalyzed Poly(ortho ester)s.* Macromolecules, 1997. **30**(4): p. 770-772.
62. Heller, J., *Development of poly(ortho esters): a historical overview.* Biomaterials, 1990. **11**(9): p. 659-665.
63. Heller, J., J. Barr, S.Y. Ng, K.S. Abdellauoi, and R. Gurny, *Poly(ortho esters): synthesis, characterization, properties and uses.* Advanced Drug Delivery Reviews, 2002. **54**(7): p. 1015-1039.
64. Einmahl, S., S. Ponsart, R.A. Bejjani, F. D'Hermies, M. Savoldelli, J. Heller, C. Tabatabay, R. Gurny, and F. Behar-Cohen, *Ocular biocompatibility of a poly(ortho ester) characterized by autocatalyzed degradation.* Journal of biomedical materials research. Part A, 2003. **67A**(1): p. 44-53.
65. Heller, J., *Ocular delivery using poly(ortho esters).* Advanced Drug Delivery Reviews, 2005. **57**(14): p. 2053-2062.
66. Zignani, M., S. Einmahl, V. Baeyens, E. Varesio, J.L. Veuthey, J. Anderson, J. Heller, C. Tabatabay, and R. Gurny, *A poly(ortho ester) designed for combined ocular delivery of dexamethasone sodium phosphate and 5-fluorouracil: subconjunctival tolerance and in vitro release.* European Journal of Pharmaceutics and Biopharmaceutics, 2000. **50**(2): p. 251-255.
67. Anderson, D.G., D.M. Lynn, and R. Langer, *Semi-automated synthesis and screening of a large library of degradable cationic polymers for gene delivery.* Angew Chem Int Ed Engl, 2003. **42**(27): p. 3153-8.

68. Anderson, D.G., W. Peng, A. Akinc, N. Hossain, A. Kohn, R. Padera, R. Langer, and J.A. Sawicki, *A polymer library approach to suicide gene therapy for cancer.* Proceedings of the National Academy of Sciences of the United States of America, 2004. **101**(45): p. 16028-16033.
69. Anderson, D.G., C.A. Tweedie, N. Hossain, S.M. Navarro, D.M. Brey, K.J. Van Vliet, R. Langer, and J.A. Burdick, *A combinatorial library of photocrosslinkable and degradable materials.* Advanced Materials, 2006. **18**(19): p. 2614-2618.
70. Hawkins, A.M., T.A. Milbrandt, D.A. Puleo, and J.Z. Hilt, *Synthesis and analysis of degradation, mechanical and toxicity properties of poly(β-amino ester) degradable hydrogels.* Acta Biomaterialia, 2011. **7**(5): p. 1956-1964.
71. Hawkins, A.M., D.A. Puleo, and J.Z. Hilt, *Effect of macromer synthesis time on the properties of the resulting poly(β-amino ester) degradable hydrogel.* Journal of Applied Polymer Science, 2011. **122**(2): p. 1420-1426.
72. Little, S.R., D.M. Lynn, S.V. Puram, and R. Langer, *Formulation and characterization of poly (β amino ester) microparticles for genetic vaccine delivery.* Journal of Controlled Release, 2005. **107**(3): p. 449-462.
73. Little, S.R., D.M. Lynn, Q. Ge, D.G. Anderson, S.V. Puram, J. Chen, H.N. Eisen, and R. Langer, *Poly-β amino ester-containing microparticles enhance the activity of nonviral genetic vaccines.* Proceedings of the National Academy of Sciences of the United States of America, 2004. **101**(26): p. 9534-9539.
74. Anderson, D.G., A. Akinc, N. Hossain, and R. Langer, *Structure/property studies of polymeric gene delivery using a library of poly([beta]-amino esters).* Mol Ther, 2005. **11**(3): p. 426-434.
75. Ko, J., K. Park, Y.-S. Kim, M.S. Kim, J.K. Han, K. Kim, R.-W. Park, I.-S. Kim, H.K. Song, D.S. Lee, and I.C. Kwon, *Tumoral acidic extracellular pH targeting of pH-responsive MPEG-poly(β-amino ester) block copolymer micelles for cancer therapy.* Journal of Controlled Release, 2007. **123**(2): p. 109-115.
76. Shen, Y., H. Tang, Y. Zhan, E.A. Van Kirk, and W.J. Murdoch, *Degradable Poly(β-amino ester) nanoparticles for cancer cytoplasmic drug delivery.* Nanomedicine: Nanotechnology, Biology and Medicine, 2009. **5**(2): p. 192-201.
77. Min, K.H., J.-H. Kim, S.M. Bae, H. Shin, M.S. Kim, S. Park, H. Lee, R.-W. Park, I.-S. Kim, K. Kim, I.C. Kwon, S.Y. Jeong, and D.S. Lee, *Tumoral acidic pH-responsive MPEG-poly(β-amino ester) polymeric micelles for cancer targeting therapy.* Journal of Controlled Release, 2010. **144**(2): p. 259-266.
78. Orellana, B.R., J.Z. Hilt, and D.A. Puleo, *Drug release from calcium sulfate-based composites.* Journal of Biomedical Materials Research Part B: Applied Biomaterials, 2014: p. n/a-n/a.
79. Orellana, B.R., M.V. Thomas, T.D. Dziubla, N.M. Shah, J.Z. Hilt, and D.A. Puleo, *Bioerodible calcium sulfate/poly(β-amino ester) hydrogel composites.* Journal of the Mechanical Behavior of Biomedical Materials, 2013. **26**(0): p. 43-53.
80. Clark, A., T.A. Milbrandt, J.Z. Hilt, and D.A. Puleo, *Mechanical properties and dual drug delivery application of poly(lactic-co-glycolic acid) scaffolds fabricated with a poly(β-amino ester) porogen.* Acta Biomaterialia, 2014. **10**(5): p. 2125-2132.
81. Fisher, P.D., P. Palomino, T.A. Milbrandt, J.Z. Hilt, and D.A. Puleo, *Improved small molecule drug release from in situ forming poly(lactic-co-glycolic acid) scaffolds incorporating poly(beta-amino ester) and hydroxyapatite microparticles.* Journal of Biomaterials Science. Polymer Edition, 2014. **25**(11): p. 1174-93.

82. Hawkins, A., N. Satarkar, and J.Z. Hilt, *Nanocomposite Degradable Hydrogels: Demonstration of Remote Controlled Degradation and Drug Release.* Pharmaceutical Research, 2009. **26**(3): p. 667-673.
83. Yang, Y.Y., H.H. Chia, and T.S. Chung, *Effect of preparation temperature on the characteristics and release profiles of PLGA microspheres containing protein fabricated by double-emulsion solvent extraction/evaporation method.* J Control Release, 2000. **69**(1): p. 81-96.
84. Yang, Y.-Y., T.-S. Chung, and N. Ping Ng, *Morphology, drug distribution, and in vitro release profiles of biodegradable polymeric microspheres containing protein fabricated by double-emulsion solvent extraction/evaporation method.* Biomaterials, 2001. **22**(3): p. 231-241.
85. Sansdrap, P. and A.J. Moës, *Influence of manufacturing parameters on the size characteristics and the release profiles of nifedipine from poly(DL-lactide-co-glycolide) microspheres.* International Journal of Pharmaceutics, 1993. **98**(1–3): p. 157-164.
86. Mao, S., J. Xu, C. Cai, O. Germershaus, A. Schaper, and T. Kissel, *Effect of WOW process parameters on morphology and burst release of FITC-dextran loaded PLGA microspheres.* International Journal of Pharmaceutics, 2007. **334**(1–2): p. 137-148.
87. Cohen, S., T. Yoshioka, M. Lucarelli, L. Hwang, and R. Langer, *Controlled Delivery Systems for Proteins Based on Poly(Lactic/Glycolic Acid) Microspheres.* Pharmaceutical Research, 1991. **8**(6): p. 713-720.
88. Wang, H.T., H. Palmer, R.J. Linhardt, D.R. Flanagan, and E. Schmitt, *Degradation of poly(ester) microspheres.* Biomaterials, 1990. **11**(9): p. 679-685.
89. Ikada, Y. and Y. Tabata, *Protein release from gelatin matrices.* Adv Drug Deliv Rev, 1998. **31**(3): p. 287-301.
90. Zou, Y., J.L. Brooks, V. Talwalkar, T.A. Milbrandt, and D.A. Puleo, *Development of an injectable two-phase drug delivery system for sequential release of antiresorptive and osteogenic drugs.* Journal of Biomedical Materials Research Part B: Applied Biomaterials, 2012. **100B**(1): p. 155-162.
91. Soppirnath, K.S. and T.M. Aminabhavi, *Water transport and drug release study from cross-linked polyacrylamide grafted guar gum hydrogel microspheres for the controlled release application.* European Journal of Pharmaceutics and Biopharmaceutics, 2002. **53**(1): p. 87-98.
92. Mu, L. and S.S. Feng, *Fabrication, characterization and in vitro release of paclitaxel (Taxol®) loaded poly (lactic-co-glycolic acid) microspheres prepared by spray drying technique with lipid/cholesterol emulsifiers.* Journal of Controlled Release, 2001. **76**(3): p. 239-254.
93. Bodmeier, R. and H. Chen, *Preparation of Biodegradable Poly(±)lactide Microparticles Using a Spray-Drying Technique.* Journal of Pharmacy and Pharmacology, 1988. **40**(11): p. 754-757.
94. Gavini, E., P. Chetoni, M. Cossu, M.G. Alvarez, M.F. Saettone, and P. Giunchedi, *PLGA microspheres for the ocular delivery of a peptide drug, vancomycin using emulsification/spray-drying as the preparation method: in vitro/in vivo studies.* European Journal of Pharmaceutics and Biopharmaceutics, 2004. **57**(2): p. 207-212.
95. Pavanetto, F., I. Genta, P. Giunchedi, and B. Conti, *Evaluation of spray drying as a method for polylactide and polylactide-co-glycolide microsphere preparation.* Journal of Microencapsulation, 1993. **10**(4): p. 487-497.
96. Mathiowitz, E. and R. Langer, *Polyanhydride microspheres as drug carriers I. Hot-melt microencapsulation.* Journal of Controlled Release, 1987. **5**(1): p. 13-22.

97. Chickering, D., J. Jacob, and E. Mathiowitz, *Poly(fumaric-co-sebacic) microspheres as oral drug delivery systems.* Biotechnol Bioeng, 1996. **52**(1): p. 96-101.
98. Godbee, J., E. Scott, P. Pattamunuch, S. Chen, and E. Mathiowitz, *Role of solvent/non-solvent ratio on microsphere formation using the solvent removal method.* Journal of Microencapsulation, 2004. **21**(2): p. 151-160.
99. Arshady, R., *Preparation of microspheres and microcapsules by interfacial polycondensation techniques.* Journal of Microencapsulation, 1989. **6**(1): p. 13-28.
100. Sun, Q. and Y. Deng, *In Situ Synthesis of Temperature-Sensitive Hollow Microspheres via Interfacial Polymerization.* Journal of the American Chemical Society, 2005. **127**(23): p. 8274-8275.
101. Grizzi, I., H. Garreau, S. Li, and M. Vert, *Hydrolytic degradation of devices based on poly(DL-lactic acid) size-dependence.* Biomaterials, 1995. **16**(4): p. 305-11.
102. Kempe, S. and K. Mäder, *In situ forming implants — an attractive formulation principle for parenteral depot formulations.* Journal of Controlled Release, 2012. **161**(2): p. 668-679.
103. Hatefi, A. and B. Amsden, *Biodegradable injectable in situ forming drug delivery systems.* Journal of Controlled Release, 2002. **80**(1–3): p. 9-28.
104. Zhang, X., J.K. Jackson, W. Wong, W. Min, T. Cruz, W.L. Hunter, and H.M. Burt, *Development of biodegradable polymeric paste formulations for taxol: An in vitro and in vivo study.* International Journal of Pharmaceutics, 1996. **137**(2): p. 199-208.
105. Winternitz, C.I., J.K. Jackson, A.M. Oktaba, and H.M. Burt, *Development of a polymeric surgical paste formulation for taxol.* Pharm Res, 1996. **13**(3): p. 368-75.
106. Einmahl, S., S. Capancioni, K. Schwach-Abdellaoui, M. Moeller, F. Behar-Cohen, and R. Gurny, *Therapeutic applications of viscous and injectable poly(ortho esters).* Adv Drug Deliv Rev, 2001. **53**(1): p. 45-73.
107. Heller, J., J. Barr, S. Ng, H.R. Shen, R. Gurny, K. Schwach-Abdelaoui, A. Rothen-Weinhold, and M. van de Weert, *Development of poly(ortho esters) and their application for bovine serum albumin and bupivacaine delivery.* J Control Release, 2002. **78**(1-3): p. 133-41.
108. Brinker, C.J. and G.W. Scherer, *Sol-gel science: the physics and chemistry of sol-gel processing*. 1990: Gulf Professional Publishing.
109. Jeong, B., S.W. Kim, and Y.H. Bae, *Thermosensitive sol–gel reversible hydrogels.* Advanced Drug Delivery Reviews, 2002. **54**(1): p. 37-51.
110. Liu, W., B. Zhang, W.W. Lu, X. Li, D. Zhu, K. De Yao, Q. Wang, C. Zhao, and C. Wang, *A rapid temperature-responsive sol–gel reversible poly(N-isopropylacrylamide)-g-methylcellulose copolymer hydrogel.* Biomaterials, 2004. **25**(15): p. 3005-3012.
111. Yoshioka, H., M. Mikami, Y. Mori, and E. Tsuchida, *A Synthetic Hydrogel with Thermoreversible Gelation. I. Preparation and Rheological Properties.* Journal of Macromolecular Science, Part A, 1994. **31**(1): p. 113-120.
112. Feil, H., Y.H. Bae, J. Feijen, and S.W. Kim, *Effect of comonomer hydrophilicity and ionization on the lower critical solution temperature of N-isopropylacrylamide copolymers.* Macromolecules, 1993. **26**(10): p. 2496-2500.
113. Vihola, H., A. Laukkanen, L. Valtola, H. Tenhu, and J. Hirvonen, *Cytotoxicity of thermosensitive polymers poly(N-isopropylacrylamide), poly(N-vinylcaprolactam) and amphiphilically modified poly(N-vinylcaprolactam).* Biomaterials, 2005. **26**(16): p. 3055-3064.
114. Uchida, K., K. Sakai, E. Ito, O. Hyeong Kwon, A. Kikuchi, M. Yamato, and T. Okano, *Temperature-dependent modulation of blood platelet movement and morphology on poly(N-isopropylacrylamide)-grafted surfaces.* Biomaterials, 2000. **21**(9): p. 923-929.

115. Neradovic, D., M.J. van Steenbergen, L. Vansteelant, Y.J. Meijer, C.F. van Nostrum, and W.E. Hennink, *Degradation Mechanism and Kinetics of Thermosensitive Polyacrylamides Containing Lactic Acid Side Chains.* Macromolecules, 2003. **36**(20): p. 7491-7498.
116. Cui, Z., B.H. Lee, C. Pauken, and B.L. Vernon, *Manipulating Degradation Time in a N-isopropylacrylamide-Based Co-polymer with Hydrolysis-Dependent LCST.* Journal of Biomaterials Science, Polymer Edition, 2010. **21**(6-7): p. 913-926.
117. Edsman, K., J. Carlfors, and R. Petersson, *Rheological evaluation of poloxamer as an in situ gel for ophthalmic use.* European Journal of Pharmaceutical Sciences, 1998. **6**(2): p. 105-112.
118. Kwon, J.W., Y.K. Han, W.J. Lee, C.S. Cho, S.J. Paik, D.I. Cho, J.H. Lee, and W.R. Wee, *Biocompatibility of poloxamer hydrogel as an injectable intraocular lens: a pilot study.* J Cataract Refract Surg, 2005. **31**(3): p. 607-13.
119. Veyries, M.L., G. Couarraze, S. Geiger, F. Agnely, L. Massias, B. Kunzli, F. Faurisson, and B. Rouveix, *Controlled release of vancomycin from Poloxamer 407 gels.* International Journal of Pharmaceutics, 1999. **192**(2): p. 183-193.
120. Ricci, E.J., M.V.L.B. Bentley, M. Farah, R.E.S. Bretas, and J.M. Marchetti, *Rheological characterization of Poloxamer 407 lidocaine hydrochloride gels.* European Journal of Pharmaceutical Sciences, 2002. **17**(3): p. 161-167.
121. Moore, T., S. Croy, S. Mallapragada, and N. Pandit, *Experimental investigation and mathematical modeling of Pluronic® F127 gel dissolution: drug release in stirred systems.* Journal of Controlled Release, 2000. **67**(2–3): p. 191-202.
122. Gong, C.Y., S. Shi, P.W. Dong, B. Yang, X.R. Qi, G. Guo, Y.C. Gu, X. Zhao, Y.Q. Wei, and Z.Y. Qian, *Biodegradable in situ gel-forming controlled drug delivery system based on thermosensitive PCL-PEG-PCL hydrogel: part 1--Synthesis, characterization, and acute toxicity evaluation.* J Pharm Sci, 2009. **98**(12): p. 4684-94.
123. Gong, C.Y., P.W. Dong, S. Shi, S.Z. Fu, J.L. Yang, G. Guo, X. Zhao, Y.Q. Wei, and Z.Y. Qian, *Thermosensitive PEG–PCL–PEG hydrogel controlled drug delivery system: Sol–gel–sol transition and in vitro drug release study.* Journal of Pharmaceutical Sciences, 2009. **98**(10): p. 3707-3717.
124. Jeong, B., Y.H. Bae, and S.W. Kim, *Drug release from biodegradable injectable thermosensitive hydrogel of PEG–PLGA–PEG triblock copolymers.* Journal of Controlled Release, 2000. **63**(1–2): p. 155-163.
125. Cowsar, D.R., R.L. Dunn, J.P. English, and D.P. Vanderbilt, *Biodegradable in-situ forming implants and methods of producing the same*. 1994, Google Patents.
126. Cowsar, D.R., R.L. Dunn, J.P. English, and D.D. Vanderbilt, *Biodegradable in-situ forming implants and methods for producing the same*. 1994, Google Patents.
127. Cowsar, D.R., R.L. Dunn, J.P. English, and D.D. Vanderbilt, *Biodegradable in-situ forming implants and methods of producing the same*. 1994, Google Patents.
128. Cramer, N., J. Stansbury, and C. Bowman, *Recent advances and developments in composite dental restorative materials.* Journal of dental research, 2011. **90**(4): p. 402-416.
129. Nivasu, V.M., T.T. Reddy, and S. Tammishetti, *In situ polymerizable polyethyleneglycol containing polyesterpolyol acrylates for tissue sealant applications.* Biomaterials, 2004. **25**(16): p. 3283-91.
130. Burdick, J.A., L.M. Philpott, and K.S. Anseth, *Synthesis and characterization of tetrafunctional lactic acid oligomers: A potential in situ forming degradable orthopaedic biomaterial.* Journal of Polymer Science Part A: Polymer Chemistry, 2001. **39**(5): p. 683-692.

131. Leach, J.B. and C.E. Schmidt, *Characterization of protein release from photocrosslinkable hyaluronic acid-polyethylene glycol hydrogel tissue engineering scaffolds.* Biomaterials, 2005. **26**(2): p. 125-35.
132. Schmitz, S., C. Garbe, B. Tebbe, and C.E. Orfanos, *[Long-wave ultraviolet radiation (UVA) and skin cancer].* Hautarzt, 1994. **45**(8): p. 517-25.
133. Qiu, B., S. Stefanos, J. Ma, A. Lalloo, B.A. Perry, M.J. Leibowitz, P.J. Sinko, and S. Stein, *A hydrogel prepared by in situ cross-linking of a thiol-containing poly(ethylene glycol)-based copolymer: a new biomaterial for protein drug delivery.* Biomaterials, 2003. **24**(1): p. 11-18.
134. Cui, H. and P.B. Messersmith, *Thermally Triggered Gelation of Alginate for Controlled Release*, in *Tailored Polymeric Materials for Controlled Delivery Systems*. 1998, American Chemical Society. p. 203-211.
135. Westhaus, E. and P.B. Messersmith, *Triggered release of calcium from lipid vesicles: a bioinspired strategy for rapid gelation of polysaccharide and protein hydrogels.* Biomaterials, 2001. **22**(5): p. 453-62.
136. Cohen, S., E. Lobel, A. Trevgoda, and Y. Peled, *A novel in situ-forming ophthalmic drug delivery system from alginates undergoing gelation in the eye.* Journal of Controlled Release, 1997. **44**(2–3): p. 201-208.
137. Graham, P.D., K.J. Brodbeck, and A.J. McHugh, *Phase inversion dynamics of PLGA solutions related to drug delivery.* Journal of Controlled Release, 1999. **58**(2): p. 233-245.
138. Liu, H. and S.S. Venkatraman, *Effect of polymer type on the dynamics of phase inversion and drug release in injectable in situ gelling systems.* J Biomater Sci Polym Ed, 2012. **23**(1-4): p. 251-66.
139. Parent, M., C. Nouvel, M. Koerber, A. Sapin, P. Maincent, and A. Boudier, *PLGA in situ implants formed by phase inversion: Critical physicochemical parameters to modulate drug release.* Journal of Controlled Release, 2013. **172**(1): p. 292-304.
140. Ravivarapu, H.B., K.L. Moyer, and R.L. Dunn, *Parameters affecting the efficacy of a sustained release polymeric implant of leuprolide.* Int J Pharm, 2000. **194**(2): p. 181-91.
141. Astaneh, R., M. Erfan, H. Moghimi, and H. Mobedi, *Changes in morphology of in situ forming PLGA implant prepared by different polymer molecular weight and its effect on release behavior.* Journal of Pharmaceutical Sciences, 2009. **98**(1): p. 135-145.
142. Ahmed, T.A., H.M. Ibrahim, F. Ibrahim, A.M. Samy, A. Kaseem, M.T. H. Nutan, and M.D. Hussain, *Development of biodegradable in situ implant and microparticle injectable formulations for sustained delivery of haloperidol.* Journal of Pharmaceutical Sciences, 2012. **101**(10): p. 3753-3762.
143. Brodbeck, K.J., S. Pushpala, and A.J. McHugh, *Sustained release of human growth hormone from PLGA solution depots.* Pharm Res, 1999. **16**(12): p. 1825-9.
144. Wang, L., S. Venkatraman, and L. Kleiner, *Drug release from injectable depots: two different in vitro mechanisms.* Journal of Controlled Release, 2004. **99**(2): p. 207-216.
145. Wang, L., L. Kleiner, and S. Venkatraman, *Structure formation in injectable poly(lactide–co-glycolide) depots.* Journal of Controlled Release, 2003. **90**(3): p. 345-354.
146. Lambert, W.J. and K.D. Peck, *Development of an in situ forming biodegradable poly-lactide-coglycolide system for the controlled release of proteins.* Journal of Controlled Release, 1995. **33**(1): p. 189-195.
147. Royals, M.A., S.M. Fujita, G.L. Yewey, J. Rodriguez, P.C. Schultheiss, and R.L. Dunn, *Biocompatibility of a biodegradable in situ forming implant system in rhesus monkeys.* Journal of Biomedical Materials Research, 1999. **45**(3): p. 231-9.

148. Sartor, O., *Eligard: leuprolide acetate in a novel sustained-release delivery system.* Urology, 2003. **61**(2 Suppl 1): p. 25-31.
149. Boraiah, S., O. Paul, D. Hawkes, M. Wickham, and D. Lorich, *Complications of Recombinant Human BMP-2 for Treating Complex Tibial Plateau Fractures: A Preliminary Report.* Clinical Orthopaedics and Related Research®, 2009. **467**(12): p. 3257-3262.
150. Benglis, D., M.Y. Wang, and A.D. Levi, *A comprehensive review of the safety profile of bone morphogenetic protein in spine surgery.* Neurosurgery, 2008. **62**(5).
151. Pihlstrom, B.L., B.S. Michalowicz, and N.W. Johnson, *Periodontal diseases.* The Lancet, 2005. **366**(9499): p. 1809-1820.
152. Albandar, J.M., *Epidemiology and risk factors of periodontal diseases.* Dent Clin North Am, 2005. **49**(3): p. 517-32, v-vi.
153. Taylor, G.W., *Bidirectional interrelationships between diabetes and periodontal diseases: an epidemiologic perspective.* Ann Periodontol, 2001. **6**(1): p. 99-112.
154. Scannapieco, F.A., R.B. Bush, and S. Paju, *Associations between periodontal disease and risk for atherosclerosis, cardiovascular disease, and stroke. A systematic review.* Annals of periodontology / the American Academy of Periodontology, 2003. **8**(1): p. 38-53.
155. Rosan, B. and R.J. Lamont, *Dental plaque formation.* Microbes and Infection, 2000. **2**(13): p. 1599-1607.
156. Morrison, E.C., S.P. Ramfjord, and R.W. Hill, *Short-term effects of initial, nonsurgical periodontal treatment (hygienic phase).* J Clin Periodontol, 1980. **7**(3): p. 199-211.
157. Cobb, C.M., *Clinical significance of non-surgical periodontal therapy: an evidence-based perspective of scaling and root planing.* Journal of Clinical Periodontology, 2002. **29**: p. 22-32.
158. Jorgensen, M.G. and J. Slots, *Practical antimicrobial periodontal therapy.* Compend Contin Educ Dent, 2000. **21**(2): p. 111-4, 116, 118-20 passim; quiz 124.
159. Slots, J. and T.E. Rams, *Antibiotics in periodontal therapy: advantages and disadvantages.* J Clin Periodontol, 1990. **17**(7 (Pt 2)): p. 479-93.
160. Zambon, J.J., *Actinobacillus actinomycetemcomitans in human periodontal disease.* J Clin Periodontol, 1985. **12**(1): p. 1-20.
161. McCulloch, C.A.G., P. Birek, C. Overall, S. Aitken, W. Lee, and G. Kulkarni, *Randomized controlled trial of doxycycline in prevention of recurrent periodontitis in high-risk patients: antimicrobial activity and collagenase inhibition.* Journal of Clinical Periodontology, 1990. **17**(9): p. 616-622.
162. Golub, L.M., T. Sorsa, H.-M. Lee, S. Ciancio, D. Sorbi, N.S. Ramamurthy, B. Gruber, T. Salo, and Y.T. Konttinen, *Doxycycline inhibits neutrophil (PMN)-type matrix metalloproteinases in human adult periodontitis gingiva.* Journal of Clinical Periodontology, 1995. **22**(2): p. 100-109.
163. Golub, L.M., H.M. Lee, M.E. Ryan, W.V. Giannobile, J. Payne, and T. Sorsa, *Tetracyclines inhibit connective tissue breakdown by multiple non-antimicrobial mechanisms.* Adv Dent Res, 1998. **12**(2): p. 12-26.
164. Caton, J.G., S.G. Ciancio, T.M. Blieden, M. Bradshaw, R.J. Crout, A.F. Hefti, J.M. Massaro, A.M. Polson, J. Thomas, and C. Walker, *Treatment with subantimicrobial dose doxycycline improves the efficacy of scaling and root planing in patients with adult periodontitis.* J Periodontol, 2000. **71**(4): p. 521-32.
165. Webster, G. and J.Q. Del Rosso, *Anti-Inflammatory Activity of Tetracyclines.* Dermatologic Clinics, 2007. **25**(2): p. 133-135.

166. Mavragani, M., P. Brudvik, and K.A. Selvig, *Orthodontically induced root and alveolar bone resorption: inhibitory effect of systemic doxycycline administration in rats.* The European Journal of Orthodontics, 2005. **27**(3): p. 215-225.
167. Vernillo, A.T. and B.R. Rifkin, *Effects of tetracyclines on bone metabolism.* Adv Dent Res, 1998. **12**(2): p. 56-62.
168. Damien, C.J. and J.R. Parsons, *Bone graft and bone graft substitutes: a review of current technology and applications.* J Appl Biomater, 1991. **2**(3): p. 187-208.
169. Reynolds, M.A., M.E. Aichelmann-Reidy, G.L. Branch-Mays, and J.C. Gunsolley, *The efficacy of bone replacement grafts in the treatment of periodontal osseous defects. A systematic review.* Ann Periodontol, 2003. **8**(1): p. 227-65.
170. Lavernia, C.J., R.J. Sierra, and F.R. Grieco, *Osteonecrosis of the femoral head.* J Am Acad Orthop Surg, 1999. **7**(4): p. 250-61.
171. Kang, J.S., S. Park, J.H. Song, Y.Y. Jung, M.R. Cho, and K.H. Rhyu, *Prevalence of Osteonecrosis of the Femoral Head: A Nationwide Epidemiologic Analysis in Korea.* The Journal of Arthroplasty, 2009. **24**(8): p. 1178-1183.
172. Assouline-Dayan, Y., C. Chang, A. Greenspan, Y. Shoenfeld, and M.E. Gershwin, *Pathogenesis and natural history of osteonecrosis.* Seminars in Arthritis and Rheumatism, 2002. **32**(2): p. 94-124.
173. Crock, H.V., *An Atlas of the Arterial Supply of the Head and Neck of the Femur in Man.* Clinical Orthopaedics and Related Research, 1980. **152**.
174. Atsumi, T. and Y. Kuroki, *Role of Impairment of Blood Supply of the Femoral Head in the Pathogenesis of Idiopathic Osteonecrosis.* Clinical Orthopaedics and Related Research, 1992. **277**.
175. Ohzono, K., M. Saito, K. Takaoka, K. Ono, S. Saito, T. Nishina, and T. Kadowaki, *Natural history of nontraumatic avascular necrosis of the femoral head.* Journal of Bone & Joint Surgery, British Volume, 1991. **73-B**(1): p. 68-72.
176. Glimcher, M.J. and J.E. Kenzora, *The Biology of Osteonecrosis of the Human Femoral Head and its Clinical Implications: III. Discussion of the Etiology and Genesis of the Pathological Sequelae; Comments on Treatment.* Clinical Orthopaedics and Related Research, 1979. **140**.
177. Glimcher Mj Fau - Kenzora, J.E. and J.E. Kenzora, *The biology of osteonecrosis of the human femoral head and its clinical implications: II. The pathological changes in the femoral head as an organ and in the hip joint.* (0009-921X (Print)).
178. Lieberman, J.R., *Core Decompression for Osteonecrosis of the Hip.* Clinical Orthopaedics and Related Research, 2004. **418**.
179. Fairbank, A.C., D. Bhatia, R.H. Jinnah, and D.S. Hungerford, *Long-term results of core decompression for ischaemic necrosis of the femoral head.* Journal of Bone and Joint Surgery, 1995. **77-B**(1): p. 42-49.
180. Bozic, K.J., D. Zurakowski, and T.S. Thornhill, *Survivorship Analysis of Hips Treated with Core Decompression for Nontraumatic Osteonecrosis of the Femoral Head.* The Journal of Bone & Joint Surgery, 1999. **81**(2): p. 200-209.
181. Little, D.G., R.A. Peat, A. McEvoy, P.R. Williams, E.J. Smith, and P.A. Baldock, *Zoledronic Acid Treatment Results in Retention of Femoral Head Structure After Traumatic Osteonecrosis in Young Wistar Rats.* Journal of Bone and Mineral Research, 2003. **18**(11): p. 2016-2022.
182. Ramachandran, M., K. Ward, R.R. Brown, C.F. Munns, C.T. Cowell, and D.G. Little, *Intravenous Bisphosphonate Therapy for Traumatic Osteonecrosis of the Femoral Head in Adolescents.* The Journal of Bone & Joint Surgery, 2007. **89**(8): p. 1727-1734.

183. Chen Ch Fau - Chang, J.-K., K.-A. Chang Jk Fau - Lai, S.-M. Lai Ka Fau - Hou, C.-H. Hou Sm Fau - Chang, G.-J. Chang Ch Fau - Wang, and G.J. Wang, *Alendronate in the prevention of collapse of the femoral head in nontraumatic osteonecrosis: a two-year multicenter, prospective, randomized, double-blind, placebo-controlled study.* Arthritis and Rheumatism, 2012. **64**(5): p. 1572-1578.
184. Lai, K.-A., W.-J. She, C.-Y. Yang, C.-J. Shao, J.-T. Hsu, and R.-M. Lin, *The use of alendronate to prevent early collapse of the femoral head in patients with nontraumatic osteonecrosis.* Journal of Bone and Joint Surgery, 2005. **87A**(10): p. 2155-2159.
185. Aya-ay, J., S. Athavale, S. Morgan-Bagley, H. Bian, F. Bauss, and H.K.W. Kim, *Retention, Distribution, and Effects of Intraosseously Administered Ibandronate in the Infarcted Femoral Head.* Journal of Bone and Mineral Research, 2007. **22**(1): p. 93-100.
186. Vandermeer, J.S., N. Kamiya, J. Aya-ay, A. Garces, R. Browne, and H.K.W. Kim, *Local administration of ibandronate and bone morphogenetic protein-2 after ischemic osteonecrosis of the immature femoral head: a combined therapy that stimulates bone formation and decreases femoral head deformity.* J Bone Joint Surg Am, 2011. **93**: p. 905-13.
187. Sugiyama, M., T. Kodama, K. Konishi, K. Abe, S. Asami, and S. Oikawa, *Compactin and Simvastatin, but Not Pravastatin, Induce Bone Morphogenetic Protein-2 in Human Osteosarcoma Cells.* Biochemical and Biophysical Research Communications, 2000. **271**(3): p. 688-692.
188. Russell, R.G.G., *Determinants of structure–function relationships among bisphosphonates.* Bone, 2007. **40**(5, Supplement 2): p. S21-S25.
189. Frith, J.C., J. Mönkkönen, S. Auriola, H. Mönkkönen, and M.J. Rogers, *The molecular mechanism of action of the antiresorptive and antiinflammatory drug clodronate: Evidence for the formation in vivo of a metabolite that inhibits bone resorption and causes osteoclast and macrophage apoptosis.* Arthritis & Rheumatism, 2001. **44**(9): p. 2201-2210.
190. Mundy, G., R. Garrett, S. Harris, J. Chan, D. Chen, G. Rossini, B. Boyce, M. Zhao, and G. Gutierrez, *Stimulation of bone formation in vitro and in rodents by statins.* Science, 1999. **286**(5446): p. 1946-9.
191. Allen, T.M. and P.R. Cullis, *Drug Delivery Systems: Entering the Mainstream.* Science, 2004. **303**(5665): p. 1818-1822.
192. Veber, D.F., S.R. Johnson, H.-Y. Cheng, B.R. Smith, K.W. Ward, and K.D. Kopple, *Molecular Properties That Influence the Oral Bioavailability of Drug Candidates.* Journal of Medicinal Chemistry, 2002. **45**(12): p. 2615-2623.
193. Uhrich, K.E., S.M. Cannizzaro, R.S. Langer, and K.M. Shakesheff, *Polymeric systems for controlled drug release.* Chemical Reviews, 1999. **99**(11): p. 3181-98.
194. Garg, T., O. Singh, S. Arora, and R. Murthy, *Scaffold: a novel carrier for cell and drug delivery.* Critical Reviews in Therapeutic Drug Carrier Systems, 2012. **29**(1): p. 1-63.
195. Hatefi, A. and B. Amsden, *Biodegradable injectable in situ forming drug delivery systems.* Journal of Controlled Release, 2002. **80**(1-3): p. 9-28.
196. Packhaeuser, C.B., J. Schnieders, C.G. Oster, and T. Kissel, *In situ forming parenteral drug delivery systems: an overview.* European Journal of Pharmaceutics and Biopharmaceutics, 2004. **58**(2): p. 445-455.
197. Anderson, J.M. and M.S. Shive, *Biodegradation and biocompatibility of PLA and PLGA microspheres.* Advanced Drug Delivery Reviews, 1997. **28**(1): p. 5-24.
198. Shah, N.H., A.S. Railkar, F.C. Chen, R. Tarantino, S. Kumar, M. Murjani, D. Palmer, M.H. Infeld, and A.W. Malick, *A biodegradable injectable implant for delivering micro and*

macromolecules using poly (lactic-co-glycolic) acid (PLGA) copolymers. Journal of Controlled Release, 1993. **27**(2): p. 139-147.
199. Eliaz, R.E., D. Wallach, and J. Kost, *Delivery of soluble tumor necrosis factor receptor from in-situ forming PLGA implants: in-vivo.* Pharmaceutical Research, 2000. **17**(12): p. 1546-50.
200. Shively, M.L., B.A. Coonts, W.D. Renner, J.L. Southard, and A.T. Bennett, *Physico-chemical characterization of a polymeric injectable implant delivery system.* Journal of Controlled Release, 1995. **33**(2): p. 237-243.
201. Brodbeck, K.J., J.R. DesNoyer, and A.J. McHugh, *Phase inversion dynamics of PLGA solutions related to drug delivery: Part II. The role of solution thermodynamics and bath-side mass transfer.* Journal of Controlled Release, 1999. **62**(3): p. 333-344.
202. Kranz, H. and R. Bodmeier, *Structure formation and characterization of injectable drug loaded biodegradable devices: In situ implants versus in situ microparticles.* European Journal of Pharmaceutical Sciences, 2008. **34**(2–3): p. 164-172.
203. Jeon, O., M. Krebs, and E. Alsberg, *Controlled and sustained gene delivery from injectable, porous PLGA scaffolds.* Journal of biomedical materials research. Part A, 2011. **98A**(1): p. 72-9.
204. Meenach, S.A., C.G. Otu, K.W. Anderson, and J.Z. Hilt, *Controlled synergistic delivery of paclitaxel and heat from poly(β-amino ester)/iron oxide-based hydrogel nanocomposites.* International Journal of Pharmaceutics, 2012. **427**(2): p. 177-184.
205. Potineni, A., D.M. Lynn, R. Langer, and M.M. Amiji, *Poly(ethylene oxide)-modified poly(β-amino ester) nanoparticles as a pH-sensitive biodegradable system for paclitaxel delivery.* Journal of Controlled Release, 2003. **86**(2–3): p. 223-234.
206. Miguel, B.S., C. Ghayor, M. Ehrbar, R.E. Jung, R.A. Zwahlen, P. Hortschansky, H.G. Schmoekel, and F.E. Weber, *N-methyl pyrrolidone as a potent bone morphogenetic protein enhancer for bone tissue regeneration.* Tissue Engineering Part A, 2009. **15**(10): p. 2955-63.
207. Ghayor, C., R. Correro, K. Lange, L.S. Karfeld-Sulzer, K.W. Gratz, and F.E. Weber, *Inhibition of Osteoclast Differentiation and Bone Resorption by N-Methyl Pyrrolidone.* Journal of Biological Chemistry, 2011. **286**(27): p. 24458-24466.
208. Maeda, T., A. Matsunuma, I. Kurahashi, T. Yanagawa, H. Yoshida, and N. Horiuchi, *Induction of osteoblast differentiation indices by statins in MC3T3-E1 cells.* Journal of Cellular Biochemistry, 2004. **92**: p. 458-471.
209. Ostovic, D., C. Stelmach, and B. Hulshizer, *Formation of a chromophoric complex between alendronate and copper(II) ions.* Pharmaceutical Research, 1993. **10**(3): p. 470-2.
210. Siepmann, J. and N.A. Peppas, *Modeling of drug release from delivery systems based on hydroxypropyl methylcellulose (HPMC).* Advanced Drug Delivery Reviews, 2001. **48**(2–3): p. 139-157.
211. Kim, S., Y. Bae, and T. Okano, *Hydrogels: Swelling, Drug Loading, and Release.* Pharmaceutical Research, 1992. **9**(3): p. 283-290.
212. Tang, Y. and J. Singh, *Controlled delivery of aspirin: effect of aspirin on polymer degradation and in vitro release from PLGA based phase sensitive systems.* International Journal of Pharmaceutics, 2008. **357**(1-2): p. 119-25.
213. Bakhshi, R., E. Vasheghani-Farahani, H. Mobedi, A. Jamshidi, and M. Khakpour, *The effect of additives on naltrexone hydrochloride release and solvent removal rate from an injectable in situ forming PLGA implant.* Polymers for Advanced Technologies, 2006. **17**(5): p. 354-359.

214. Nancollas, G.H., R. Tang, R.J. Phipps, Z. Henneman, S. Gulde, W. Wu, A. Mangood, R.G. Russell, and F.H. Ebetino, *Novel insights into actions of bisphosphonates on bone: differences in interactions with hydroxyapatite.* Bone, 2006. **38**(5): p. 617-27.
215. Fredenberg, S., M. Wahlgren, M. Reslow, and A. Axelsson, *The mechanisms of drug release in poly(lactic-co-glycolic acid)-based drug delivery systems—A review.* International Journal of Pharmaceutics, 2011. **415**(1–2): p. 34-52.
216. Yewey, G.L., E.G. Duysen, S.M. Cox, and R.L. Dunn, *Delivery of proteins from a controlled release injectable implant.* Pharmaceutical Biotechnology, 1997. **10**: p. 93-117.
217. Burkersroda, F., L. Schedl, and A. Gopferich, *Why degradable polymers undergo surface erosion or bulk erosion.* Biomaterials, 2002. **23**(21): p. 4221-31.
218. Kenley, R.A., M.O. Lee, T.R. Mahoney, and L.M. Sanders, *Poly(lactide-co-glycolide) decomposition kinetics in vivo and in vitro.* Macromolecules, 1987. **20**(10): p. 2398-2403.
219. Biondi, M., F. Ungaro, F. Quaglia, and P.A. Netti, *Controlled drug delivery in tissue engineering.* Advanced Drug Delivery Reviews, 2008. **60**(2): p. 229-242.
220. Zhang, L., A.F. Radovic-Moreno, F. Alexis, F.X. Gu, P.A. Basto, V. Bagalkot, S. Jon, R.S. Langer, and O.C. Farokhzad, *Co-Delivery of Hydrophobic and Hydrophilic Drugs from Nanoparticle–Aptamer Bioconjugates.* ChemMedChem, 2007. **2**(9): p. 1268-1271.
221. Sokolsky-Papkov, M., K. Agashi, A. Olaye, K. Shakesheff, and A.J. Domb, *Polymer carriers for drug delivery in tissue engineering.* Advanced Drug Delivery Reviews, 2007. **59**(4–5): p. 187-206.
222. Zhou, T., H. Lewis, R.E. Foster, and S.P. Schwendeman, *Development of a multiple-drug delivery implant for intraocular management of proliferative vitreoretinopathy.* Journal of Controlled Release, 1998. **55**(2–3): p. 281-295.
223. Schloegl, W., V. Marschall, M.Y. Witting, E. Volkmer, I. Drosse, U. Leicht, M. Schieker, M. Wiggenhorn, F. Schaubhut, S. Zahler, and W. Friess, *Porosity and mechanically optimized PLGA based in situ hardening systems.* European Journal of Pharmaceutics and Biopharmaceutics, 2012. **82**(3): p. 554-562.
224. Huang, Y.X., J. Ren, C. Chen, T.B. Ren, and X.Y. Zhou, *Preparation and Properties of Poly(lactide-co-glycolide) (PLGA)/ Nano-Hydroxyapatite (NHA) Scaffolds by Thermally Induced Phase Separation and Rabbit MSCs Culture on Scaffolds.* Journal of Biomaterials Applications, 2008. **22**(5): p. 409-432.
225. Kim, S.-S., M. Sun Park, O. Jeon, C. Yong Choi, and B.-S. Kim, *Poly(lactide-co-glycolide)/hydroxyapatite composite scaffolds for bone tissue engineering.* Biomaterials, 2006. **27**(8): p. 1399-1409.
226. Kothapalli, C.R., M.T. Shaw, and M. Wei, *Biodegradable HA-PLA 3-D porous scaffolds: effect of nano-sized filler content on scaffold properties.* Acta Biomater, 2005. **1**(6): p. 653-62.
227. Li, B. and R.M. Aspden, *Composition and Mechanical Properties of Cancellous Bone from the Femoral Head of Patients with Osteoporosis or Osteoarthritis.* Journal of Bone and Mineral Research, 1997. **12**(4): p. 641-651.
228. Brown, T.D., M.E. Way, and A.B. Ferguson, Jr., *Mechanical characteristics of bone in femoral capital aseptic necrosis.* Clin Orthop Relat Res, 1981(156): p. 240-7.
229. Wang, J.X., *A biomechanical study in the repairing process of avascular necrosis of the femoral head in dogs.* Zhonghua Wai Ke Za Zhi, 1993. **31**(6): p. 374-7.
230. Wei, G. and P.X. Ma, *Structure and properties of nano-hydroxyapatite/polymer composite scaffolds for bone tissue engineering.* Biomaterials, 2004. **25**(19): p. 4749-4757.

231. Verheyen, C.C.P.M., J.R. De Wijn, C.A. Van Blitterswijk, and K. De Groot, *Evaluation of hydroxylapatite/poly(l-lactide) composites: Mechanical behavior.* Journal of Biomedical Materials Research, 1992. **26**(10): p. 1277-1296.
232. Guan, L. and J.E. Davies, *Preparation and characterization of a highly macroporous biodegradable composite tissue engineering scaffold.* Journal of biomedical materials research. Part A, 2004. **71A**(3): p. 480-487.
233. Fu, S.-Y., X.-Q. Feng, B. Lauke, and Y.-W. Mai, *Effects of particle size, particle/matrix interface adhesion and particle loading on mechanical properties of particulate–polymer composites.* Composites Part B: Engineering, 2008. **39**(6): p. 933-961.
234. Gad, H., M. El-Nabarawi, and S. Abd El-Hady, *Formulation and Evaluation of PLA and PLGA In Situ Implants Containing Secnidazole and/or Doxycycline for Treatment of Periodontitis.* AAPS PharmSciTech, 2008. **9**(3): p. 878-884.
235. Schoenfeld, C.M., E.P. Lautenschlager, and P.R. Meyer, Jr., *Mechanical properties of human cancellous bone in the femoral head.* Medical and biological engineering, 1974. **12**(3): p. 313-317.
236. Rezwan, K., Q.Z. Chen, J.J. Blaker, and A.R. Boccaccini, *Biodegradable and bioactive porous polymer/inorganic composite scaffolds for bone tissue engineering.* Biomaterials, 2006. **27**(18): p. 3413-3431.
237. Bohner, M. and G. Baroud, *Injectability of calcium phosphate pastes.* Biomaterials, 2005. **26**(13): p. 1553-1563.
238. Alves, H.L., L.A. Santos, and C.P. Bergmann, *Injectability evaluation of tricalcium phosphate bone cement.* Journal of Materials Science: Materials in Medicine, 2008. **19**(5): p. 2241-2246.
239. Khairoun, I., M.G. Boltong, F.C.M. Driessens, and J.A. Planell, *Some factors controlling the injectability of calcium phosphate bone cements.* Journal of Materials Science: Materials in Medicine, 1998. **9**(8): p. 425-428.
240. Leroux, L., Z. Hatim, M. Frèche, and J.L. Lacout, *Effects of various adjuvants (lactic acid, glycerol, and chitosan) on the injectability of a calcium phosphate cement.* Bone, 1999. **25**(2, Supplement 1): p. 31S-34S.
241. Kempe, S., H. Metz, and K. Mäder, *Do in situ forming PLG/NMP implants behave similar in vitro and in vivo? A non-invasive and quantitative EPR investigation on the mechanisms of the implant formation process.* Journal of Controlled Release, 2008. **130**(3): p. 220-225.
242. DiPisa Ja Fau - Sih, G.S., A.T. Sih Gs Fau - Berman, and A.T. Berman, *The temperature problem at the bone-acrylic cement interface of the total hip replacement.* Clinical Orthopaedics and Related Research, 1976. **121**: p. 95-98.
243. Saha, S. and S. Pal, *Mechanical properties of bone cement: A review.* Journal of Biomedical Materials Research, 1984. **18**(4): p. 435-462.
244. Mundargi, R.C., S. Srirangarajan, S.A. Agnihotri, S.A. Patil, S. Ravindra, S.B. Setty, and T.M. Aminabhavi, *Development and evaluation of novel biodegradable microspheres based on poly(d,l-lactide-co-glycolide) and poly(ε-caprolactone) for controlled delivery of doxycycline in the treatment of human periodontal pocket: In vitro and in vivo studies.* Journal of Controlled Release, 2007. **119**(1): p. 59-68.
245. Sundararaj, S.C., M.V. Thomas, R. Peyyala, T.D. Dziubla, and D.A. Puleo, *Design of a multiple drug delivery system directed at periodontitis.* Biomaterials, 2013. **34**(34): p. 8835-8842.
246. Joshi, D., T. Garg, A.K. Goyal, and G. Rath, *Advanced drug delivery approaches against periodontitis.* Drug Delivery, 2014: p. 1-15.

247. Izumi, Y., A. Aoki, Y. Yamada, H. Kobayashi, T. Iwata, T. Akizuki, T. Suda, S. Nakamura, N. Wara-Aswapati, M. Ueda, and I. Ishikawa, *Current and future periodontal tissue engineering.* Periodontology 2000, 2011. **56**(1): p. 166-187.
248. Krebs, M.D., K.A. Sutter, A.S.P. Lin, R.E. Guldberg, and E. Alsberg, *Injectable poly(lactic-co-glycolic) acid scaffolds with in situ pore formation for tissue engineering.* Acta Biomaterialia, 2009. **5**(8): p. 2847-2859.
249. Do, M.P., C. Neut, E. Delcourt, T. Seixas Certo, J. Siepmann, and F. Siepmann, *In situ forming implants for periodontitis treatment with improved adhesive properties.* European journal of pharmaceutics and biopharmaceutics : official journal of Arbeitsgemeinschaft fur Pharmazeutische Verfahrenstechnik e.V, 2014: p. [Epub ahead of print].
250. Goktas, S., J.J. Dmytryk, and P.S. McFetridge, *Biomechanical behavior of oral soft tissues.* J Periodontol, 2011. **82**(8): p. 1178-86.
251. Izumi, K., T. Tobita, and S.E. Feinberg, *Isolation of human oral keratinocyte progenitor/stem cells.* Journal of Dental Research, 2007. **86**(4): p. 341-346.
252. Lavenus, S., P. Pilet, J. Guicheux, P. Weiss, G. Louarn, and P. Layrolle, *Behaviour of mesenchymal stem cells, fibroblasts and osteoblasts on smooth surfaces.* Acta Biomaterialia, 2011. **7**(4): p. 1525-1534.
253. Hawkins, A.M., M.E. Tolbert, B. Newton, T.A. Milbrandt, D.A. Puleo, and J.Z. Hilt, *Tuning biodegradable hydrogel properties via synthesis procedure.* Polymer, 2013. **54**(17): p. 4422-4426.
254. Hawkins, A.M., T.A. Milbrandt, D.A. Puleo, and J.Z. Hilt, *Composite hydrogel scaffolds with controlled pore opening via biodegradable hydrogel porogen degradation.* Journal of biomedical materials research. Part A, 2014. **102**(2): p. 400-412.
255. Spencer, D., *Oswald physical and engineering sciences second place: multiple macromer hydrogels for multiphase drug release.* Kaleidoscope, 2014. **11**(1): p. 20.
256. Li, H., S.M. Oppenheimer, S.I. Stupp, D.C. Dunand, and L.C. Brinson, *Effects of pore morphology and bone ingrowth on mechanical properties of microporous titanium as an orthopaedic implant material.* Materials Transactions, 2004. **45**(4): p. 1124-1131.
257. Yu, H., H.W. Matthew, P.H. Wooley, and S.-Y. Yang, *Effect of porosity and pore size on microstructures and mechanical properties of poly-ε-caprolactone- hydroxyapatite composites.* Journal of Biomedical Materials Research Part B: Applied Biomaterials, 2008. **86B**(2): p. 541-547.
258. Anderson, H.H., *Treatment of chronic periodontitis: a site-specific fiber placement technique.* Practical periodontics and aesthetic dentistry : PPAD, 1996. **8**(6): p. 565-70.
259. Andersen, K.L., E.H. Pedersen, and B. Melsen, *Material parameters and stress profiles within the periodontal ligament.* American Journal of Orthodontics and Dentofacial Orthopedics, 1991. **99**(5): p. 427-440.
260. Beertsen, W., C.A.G. McCulloch, and J. Sodek, *The periodontal ligament: a unique, multifunctional connective tissue.* Periodontology 2000, 1997. **13**(1): p. 20-40.
261. Sawada, A., N. Wakabayashi, M. Ona, and T. Suzuki, *Viscoelasticity of human oral mucosa: implications for masticatory biomechanics.* Journal of Dental Research, 2011. **90**(5): p. 590-595.
262. Tanaka, E., E. Yamano, D.A. Dalla-Bona, M. Watanabe, T. Inubushi, M. Shirakura, R. Sano, K. Takahashi, T. van Eijden, and K. Tanne, *Dynamic compressive properties of the mandibular condylar cartilage.* Journal of Dental Research, 2006. **85**(6): p. 571-575.
263. Qin, Y., M. Yuan, L. Li, W. Li, and J. Xue, *Formulation and evaluation of in situ forming PLA implant containing tinidazole for the treatment of periodontitis.* Journal of

Biomedical Materials Research Part B: Applied Biomaterials, 2012. **100B**(8): p. 2197-2202.
264. Karimbux, N., *Clinical cases in periodontics*. 2012, Chichester, West Sussex, UK: Wiley-Blackwell.
265. Drisko, C.H., *The use of locally-delivered doxycycline in the treatment of periodontitis. Clinical results*.* Journal of Clinical Periodontology, 1998. **25**(11): p. 947-952.
266. Inoue, K., H. Arikawa, K. Fujii, N. Shinohara, and N. Kawahata, *Viscoelastic properties of oral soft tissue. 1. A method of determining elastic modulus of oral soft tissue.* Dent Mater J, 1985. **4**(1): p. 47-53.
267. Chang, S.J., Y.-T. Huang, S.-C. Yang, S.-M. Kuo, and M.-W. Lee, *In vitro properties of gellan gum sponge as the dental filling to maintain alveolar space.* Carbohydrate Polymers, 2012. **88**(2): p. 684-689.

Vita

Education
University of California, Irvine. Irvine, California, June 2009
B.S. Biomedical Engineering

Research Experience
National Science Foundation IGERT Graduate Trainee
University of Kentucky, Lexington, KY, August 2010 – present
Advisors: Dr. D.A. Puleo, Department of Biomedical Engineering, Dr. J.Z. Hilt, Department of Chemical and Materials Engineering

Graduate Research Assistant
University of Kentucky, Lexington, KY, August 2013 – present
Advisors: Dr. D.A. Puleo, Department of Biomedical Engineering, Dr. J.Z. Hilt, Department of Chemical and Materials Engineering

Research Associate
Alere, Inc., San Diego, CA, November 2009 – August 2010

Awards / Honors
- NSF-IGERT Fellow (August 2010 – present)
- Graduate Certificate in Bioactive Interfaces and Devices (December 2013)
- First Place – Society For Biomaterials Education Challenge (April 2014)
- UC Irvine Regents' Scholarship (September 2005 – June 2009)

Publications
- P.D. Fisher, G. Venugopal, T.A. Milbrandt, J.Z. Hilt, D.A. Puleo. Hydroxyapatite-reinforced in situ forming PLGA systems for intraosseous injection. J Biomed Mater Res A (in press), 2014.

- S. Ramineni, C. Fowler, P. Fisher, L. Cunningham, D. Puleo. Effects of Epidermal Growth Factor-Loaded Mucoadhesive Films on Wounded Oral Tissue Rafts. Biomed Mater (in review), 2014.

- P.D. Fisher*, B.R. Orellana*, A. Clark, A.M. Hawkins, J.Z. Hilt, T.A. Milbrandt, D.A. Puleo. In vivo biocompatibility of poly(β-amino ester) bone implants. In preparation, 2014. (*Authors contributed equally to this work)

- P.D. Fisher, J.Z. Hilt, D.A. Puleo. Poly(β-amino ester) microparticles as porogen and drug delivery vehicles in in situ forming scaffolds. In progress, 2014.

- Y. Zou*, P.D. Fisher*, J.K. Horstmann, J.L. Brooks, V. Talwalkar, T.A. Milbrandt, D.A. Puleo. Synergistic local drug delivery in a pig model of Legg-Calvé-Perthes Disease. The Bone and Joint Journal (submitted), 2014. (*Authors contributed equally to this work)

- P.D. Fisher, P. Palomino, T.A. Milbrandt, J.Z. Hilt, D.A. Puleo. Improved small molecule drug release from in situ forming poly(lactic-co-glycolic acid) scaffolds incorporating poly(β-amino ester) and hydroxyapatite microparticles. J. Biomat. Sci., Polymer Ed., 25, 1174-1193, 2014.

Professional Conference Presentations

- P. Fisher, T. Milbrandt, J.Z. Hilt, D. Puleo, "Improving Properties of *In Situ* Forming PLGA Implants via Poly(β-Amino Ester) and Hydroxyapatite Additives", Biomedical Engineering Society Annual Meeting, San Antonio, TX (October 7-10, 2014) – Poster

- P. Fisher, J.Z. Hilt, T. Milbrandt, D. Puleo, Drug Release and Mechanical Effects of Poly(β-Amino Ester) and Hydroxyapatite on In Situ Forming PLGA Systems", Society For Biomaterials Annual Meeting, Denver, CO (April 16-19, 2014) – Oral Presentation

- P. Fisher, J.Z. Hilt, D. Puleo, "In Situ Forming Drug Delivery Scaffold for Treating Avascular Necrosis of the Femoral Head", Society For Biomaterials Annual Meeting, Boston, MA (April 10-13, 2013) – Poster

- P. Fisher, J.Z. Hilt, D. Puleo, "In situ Forming, Mechanically Supportive Drug Delivery System for Avascular Necrosis of the Femoral Head", 4th Annual Biomaterials Day, Lexington, KY (September 22, 2012) – Oral Presentation

- P. Fisher, J.Z. Hilt, D. Puleo, "An Injectable, Mechanically Supportive Drug Delivery Scaffold For Osteogenic Applications", 3rd Annual Biomaterials Day, West Lafayette, IN (October 29, 2011) – Oral Presentation